INFORMATION TO USERS

This manuscript has been reproduced from the microfilm master. UMI films the text directly from the original or copy submitted. Thus, some thesis and dissertation copies are in typewriter face, while others may be from any type of computer printer.

The quality of this reproduction is dependent upon the quality of the copy submitted. Broken or indistinct print, colored or poor quality illustrations and photographs, print bleedthrough, substandard margins, and improper alignment can adversely affect reproduction.

In the unlikely event that the author did not send UMI a complete manuscript and there are missing pages, these will be noted. Also, if unauthorized copyright material had to be removed, a note will indicate the deletion.

Oversize materials (e.g., maps, drawings, charts) are reproduced by sectioning the original, beginning at the upper left-hand corner and continuing from left to right in equal sections with small overlaps.

Photographs included in the original manuscript have been reproduced xerographically in this copy. Higher quality 6" x 9" black and white photographic prints are available for any photographs or illustrations appearing in this copy for an additional charge. Contact UMI directly to order.

Bell & Howell Information and Learning
300 North Zeeb Road, Ann Arbor, MI 48106-1346 USA
800-521-0600

UMI®

RAMAN SPECTROSCOPY OF MASS-SELECTED METAL CLUSTERS

By

XIAOLE SHEN

A dissertation submitted to the Graduate Faculty in Chemistry in partial fulfillment of the requirements for the degree of Doctor of Philosophy, The City University of New York.

2000

This manuscript has been read and accepted for the Graduate Faculty in Chemistry in satisfaction of the dissertation requirement for the degree of Doctor of Phylosophy.

6 · 30 · 00
date

Chairman of Examining Committee

7/10/00
date

Executive Officer

Supervisory Committee

The City University of New York

ABSTRACT

Raman Spectroscopy of Mass-Selected Metal Clusters

By

Xiaole Shen

Advisor: John R. Lombardi and Derek M. Lindsay

Absorption and Resonance Raman spectroscopy has been employed to interrogate mass-selected metal clusters in argon matrices. With the CCNY metal cluster deposition source, metal cluster cations (produced by bombardment) are mass selected using a velocity Wien Filter, and then co-deposited with rare gas on a cold window in the presence of low energy electrons. Neutralized cluster samples are interrogated by absorption, excitation, fluorescence and Raman spectroscopy. Following previous work on transition metal clusters, we focused on the IIIB group and lanthanide dimers. Good quality Raman spectra of Y_2, La_2, Ce_2, Pr_2, Nd_2, Gd_2, Tb_2, Lu_2 are reported. At the same time, investigation on triatomic clusters resulted in reports on Rh_3, Ta_3, and Ru_3. Electronic transitions have been assigned with little ambiguity as to spectral carrier. Vibrational parameters were obtained for the first time. These results provided bonding properties and structural information. They give us further understanding of bonding character.

Dedication

I would like to thank all my colleagues during the research about this thesis. Dr. Li Fang, Dr. Yifei Liu and Mr. Xiaoyu Chen, who provide me a free space of learning and thinking; Prof. Ronald Birke and Prof. Louis Massa, who keep eyes on every improvement of me. Without them, I could not finish so far.

I am deeply indebted to Prof. John R. Lombardi, my academic mentor. He taught me not only the knowledge but also the art of science. His courage and support brought all my work through tough situations. This thesis is dedicated to Prof. Derek. Lindsay, who brought me into science field. His dedication to research and strictness in experiment will teach me all my life. Without them, I could never finish this work.

Not surprisingly, I owe much to my family, especially my wife, who give me all the motivation to finish the degree.

Thank you very much!

TABLE OF CONTENTS

LIST OF FIGURES

Chapter **Page**

LIST OF TABLES

Chapter **Page**

CHAPTER I. INTRODUCTION

While the two extrema, the free atom and the bulk metal are quite well understood, much less is known about the transition region in between. Properties of molecular cluster could be quite different from those of the bulk or atom. Investigation of clusters will provide insight into the forces that govern physical and chemical properties of many interesting phases of metals.

In the past 20 years or so, metal clusters without ligand support have come under both experimental and theoretical examination. The potential applications could be in fields from solid state physics to chemical catalysis, or from material science to chemical synthesis. The knowledge of clusters provides not only clues as to interaction within and between material, but also provide a template for designing new materials. The technology developed on the way to achieving the knowledge such as molecular beam instrumentation, spectroscopy, as well as theoretical methods present a great contribution to all science fields.

An overwhelming array of techniques has been brought to bear in cluster science. Experimental studies have focused on absorption spectroscopy, excitation spectroscopy, surface scattering and depletion, ionization

potential, stability and thermodynamic, photochemical process. In the following, we will focus on details of several previous experimental studies for the vibronic property of the cluster.

Knudson Effusion Mass Spectroscopy is probably the earliest investigation of clusters. The major concern of this method is to determine the dissociation energy by setting up thermal equilibrium between cluster and atom. Results for almost all transition metal dimers have been published 20 years ago [1]. The second law is applied to the equilibrium constant vs. temperature which in turn gives the dissociation energy D_e. Another way is to use the third law and to predict some parameter such as frequency, degeneracy for both ground state and excited. The third law method always provides better and more reasonable results than second law. For the second law method, the relatively high deviation is from the uncertainty in the mass determination and therefore in the equilibrium constants. Furthermore, experiments are limited by a technology 20 years old so that there are problems in ionization, measurement, as well as purity. The equilibrium is a slow process and the result may be different from spectroscopic dissociation. The real process would not always be from the cluster ground state to atomic ground state.

Study of gas phase clusters is hampered by insufficient sensitivity. Nevertheless, there are still some elegant experiments. The following two method change the essence of detection by ionization, substituting photon detection by more sensitive ion detection.

Photoelectron Spectroscopy of negative cluster ions provides information on neutral cluster. It reveals the accurate electron affinity (EA) of a cluster. The ground state gas phase information from this experiment is always reliable. The vibrational frequency result for Cr_2 and Pd_2 [2] is selected as our standard in the dimer periodical table. Sometime even the anharmonicity constant could be quite similar to matrix isolation result too. However, the frequency data acquired from this method is not as precise as from Raman spectroscopy. The method is also limited to those dimers whose diatomic anion may be formed from the discharge of carbonyl complex. ZEKE is a special way to detect a photoelectron, which is successfully applied in cluster investigation such as in Y_2 [3].

The review [4] of Dr. Michael Morse summarized cluster investigation as of 1986. Soon after that, his group at the University of Utah began their studies on resonance two-photon ionization (R2PI) spectroscopy of clusters. From such studies they obtained information on molecular term

symbols, dissociation energy through predissociation threshold measurements, equilibrium distance (r_e) between atoms by rotational resolved studies, precise force constant or vibrational frequency (ω) measurements by fluorescence and ionization energy for clusters. They provided the most reliable spectroscopic D_e. The precision of the parameters, around 0.2% deviation of ω, D_e and r_e, is astonishing. That is due to the application of extremely sensitive R2PI or fluorescence [5] detection, as well as a 0.04 cm^{-1} line width scannable dye laser. They published numerous results about several homonuclear [5a] and especially heteronuclear [5b] clusters. Such experiment on gas phase cluster revealed the geometric information through rotational structure, and this has an advantage over matrix isolation. The obvious limitation of this method is that the resonance process must take place in the region that dye laser can be continuously lasing. The assignment of electronic state energy levels is another problem.

A purely spectroscopic method with detection of photons always needs accumulation of the clusters such as in a deposition process. Fluorescence and resonance Raman are always applicable. Cu_2, Mo_2, and Pt_2 [6] are three special species only determined by fluorescence. Normally, the

fluorescence spectrum is easier to detect due to its high intensity. Because of the huge number of excited states located between ground and the excited state, and being a relatively slow process, fluorescence is often quenched in metal clusters. On the contrary, a faster process as Raman is more generally applicable. Fluorescence is so sensitive that gas phase clusters are sometimes detectable. The shortcoming of fluorescence is the uncertainty of the ground state assignment.

Resonance Raman spectroscopy is a powerful tool for the study of molecular vibrations that are coupled to electronic transitions in clusters. Much information can be obtained about the potential surfaces of both ground and excited states. Matrix Isolation and resonance Raman spectroscopy of clusters has been investigated by the Moskovits group at the University of Toronto. In the late 80's they almost finished the measurement of all the third row dimers and several trimers. By the furnace method they produced cluster mixture of all sizes, analyzed and assigned the spectroscopy. Some other ambiguous but interesting evidences are obtained from varying working condition such as: cluster to matrix gas ratio, temperature, pressure, photo-dissociation and aggregation. Some of their assignments for absorption are successful

especially those with Resonance Raman evidence. But some others, including features for cluster larger than a dimer failed. Their work provided a great incentive for further cluster studies. The ground state force constants of Sc_2, Ti_2, Mn_2, Fe_2 [7] from their work are suggested to be standard in our dimer periodical table.

To conquer this difficulty, mass and matrix isolated neutralized clusters are synthesized and characterized in our lab. With this instrument, 14 transition metal dimers (V_2, Co_2, Ni_2, Y_2, Zr_2, Nb_2, Ru_2, Rh_2, La_2, Hf_2, Ta_2, W_2, Re_2, Pt_2) as well as 7 lanthanide (La_2, Ce_2, Pr_2, Nd_2, Gd_2, Tb_2, Lu_2) are reported. Furthermore, 5 trimers (Zr_3, Nb_3, Ru_3, Rh_3, Hf_3) and one tetramer (Ta_4) have been published. Most of these are the first available experimental data. High quality Raman spectra reveal vibrational frequency and force constant, anharmonicity constants and spectroscopic dissociation energy, parameters of low-lying state and geometry of higher clusters. The force constants of transition metal dimers are summarized in Table 1.1. Absorption spectra provide more information on excited states, transitions, and useful knowledge of resonance. The assignment without ambiguity for the absorption band is the major advantage of this mass-selected cluster deposition device.

There are only three machines of neutralization matrix isolation of mass selected clusters in the world. The contribution of the first in Switzerland is basic mechanisms such as sputtering, neutralization, soft-landing, fragmentation and deposition process [8]. We studied clusters across the periodical table. A recent goal by Moskovits group at University of Toronto focuses their interest on size dependent bonding and geometry, especially from coinage clusters [9].

The configuration of electronic states is important knowledge for all clusters. Electron Spin Resonance (ESR) is another important way to go deeply into essence of bonding [10]. This method focuses more on the electron character, especially paramagnetic properties instead of nuclear vibration parameters. Normally, ESR is very sensitive measurement in matrix isolation sample. Geometry is an indirect result of ESR analysis comparable with Raman results. However, ESR detects a slow process compared to molecular stretching so that it shows average in geometry effect. Thus it is sometimes the case that ESR gives different structural conclusions from spectroscopy.

Besides those experimental methods mentioned above, there are a lot of other investigation about such topics as ionization potential, electron affinity, structure and

internuclear distance, and potential application of cluster chemical reactions. They are all relative to bonding characters.

Investigation of clusters area has been divided into experimental and theoretical. Theoretical calculation predicted the results of experiment and the experimental results modify in some theories. They are normally based on traditional ab initio method or semi-empirical method. Calculation on metal clusters, especially for heavy element of third row, are challenging because of the large number of electrons, relativistic effects, electron spin orbital coupling effect etc. There is no single calculation model that could explain all experimental results. During our studies, density functional calculations employing pseudopotentials with configuration interaction applied in lanthanide dimers [11], and Complete Active Space Multi-Configuration Self-Interaction (CASSCF) + Muti-Reference Configuration Interaction (MRSDCI) for trimer [12] energy levels and symmetry appear more reliable. However, it is still hard to predict the correct parameters before experimental work.

The high sensitivity of ESR enables our neutralization method applicable for sample preparation. The mass-selected matrix isolation device can be modified for such an

application. On the other hand, the heteronuclear properties have become attractive along with homonuclear cluster study. The force constant, dissociation energy, and even absorption character can be predicted from homonulear dimer parameters. For example, the dissociation energy can be predicted by Pauling's rule, force constant is always believed to be between two component homonuclear dimers, excited states levels are sometimes foreseen especially for heteronuclear dimer by two atoms from same group. However, the experimental details are still so sparse that it is hard to summarize. It can be suggested that additional investigation of heteronuclear dimers with our experimental set-up should be undertaken.

Table 1.1

Ground State Harmonic Frequency of Diatomic Transition Metal Dimers (cm^{-1}) and the Corresponding Force Constants (mdyn/Å)

Sc_2	Ti_2	V_2	Cr_2	Mn_2	Fe_2	Co_2[i]	Ni_2[k]	Cu_2	Zn_2
238.9	407.9	536.9	479.0	76.4	299.5	296.8	259.2	266.4	25.7
0.756	2.348	4.326	3.515	0.094	1.476	1.529	1.162	1.329	0.013
Y_2[a]	Zr_2	Nb_2	Mo_2	Tc_2	Ru_2[h]	Rh_2[j]	Pd_2	Ag_2	Cd_2
184.4	305.7	420.5	477.1		347.1	283.9	210.0	192.4	22.9
0.896	2.511	4.840	6.433		3.587	2.443	1.382	1.176	0.017
Lu_2[b]	Hf_2	Ta_2	W_2	Re_2[g]	Os_2	Ir_2	Pt_2[l]	Au_2	Hg_2
121.6	176.2	300.2	336.8	337.9			197.4	190.9	18.5
0.762	1.632	4.804	6.144	6.263			2.240	2.115	0.020

La_2[c]	Ce_2[d]	Pr_2[d]	Nd_2[d]	Pm_2	Sm_2	Eu_2	Gd_2[e]	Tb_2[f]	Dy_2	Ho_2	Er_2	Tm_2	Yb_2	Lu_2
236.0	245.4	244.9	148.0				138.7	137.6						121.6
2.280	2.480	2.490	0.930				0.890	0.880						0.762

References for Table 5.1

Appendix to previously published table at *J. Phys. Chem.* **97**, 9263, (1993)

[a] "Spectroscopy of Yttrium Dimers in Argon Matrices", L. Fang, X. Chen, X. Shen, Y. Liu, D. M. Lindsay and J. R. Lombardi, Accepted for publication, *Low Temperature Physics*. **26**, xxxx, (2000) in press.

[b] "Raman and Absorption Spectrum of Mass-Selected Lutetium Dimers in Argon Matrices", L. Fang, X. Shen, X. Chen, and J. R. Lombardi, submitted to *J. Chem. Phys.*

[c] "Absorption, Resonance Raman and Raman Excitation Spectra of Lanthanum Dimers in Argon Matrices", Y. Liu, L. Fang, X. Shen, X. Chen, J. R. Lombardi and D. M. Lindsay, *Chem. Phys.* (2000) to be published.

[d] "Absorption, excitation and resonance Raman spectra of Ce_2, Pr_2 and Nd_2", X. Shen, L. Fang, X. Chen, and J. R. Lombardi, *J. Chem. Phys.* **113**, xxxx (2000) in press.

[e] X. Chen, L. Fang, X. Shen and J. R. Lombardi, *J. Chem. Phys.* **112**, 9780 (2000).

[f] "Raman Spectrum of Mass-Selected Terbium Dimers in Argon Matrices", L. Fang, X. Chen, X. Shen, and J. R. Lombardi, *J. Phys. Chem.* To be published.

[g] Z. Hu, J. Dong, J. R. Lombardi and D. M. Lindsay, *J. Chem. Phys.* **101**, 95 (1994).

[h] H. Wang, Y. Liu, H. Haouri, R. Craig, J. R. Lombardi, D. M. Lindsay, *J. Chem. Phys.*, **106**, 6534, (1997).

[i] J. Dong, Z. Hu, R. Craig, J. R. Lombardi and D. M. Lindsay, *J. Chem. Phys.* **101**, 9280 (1994).

[j] H. Wang, H. Haouri, R. Craig, Y. Liu, J. R. Lombardi, D. M. Lindsay, *J. Chem. Phys.*, **106**, 2101 (1997).

[k] H. Wang, H. Haouari, R. Craig, J. R. Lombardi, and D. M. Lindsay, *J. Chem. Phys.*, **104**, 3420 (1996).

[l] H. Wang, Y. Liu, H. Haouri, R. Craig, J. R. Lombardi and D. M. Lindsay, *J. Phys. Chem.* **101**, 7036 (1997).

CHAPTER II. Experimental

CCNY Mass-Selected Matrix Isolation system

Studies on clusters are severely hampered by ambiguities in assigning the spectra carrier. The assignment problem can be overcome by preparing matrices which contain known, single sized clusters. In principle, this may be accomplished by mass selecting ion clusters in the gas phase and neutralizing these during deposition. The apparatus at the CCNY deposits intense beams of neutral, mass selected metal clusters in rare gas matrices on a solid surface.

The whole instrument is well illustrated by Fig 2.1. Cluster ions were formed by sputtering from a water-cooled rotatable metal target. An intense, high energy (typically 15mA at 25keV) primary beam of Ar^+ ions was produced by a Cold Reflex Discharge Ion Source ("CORDIS") designed and manufactured by Rokion Ionenstrahl-Technologie (Darmstadt, Germany). The 50° inclination between the primary and secondary beam lines corresponds closely to the optimum ejection angle for material sputtered from a metal surface. More knowledge about sputtering can be acquired from [1].

Secondary ions were extracted with a modified Colutron model 200-B lens system and then mass-selected using a Wien filter (Colutron 600-B) in conjunction with an

approximately 175mm long drift space and a 6.5 mm diameter aperture. Using 600-B to vary the applied magnetic field allow a mass scan to be achieved. Only cluster ions of interest will go through the hole at the end of drifting. After mass separation, the ion beam is bent by 10° (in order to eliminate neutral sputtered products) and then guided to the deposition region by two einzel-like lenses. The whole route including extraction lens, Wien Filter and focusing lens are floated with around a -1.5 kV floating ground to improve output of sputtering and throughput.

The deposition region is shown in more detail (right inset of Fig 2.1). Cluster ions were co-deposited (at about 14K) with Ar and electrons on a polished CaF_2 plate (dimensions: 1 * 8 * 45 mm) mounted on a closed cycle cryostat (APD Displex, 204SL/DMX-6). Matrices were grown at 5-10μ/Hour with an Ar:metal dilution ratio of approximately 10^4:1. That ratio will insure each cluster is surrounded by only matrix atoms and there is no further interaction between clusters. Argon is selected as matrix material due to the lower lattice energy (2kcal/mol) than normal gases (N2, CO), which will bring less interference to the cluster properties [2]. The whole deposition region was held at the same voltage (about 10 V with respect to the sputtering target) and a "Faraday cage" surrounded the CaF_2 substrate

(or polished aluminum plate). The electron source consisted of an enclosed tungsten filament biased 3-4V negative with respect to the Faraday cage and positioned so that electrons were introduced 1 - 2 mm in front of the substrate. The difference in voltage (V_{dep}) between the target and Faraday cage determines the ion deposition energy (eV_{dep}), which was normally held at approximately 10eV in the deposition.

The typical total current for the secondary beam is around several hundred nanoamperes. The sputtering yield is determined by the ionization energy and the lattice structure of the sputtering metal as well as incidence angle of the incoming beam. The particles removed from a solid surface by sputtering are emitted with a broad distribution in kinetic energy at different excitation and charged states. They are predominantly neutral atoms in the ground state and generally less than 5% are ions [1]. That means there is just a small part of cluster ion distribution with a certain kinetic energy that we really need. The compensation of mass selection is low productivity. However, it is enough for experiments of absorption and resonance Raman spectroscopy.

Sputtering is obviously a more efficient way than the traditional furnace and heating for cluster formation. The

amount of our sputtering dimer is almost comparable to atomic ion, while the ratio of atom to dimer is found to be around 10^4 ~ 10^7 for Knudson effusion method which was controlled by thermoequilibrium [3]. Ion sputtering or laser ablating is widely applied in cluster formation especially for those traditionally refractory metals in the heating method.

Ionic species are neutralized during deposition. Notice that the deposition substrate is an insulator and negative charge will be accumulated and repel the incoming electrons. The ratio of electrons to ions is kept 3:1 to 2:1. The neutralization/collection efficiency is about 50% [4]. Surprisingly, deposition without electrons gave a spectrum approximately 20 times weaker. Cluster neutralization occurs when the ions are already inside the matrix or on the rare gas surface rather than in the gas phase before reaching the matrix.

Clusters ions must slow down before they hit the substrate and that is the so called soft landing. The kinetic energy distribution of the arriving ions, measured by applying a retarding potential to the Faraday plate, was centered close to eV_{dep}=0 eV with FWHM of about 10 eV. Fragmentation is estimated by comparing the intensities of atomic excitation features in a cluster deposition with

those obtained from depositions of the atom under similar conditions. Such a fragmentation ratio (F.R.) for transition metal dimers in this lab, vary from 0.1% in Ta_2 to 40% for Nd_2. Fragmentation ratio is determined by the dissociation energy of cluster, deposition condition, or stability of cluster ions. This is summarized in recent work [5]. Generally speaking, the higher D_0, the lower the ratio is. The F.R. increases with the kinetic energy of deposition. The larger the cluster, the more difficult fragmentation is. That is due to the better distribution of the kinetic energy by more atoms at landing. The F.R. is also different for deposition matrices from Kr to Xe, or to Ar. The landing process is transferring kinetic energy to the matrix particles and kicking them out like a sputtering process. Therefore, the lattice energy of matrix layer determines the softness of the deposition process.

In order to achieve high purity of matrix sample, ultrahigh vacuum up to 10e-8 Torr is kept in the deposition region. A residual gas analyzer (Leybold-Inficon, Quadruvac Q100) is applied to monitor the possible contaminants from N_2, O_2, CO_2 and especially H_2O. The analysis shows beyond 95% probability that the clusters are all surrounded by only matrix argon atoms during deposition.

Mass Spectroscopy

The advantage of our instrument over early setups is mass selection. Mass selection is preferable to non-selected experiments because the carrier of the spectrum can be assigned with certainty. Selection could hardly be achieved for neutral particles. On the contrary, for ionic species, selection by applying electric and magnetic (E-M) field is quite simple. Ion beam is extracted by a series electronic lens after sputtering. It is guided into Wien Filter composed by electric plates and magnetic shields perpendicular to each other. The selection is achieved by scanning the magnetic field. Compromise between the throughput and resolution leaves the resolution of our Wien Filter at $M/\Delta M=6\sim7$. This is adequate for separation between clusters and oxides. The resolution of selection is determined by the aperture after the free drift space of the E-M field as well as the sputtering ion kinetic energy distribution. The resolution could ensure the reliability of our deposition species and spectral carrier.

The sputtering mass spectrum for almost all transition metal and several lanthanides have been recorded. The secondary current of each ion is an amount criterion before deposition. Most of transition dimers have more than 10 nA current, which are estimated to be the minimum limit

required by our deposition and detection of absorption and resonance Raman spectroscopy. Some of transition metals have their trimer currents high enough for experiment as well. One of the good tetramer candidates, which has quadratic increase of current, the Ta_4 gives an elegant Raman spectrum. Some time the sputtering spectrum shows kind of magic rule with sputtering ions. Coinage metals, as in the IB group, give long progressions in the mass spectrum and their clusters composed of odd number atoms show more stability, compared with even neighbor. While for Ta and Pd the tetramer show special intensity. From the sputtering mass spectrum of transition metals, we can see metals of early transition series are good sputtering samples in that they have more intense dimer or trimer current. It may be because the early transition cluster bonds are mainly d orbital but the late transition are s orbitals. Losing the s-bonding during sputtering ionization will decrease the stability.

Mass selection is determined by the charge to mass ratio in E-M method. Sometimes a small amount of doubly charged clusters will degrade the resolution of the mass spectrum. Hf has a most complicated mass spectrum due to this. Deposition of smaller clusters may include larger sized cluster with higher charge and the same q/m ratio,

which appear at the same place. The atomic peak may be totally overlapped by the dimer with two charges, for example. By comparing the Raman spectral intensity, we know the dimer component contained in atom deposition could be around 5% for gadolinium or lutetium. The same size clusters with different charge may differ in structure. Deposition of same cluster size with different charge may bring different structure. That is important for clusters larger than dimer, in which molecular geometry is concerned.

Absorption (Scattering Depletion Spectroscopy)

SDS (Scattering Depletion Spectroscopy) works as a substitute for absorption for optically thin matrix samples in which the scattering is relatively intense. For these measurements we employed a deuterium or a Tungsten lamp, dispersed by a (computer controlled) Spex ¼ m monochromater (calibrated with a Hg lamp) and focused onto the matrix sample. A mirror is mounted on a computer controlled stepping motor (Compumotor A5783), which allows the focused light to be scanned (in approximately 12 steps) across the 8 mm wide sample.

The SDS intensity is defined by the ratio of the "reference intensity" to the "signal intensity". The former

corresponds to light scattered from an edge, whereas the latter pertains to that region near the center. The optical density profile of the sample was obtained by recording single beam scattering spectra as a function of lateral position the sample on the substrate. It is generally found that the sample is non uniform, with about twice as much absorption in the center as compared to near an edge. Compared with conventional absorption spectra, using the same signal and reference position but detecting the light transmitted through the sample, the SDS signal is 20~50% more intense. Due to the relatively more flat background of scattering light, SDS should be more sensitive than normal absorption.

In our experience, the SDS signal is related to the thickness of matrix sample. Five to six hours deposition of sample and matrix gas provide suitable thickness for the scattering measurement. Another interesting characteristic is further deposition after 6 hours will not increase the scattering signal any more and the absorption curve vs. the deposition time will become flat. Such saturation may be brought by insufficient interaction of photon and sample caused by thickness.

Besides higher sensitivity, SDS is much more convenient to setup than normal absorption. Fluorescence

spectroscopy, which is also important for spectroscopic identification and fragmentation estimation, can be applied without further optical setting. Another advantage over absorption is the possibility of using a nontransparent substrate such as an Al plate.

There is a broad background in the spectra. This is due to relatively small, but wavelength dependent, difference in scattering and/or collection efficiency in the reference and signal beams. It is not easy to pick absorption peaks out from background if the absorption is too broad. Normally the absorption with less than 50nm width would not be a problem.

The SDS or absorption spectrum is an important indication of the location of resonances. It gives us a clue as to where to excite the sample with a laser. However, not all absorption regions will give high quality resonance Raman spectra. Sometimes the absorption of cluster is overlapped with that of atom. Strong atomic emission or fluorescence from impurities will diminish any dimer spectrum.

Most homonuclear transition metal dimers have been tried in our lab. Fig 2.2a and 2.2b show the SDS spectra of transition metal dimers. Some of them have strong absorption structure. However, there are also some metals

giving good resonance Raman spectra even without obvious absorption. The appearance of resonance Raman is evidence for our assignment to absorption. If we assume the most probable spectroscopic impurity is from fragmented atoms, we can assign our spectra quantitatively by comparison to the deposition of an atom.

Resonance Raman Spectroscopy

An intense light source, normally a laser is applied to excite the sample for high quality resonance Raman spectra. An argon ion laser (Spectra Physics 2045), dye laser (Coherent, 599-02) and Ti-Sapphire laser will cover almost entire range from 360nm to 910nm. Typically, about 50 mW is focused down to an estimated 50μ spot. Plasma lines are removed by dispersing the laser beam with a grating. The Raman spectrum is collected at 90° to the incident light with a Spex 1877E Triplemate Spectrometer (0.6m) and detected by a liquid nitrogen cooled CCD detector (Spex model "Spectrum One") with DM3000R software.

Resonance Raman spectra of metallic cluster are characterized as an overtone peak progression with almost the same interval for the totally symmetric vibrational mode. The intensity increment of resonance over nonresonance Raman is estimated to be 100 times. Although

resonance excitation raises the scattering power of many substances by several orders of magnitude, resonance Raman can not always be observed with ease. The scattered radiation may be abnormally attenuated by simultaneously intensified absorption and possibly concealed by superimposed fluorescence emission. Moreoever, photolysis may not only destroy the sample but also produce unknown products. Those Raman lines with small shift lower than $100cm^{-1}$ are normally hard to detect due to the intense Rayleigh scattering background especially at short wavelength excitation.

Compared to the previous experimental data obtained with a double ¼ m monochromator combined with photo-multiplier tube, the application of a Triplemate Spectrometer and detection of with a CCD increased the precision of our measurement. Furthermore, the experiment duration is greatly shortened and more exploration is possible. This is especially helpful when no obvious absorption character is shown in SDS, as with Rh_3 and Ru_3 trimers.

Raman spectra provide a lot of information on the ground state and low lying excited states, including force constant, anharmonicity, spectroscopic dissociation energy, and geometry information for clusters larger than dimer.

The Raman excitation profile is the relative Raman intensity vs. excitation wavelength. Such relative intensity can be the intensity ratio of Raman line to CaF_2 or the absolute intensity divided by the excitation laser intensity and CCD integration time. The Raman profile is often more sensitive than SDS (absorption), which reveals useful absorption detail. First of all, it provides proof of our absorption assignment. It is also helpful in extracting the dimer absorption shape from the overlap band between dimer absorption and the more intense atomic absorption. Sometimes, fine structure involving vibrations of the electronic state can be achieved clearer than with absorption. For polyatomic metal clusters, when more than one normal mode are of concern, the excitation profile is especially useful. The excitation profile gives not only resolved exhibition of all modes but also information as to symmetry and transition polarizability, which is often a clue to the transition assignment.

Raman Shift Calibration

Raman peak positions in progressions are of interest to us. Normally, the Raman shift is calibrated by using the standard CaF_2 shift at 327.0 cm^{-1} as an internal standard. The previous standard we used, 330cm^{-1}, was based on

experiment of H. Z. Cummins, etc [6]. That data is from single channel detection with PMT. There is a lot of variation for that number under different situations such as temperature. The CCD would never include both Rayleigh scattering and Raman peak within a single scan. The positions of the peaks are mainly determined relative to the CaF_2 line instead of the Rayleigh line in one scan. We always find that the position of the first peak, which is determined relatively by the CaF_2 absolute shift number, is a little higher for expected when linearly fit vibrational state intervals, see Fig 2.3. For this reason, we calibrated our system with a standard line light source and achieved a new number.

The calibration is assurance of the high precision in our reported frequencies. Furthermore, careful frequency calibration is essential especially for determination of the small number for $\omega_e x_e$ and the spectroscopic dissociation energy. The calibration is carried out by using Hg lamp or Neon lamp. The shift, relative position of the CaF_2 line to the laser is deduced by the measurable relative position of a certain Hg line to both of them. This shift number is consistent in the range from visible to IR. The previous work also mentioned that the Raman shift varies with temperature compared to the results at 300K and 77K [6]. In

our temperature dependent calibration, when the temperature is increased, the shift remains constant 327.0cm^{-1} from 16K to around 80K, and then decrease continuously to 324.5cm^{-1} at room temperature, as shown in figure 2.4. The intensity of the CaF_2 line also serves as quantitative standard in excitation profiles.

Due to the recent recalibration of the internal standard Raman line, we checked data published previously for Ni_2, Rh_2, Ru_2 (detection by CCD). Using the new CaF_2 shift, we see the fit has improved the precision (Table 2.1). The calculated D_0 is closer to third law results or theoretical work.

Figure 2.1

SCHEMATIC OF THE METAL CLUSTER DEPOSITION SOURCE

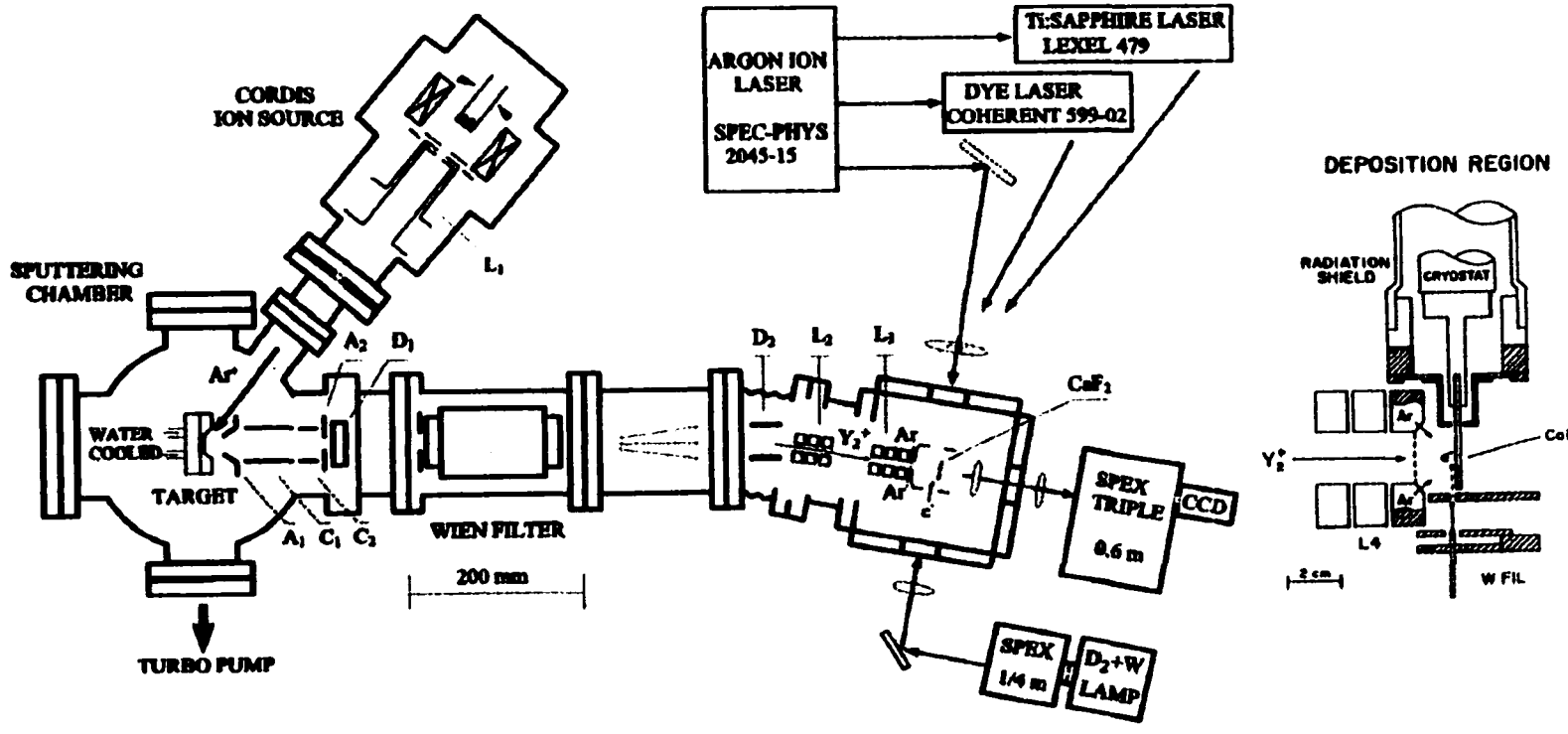

Figure 2.2a

Figure 2.2b

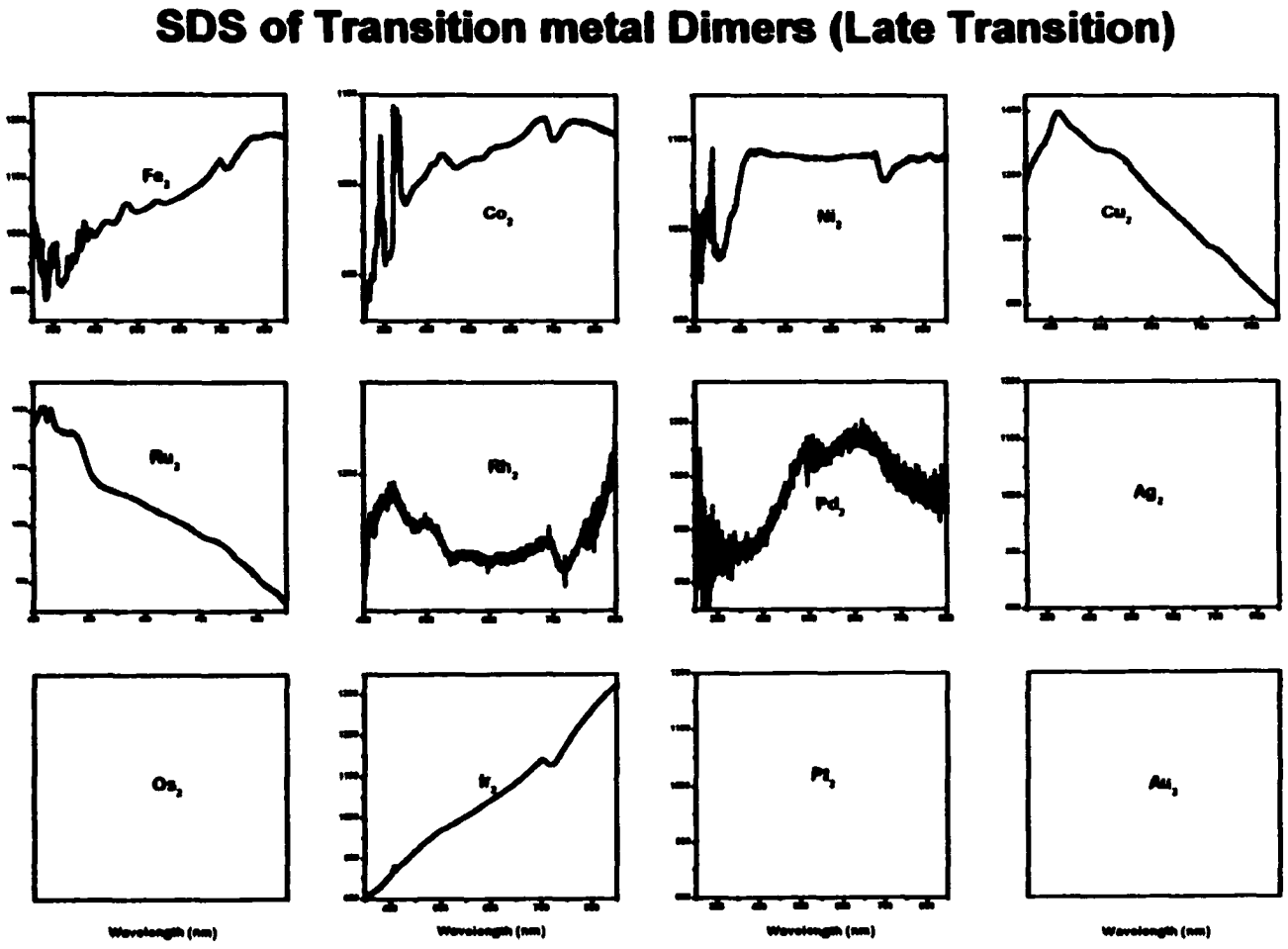

Fig 2.3 Improvement of linearity by new calibration value of CaF_2. 0-2~6 numbers are not affected.

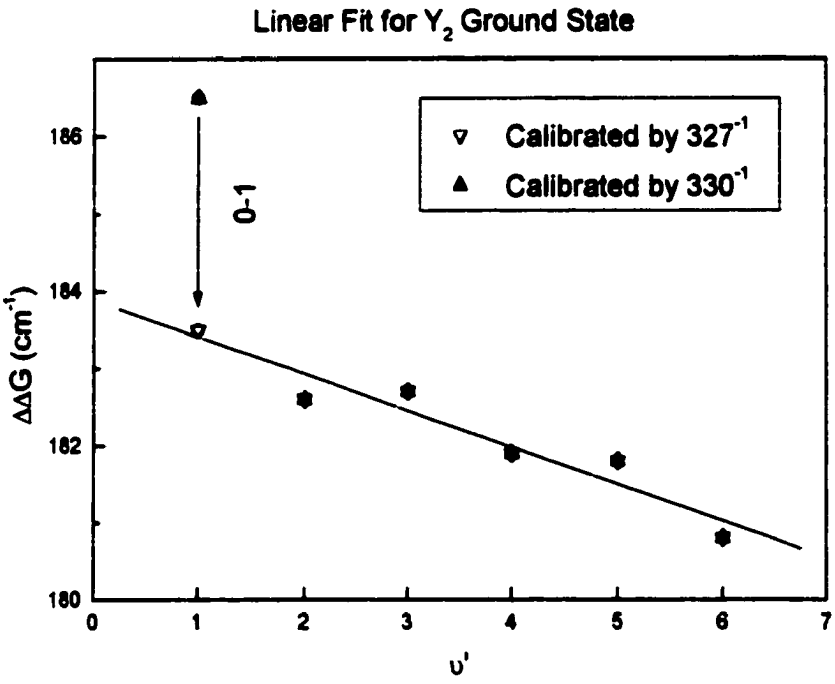

Table 2.1 Comparison of calibration results with new and previous standard of CaF_2.

		ω_e (cm^{-1})	$\omega_e x_e$	D_0 (eV)
Ni_2	Previous	259.2(30)	1.90(70)	1.1(4)
	Calibrated	255.2(11)	1.10(26)	1.8(4)
Rh_2	Previous	283.9(18)	1.83(33)	1.4(3)
	Calibrated	280.6(8)	1.47(15)	1.7(2)
Ru_2	Previous	347.1(9)	1.85(15)	2.0(2)
	Calibrated	344.0(7)	1.46(10)	2.5(2)

Figure 2.4

Temperature dependent property of internal standard CaF_2 Raman Shift.

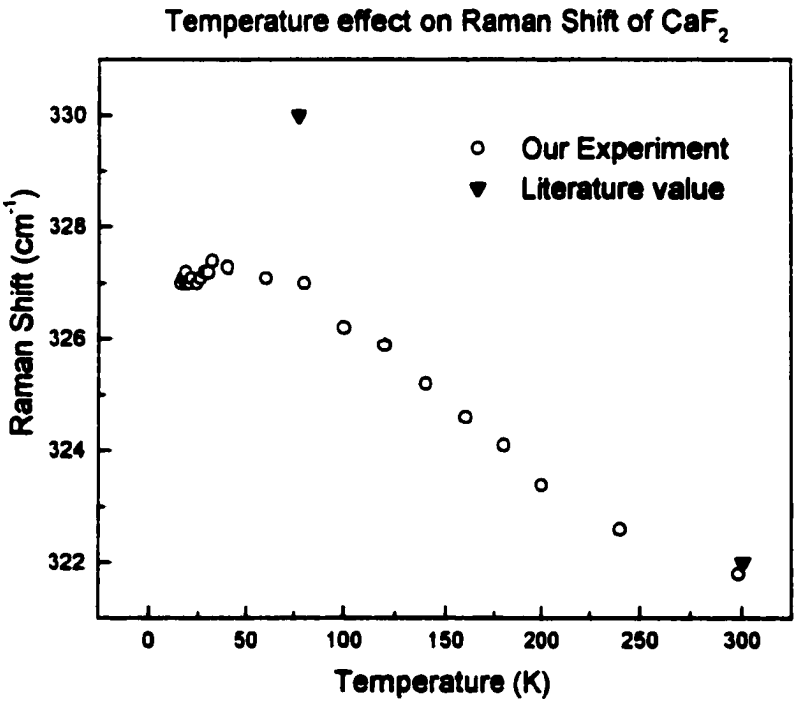

Chapter III. Resonance Raman Theory

Raman spectroscopy is concerned with the phenomenon of the change in frequency of a monochromatic beam of light when it is scattered by molecules. Consider a clear substance irradiated by a monochromatic beam of light. A small fraction will be scattered in directions different from that the incident beam. When this scattered light is analyzed spectroscopically, it is found that most of it has the same frequency as that of the incident beam. This is Rayleigh scattering, the intensity of which is proportional to υ_0^4 and α_0^2, where α_0 denotes the equilibrium value of the polarizability of the molecule.

In addition to Rayleigh scattering at frequency υ_0, the scattered radiation will contains a series of lines spaced symmetrically on either side of the Rayleigh line, at frequency of $\upsilon_0 \pm \upsilon_i$. The frequency shifts, υ_i, referred to as the Raman frequencies, provide key information (rotational, vibrational, and electronic energy)regarding the scattering species. The intensity of Raman bands are, among other factors, proportional to $(\upsilon_0 \pm \upsilon_i)^4$ and $(\partial\alpha/\partial Q_i)_0$ denotes the equilibrium value of the rate of change of α with the normal coordinate Q_i. By the selection rules, only

totally symmetric vibrations of a centrosymmetric molecules like a metal clusters are only Raman active.

However, the Raman effect is very weak, and it is essential for a Raman spectrometer to discriminate the Raman signal from Rayleigh and stray light. This requires high efficient collection optics, a sensitive detector and an intense light source.

For a Raman transition between states g and f, the scattering intensity is

$$I_s = \frac{8\pi\nu_s^4}{9c^4} I_0 \sum_{\rho\sigma} |(\alpha_{\rho\sigma})_{gf}|^2, \qquad (2.1)$$

I_0 is the incident intensity at frequency ν_0, ν_s is the scattered frequency, c is the velocity of light, and $(\alpha_{\rho\sigma})_{gf}$ is the transition polarizability tensor, with incident and scattering polarizations indicated by ρ and σ. With second order perturbation theory, Kramers, Heisenberg[1] and Dirac[2] give the following expression (KHD) for the polarizability

$$(\alpha_{\rho\sigma})_{gf} = \frac{1}{\hbar} \sum_e \left(\frac{\langle f|\mu_\rho|e\rangle\langle e|\mu_\sigma|g\rangle}{\nu_{eg} - \nu_0 + i\Gamma_e} + \frac{\langle f|\mu_\sigma|e\rangle\langle e|\mu_\rho|g\rangle}{\nu_{ef} + \nu_0 + i\Gamma_e} \right) \qquad (2.2)$$

M is pure transition moment and

$$M_e = M_e^0 + (\partial M/\partial Q)^0 Q \ldots\ldots, \qquad (2.3)$$

With the Born-Oppenheimer approximation α can be expressed as a sum of two terms

$$\alpha = A + B, \tag{2.4}$$

$$A = (M_e^0)^2 \frac{1}{\hbar} \sum_e \frac{\langle j|\nu\rangle\langle\nu|i\rangle}{\nu_{\nu i} - \nu_0 + i\Gamma_\nu}, \tag{2.5}$$

$$B = M_e^0 (\partial M/\partial Q)^0 \frac{1}{\hbar} \sum_e \frac{\langle j|Q|\nu\rangle\langle\nu|i\rangle + \langle j|\nu\rangle\langle\nu|Q|i\rangle}{\nu_{\nu i} - \nu_0 + i\Gamma_\nu} \tag{2.6}$$

Term A in (2.6), the Frank-Condon term, is always the leading term and usually the dominant contribution to intensity for resonance spectra. Only totally symmetric modes give non-zero Frank-Condon overlaps. That is the reason we expect a long progressions of totally symmetric overtones and combination bands. Term B is determined by non-totally symmetric modes and is normally a minor term near resonance. Detailed discussion and examples of resonance Raman are available [3].

An alternative way to understand resonance Raman is by time-dependent perturbation theory [4]. When the incident wavelength is approaching the absorption band of molecules, the life time of the so called virtual state is longer. The whole molecule has enough time to adjust itself so that it does not have to go back to its Frank-Condon origin of the ground state. That means the substitution of Rayleigh intensity with Raman intensity. Overtones are now comparable to the fundamental and therefore detectable.

CHAPTER IV. Lanthanide Dimers

Since the first published multiple metal-metal bonding of $[Re_2Cl_8]^{2-}$ was firmly established by Cotton and Harris [1], we know that the metal-metal bonding could have high bond orders. The bond strength is determined by the electron configuration of the molecule, which is from the contribution of s, d orbital. P and f orbitals are generally believed to have less effect on bonding of transitional clusters. Dimer configurations can also be derived from dissociation states of separated atoms. Normally it is believed that the atomic configuration should be promoted to $d^{n+1}s^1$ for better bonding. The second and third row shows a volcano shape and there is a drop at Mn for the first row (Fig 4.1). It exhibits the some bulk properties as with modulii [2] trends in transition metals (Fig 4.2).

The vibrational frequency and force constant of a dimer obtained from resonance Raman spectroscopy are quite valuable in determining bonding. It is extremely reliable data and the precision is within 1 cm^{-1}. In addition, the assignment of dimer and atom absorption characteristics would provide unambiguous information for cluster character studies and aggregation and dissociation mechanisms. With a long progression of overtones in resonance Raman

spectroscopy, we can determine the Morse curve of the ground state or low-lying excited states up to the dissociation extreme. Well-resolved absorption spectra, such as in Re_2, could describe the excited state potential curve. Almost all Spectroscopy theories of diatomic molecules are included in one book by G. Herzberg [3].

The first and most studied group is IB, the coinage group. That is due to the ease of experiment and importance to the theory. The IB group should not be assigned as d-transition elements because of the $d^{10}s^1$ configuration with fully occupied d shell. Only the s orbital participates in bonding which makes a simple single bond in the dimer. It is the relative standard in our Pauling's dimer bond order diagram for each IB metal as a single bond in its row. The advantage of this is that it will include the effect from atomic size, mass, and then relativistic effect within the row. Group IIB is believed to give nonbonding dimers. Group IIIB dimers could be summarized without our recent work. Sc_2, Y_2 and Lu_2 are single bond character. From IVB to VIIB, except for the third row, the d orbital contributes to bonding and the bond strength is increased by further electrons occupying the d-d bonding orbitals. The 4d, 5d orbital relative expansion is responsible for strong d-d bonding, while the 3d orbital is small and not good at

bonding. The VIII group includes three columns and nine elements. Normally those late transition dimers' characteristics are dominated by s-s character. There will be less sharp change in bond order within the row as in early transition elements.

In addition to previous contribution to d-block dimers, we tried to find out what the f-block of lanthanide would be like. Investigation of rare-earth elements was overlooked thirty years ago because these elements are believed to have the same properties and few application are found. However today rare earth elements are widely applied in field of astronomy and medicine. Our work is stimulated by the discovery of astonishingly strong bonding of the lanthanum dimer. Trying to explain this, we find an unusual low promotion energy in favor of bonding for lanthanum. Even though there is still no evidence that an f electron or orbital participates in bonding, we observe that bonding character does change across the lanthanide series. According to our results, the character of the lanthanum dimer obviously does not fit the lanthanide position in the dimer periodical table either in column IIIB or third row. We want to seek out the real representative for lanthanide. Lutetium would be best candidate. In order to know what kind of bonding really

governs f-block dimers, investigation on Ce_2, Pr_2, Nd_2, Gd_2, Tb_2 and Lu_2 were carried out. It is no wonder that f orbital just act as electron reservoir and play no direct role in bonding. However, the f electron shielding could be responsible for promotion energy and indirectly affect bonding. Another surprise is that all lanthanide dimer studied could be divided into two groups of force constants, La_2 like (Ce_2, Pr_2) or Lu_2 like (Nd_2, Gd_2, Tb_2). There is an apparent drop in bonding from Pr to Nd across lanthanide table, instead of a continuous drop parallel to the atomic radii. Bulk properties like modulii (stiffness) or melting point also shows steep change around these two elements. Normally the bonding strength of dimer is parallel to the bulk modulii, as in d block transition for example. An interesting result is the trend in lanthanide goes exactly the opposite way (See Table 4.1 and Fig. 4.3). The stronger dimer elements have the softer bulk modulus. There must be a change of bonding character since the clusters grow in size. The relative equality of energy of 4f, 5d, 6p, 7s orbitals makes the inter-change of configuration as well as spectroscopy of both atom and cluster complicated. Perturbation of low lying states and configuration interaction should be considered in a theoretical analysis.

Fig. 4.1 Bonding Order of Transition Metal Dimers.

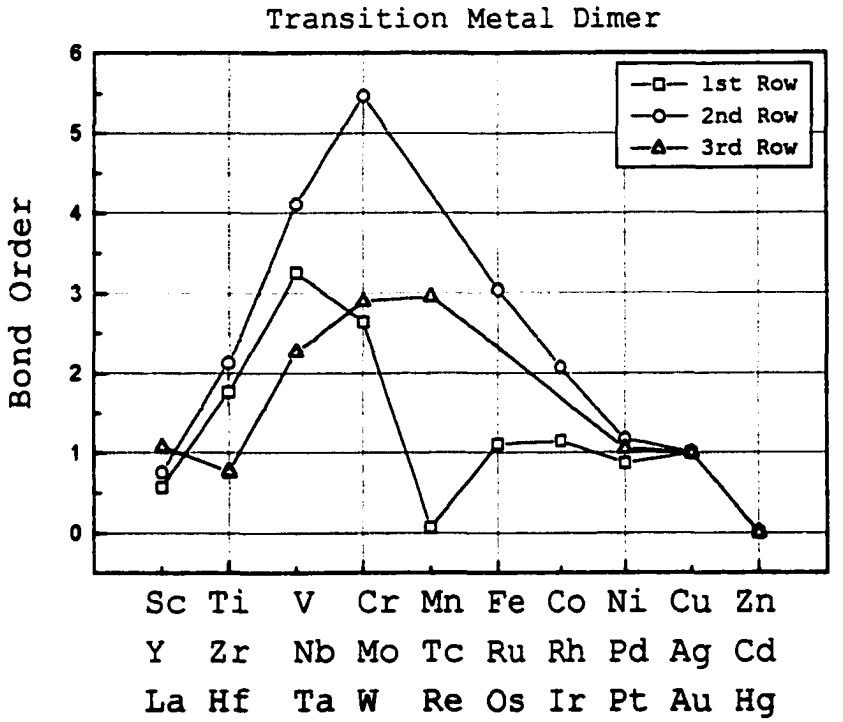

Fig. 4.2 Bulk Modulii Trends of Transition Metals

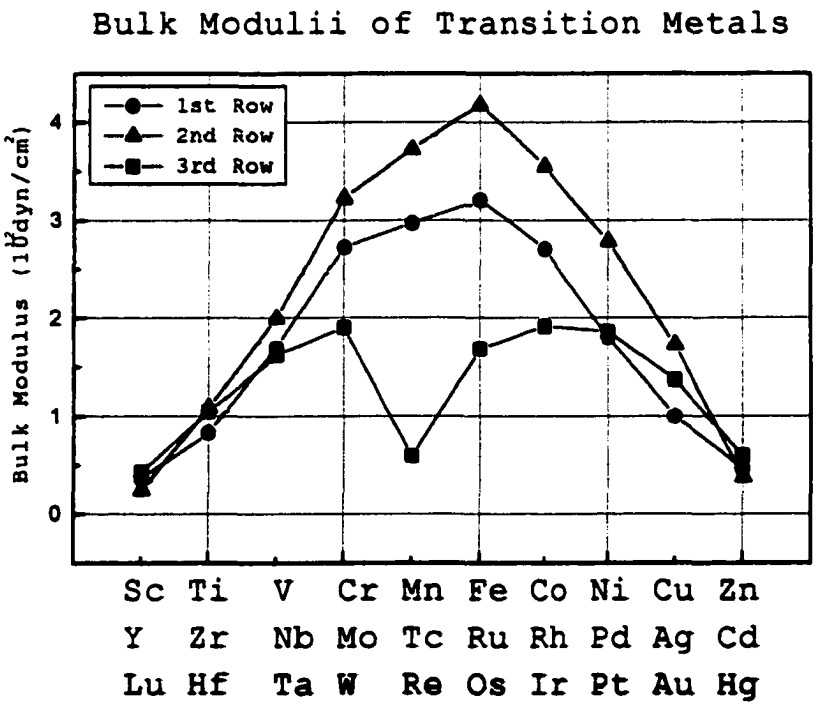

Table 4.1 Force Constant compared to bulk modulii (10^{12}dyne /cm^2) or M. P. (°C) of lanthanide metals.

	La	Ce	Pr	Nd	Gd	Tb	Lu
k_e	2.28	2.48	2.49	0.93	0.89	0.88	0.76
Modulii 10^{12}dyne/cm^2	0.243	0.239	0.306	0.327	0.383	0.399	0.411
M. P.(°C)	920	798	931	1020	1311	1360	1660

Fig. 4.3 Comparison of bulk modulii and dimer force constants of lanthanide metals.

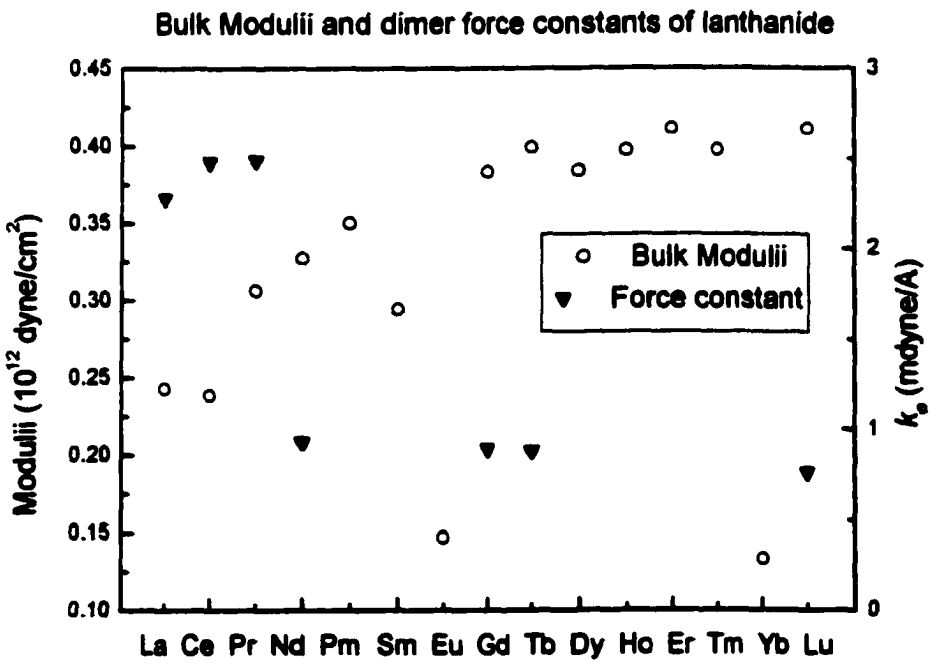

4.1 Spectroscopy of Yttrium Dimers in Argon Matrices

Low Temperature Physics **26**, xxxx (2000), in press

I. INTRODUCTION

In the past two decades, research on transition-metal clusters has attracted a number of theoretical and experimental scientists[1]. It is clear that an understanding of the multiple-metal bonding often observed in the ground states of transition metal dimers depends on accurate determination of crucial structural parameters such as vibrational frequencies, force constants, dissociation energies, etc. Work has been carried out in this regard by this and other laboratories on several second row transition metal dimers (Zr_2[2], Nb_2[3], Mo_2[4], Ru_2[5], Rh_2[6], Pd_2[7], and Ag_2[8]). However, relatively little work has been carried out on the dimer of yttrium. In this paper we report the first matrix isolation optical absorption and resonance Raman spectra of Y_2. Previous work on the atomic spectrum has been reported by Klotzbuecher and Reva[9].

Samples of Y_2 are obtained by mass selection after sputtering a metal target with high energy Ar ions. This ensures discrimination against spectral interference from atoms and higher clusters of Y, as well as various oxides of Y. We observe a weak, broad optical transition near 485nm. Exciting with Ar^+ laser radiation in this region enables us to obtain a sharp resonance Raman spectrum with a long progression of overtones. Spectral analysis gives ω_e =184.4(4) cm^{-1}, with $\omega_e x_e$ = 0.30(3) cm^{-1}, leading to a spectroscopic dissociation energy of D_e = 3.5(4) eV. Comparison of our results with several *ab initio* calculations confirms the assignment of the ground state to be $^1\Sigma_g^+$.

II. EXPERIMENT

The City College of New York (CCNY) metal cluster deposition source has been described in previous publications[2,3,10]. Briefly, an intense (typically 15mA at 25keV) argon ion beam from a CORDIS ion source sputters on a water cooled yttrium target (Alfa, 99.9%) maintained at 300V. Secondary ions are extracted with a modified Colutron model 200-B lens system and then mass selected using a Wien filter (Colutron 600-B) in conjunction with an approximately 175mm free drift distance and a 6.5mm diameter aperture. The mass resolution is 6~7, enough to discriminate against possible oxide contaminants, as well as provide unambiguous filtering and metal clusters or atoms. After mass selection, the ion beam is bent by 10° using two electric plates to eliminate neutrals and then guided and focused to the deposition region by two einzel-like lenses.

Yttrium dimer ions were codeposited with Ar and electrons (generated from a heated tungsten filament) on a polished CaF_2 substrate (~14K). Matrices were grown at ~5μm/hour with an Ar:metal dilution ratio of approximately 10^4: 1. The deposition region was surrounded by a "Faraday Cage" whose potential with respect to the sputtering target controls the kinetic energy (10eV in this experiment) of deposited ions. Ion currents under "soft landing" conditions were approximately: Y^+(250nA), Y_2^+(25nA).

Under similar conditions, we deposited the yttrium atom in an argon matrix. By comparing the intensity of known atomic excitation features in a dimer deposition with

those obtained from deposition of atom under similar conditions, the fragmentation ratio of dimers is estimated to be 10%.

Matrix samples were interrogated *in situ* using both absorption and Raman spectroscopy. As previous described[2,3,10], for the absorption measurements, both deuterium and tungsten lamps were employed as excitation light sources, dispersed by a single 1/4m monochromator, reflected by a plane mirror (controlled by a stepping motor), which allows the light to be scanned across the 8mm wide sample. The absorption measurements were made by collecting the light scattered at 90° to that incident, a technique termed "Scattering Depletion Spectroscopy (SDS)" [3].

After obtaining absorption spectra, the Raman spectra were measured by exciting the sample with appropriate laser wavelength within the absorption region. In this experiment on Y_2, the visible output (457.9nm-514.5nm) of an argon ion laser (Spectra Physics model 2045) was employed. The scattered light was collected at 90^0 and focused into a Triplemate Spectrometer (Spex 1877E, 0.6m). The scattered light was detected with a liquid nitrogen cooled CCD system (Spectrum One + CCD30 + DM3000R Software). The resolution of the detection system for the Y_2 experiment was set about $2cm^{-1}$ (at 500nm). The Raman shifts of Y_2 were calibrated using the CaF_2 (substrate at 16K) line at $327cm^{-1}$.

III. SPECTRA AND ANALYSIS

Figure 4.1.1 shows the scattering depletion spectrum (SDS) of the atom (a), which is essentially the same as Klotzbuecher's result[9], and of the dimer of yttrium (b).

Figure 4.1.2 shows a typical Raman spectrum (excited with 488nm) for Y_2 in argon matrix (14K, dimer content ~75nA-h) and, as an inset, a portion of the absorption spectrum (SDS) of the same sample compared with several excitation profiles.

The SDS shows a broad, weak band centered at 485nm, and closely parallels the excitation profile, which further confirms its assignment to the yttrium dimer.

Resonance Raman spectra of Y_2 were obtained at five different argon ion laser emissions in the visible region (465.5~496.5nm). Up to ten Stokes transitions were observed and the average value of these measurements give the Raman shifts, which are listed in table 4.1.1

Analysis of these data by standard techniques[11] (linear fit of $\Delta G_{v+1/2}$ vs v) gives ω_e =184.4(4) cm^{-1}, with $\omega_e x_e$ = 0.30(3) cm^{-1}, leading to a spectroscopic dissociation energy of D_e = 3.5(4) eV, and the force constant k_e=0.90(1) mdyne/Å. Attempts to obtain higher anharmonic corrections ($\omega_e y_e$) failed to improve the standard deviation, so it may be safely inferred that such corrections are negligible. Our observed vibrational frequency is essentially the same as that of Yang et al.[12] ω_e = 185(2) obtained by ZEKE spectroscopy.

Note that several of the observed Raman lines are accompanied by one or more weaker satellite lines. Since there are no isotopes that need to be considered, it is most likely that they are due to site effects in the Ar matrix. Similar effects have been observed in other dimer spectra[3]. We have used only the most intense line in each group for our analysis.

IV. DISCUSSION

It is of interest to compare our measured value of the force constant k_e for Y_2 with those of other members of the second row transition metal dimers. These are given in table 4.1.2

As can be seen the force constants increase almost linearly from left to right. The ground state atomic configurations are (Y) $5s^24d^1$, (Zr) $5s^24d^2$, (Nb) $5s^14d^4$, (Mo) $5s^14d^5$. However, in transition metals, bonding is usually more favorable if at least one atom has an s^1 configuration, requiring some promotion energy. Thus, considering a configuration $5s^14d^m$ (m=2-5), the force constant is proportional to the number of *d* electrons involved in bonding. (A complementary, nearly linear decline in force constant was observed[5-7] in the series Ru_2, Rh_2, Pd_2 indicating a configuration $5s^14d^m$ (m=7-9)). We can conclude that, at least for the early second row transition metal dimers, each d-electron available for bonding makes a nearly equal additional contribution to the bond order.

Of several previous publications on Y_2 only one is experimental, Verhaegan, Somoes and Drowart[13] determined the bonding energy using the third law analysis of the high temperature Knudsen effusion mass spectrum. Their result was D_0 (Y_2)=1.62±0.22 eV, in sharp disagreement with our spectroscopic value of 3.5±0.4eV. The third law technique suffers from the requirement that ω_e and r_e must be known, as well as the electronic partition function, and the results are often unreliable. However, the spectroscopic technique also has difficulties, in that a Morse potential is assumed to

govern the nuclear motion. In transition metals this assumption is not always even close. This is caused by the fact that, where both s-s and d-d bonding is important, due to their disparate spatial extensions, *d*-orbitals often have considerably different dissociation ranges than *s*-orbitals. The best example of this is the case of Cr_2[14], where serious deviations from a Morse potential are observed and the spectroscopic value is misleading. However, in Y_2 it is most likely that the bond order is small, perhaps near one. Thus, only one electron pair is involved in dissociation, and the above effect of different s and d bonding will not be important. We also have observed regular behavior all the way up to ninth harmonic (n=10). We feel, therefore, that our value for D_e is more likely to be correct.

The remaining work on Y_2 has been theoretical. Walch and Bauschlicher[15] have carried out a complete active-space multiconfiguration-self-consistent field (CAS-MCSCF) calculation followed by configuration-interaction (CI). Their results indicate that the ground state is $^5\Sigma_u^-$ ($5s\sigma_g^2 5s\sigma_u^1 4d\sigma_g^1 4d\pi_{xu}^1 4d\pi_{yu}^1$) which stems from the $5s^2 4d^1 + 5s^1 4d^2$ atomic configurations. A nearby, low-lying state (T_e = 0.87 eV) is the $^1\Sigma_g^+$ ($5s\sigma_g^2 4d\pi_{xu}^2 4d\pi_{yu}^2$) state arising from the $5s^1 4d^2 + 5s^1 4d^2$ configurations. In similar calculations in Sc_2 this latter state lies considerably higher than that in Y_2 which indicates larger contributions of *d*-electron bonding in the second row. Dai and Balasubramanian[16] have carried out similar complete active space self consistent field (CASSCF) calculations followed by multi-reference configuration interaction (MRSDCI) in which both single and double excitations are considered. Up to 2.6 million configurations are included in this calculation. Their results are quite similar to those of Walch and Bauschlicher (see table 4.1.3). Comparison of the SCF calculations both with and without

CI contributions show that increasing CI lowers the relative energy of the higher state considerably (to Te=0.55eV). In conjunction with the lack of observable ESR spectrum[17], Dai and Balasubramanian conclude that the $^1\Sigma_g^+$ state is most likely the ground state. Our Raman results (see table 4.1.3) are consistent with this conclusion. The experimental value for ω_e of 184.4 cm^{-1} is quite close to that of 180cm^{-1} in the CASSCF+MRSDCI calculation of Dai and Balasubramanian for the $^1\Sigma_g^+$ state. Similarly our D_e=3.5(4)eV compares favorably with their value of 3.09 eV for the same state.

The theoretical results are listed and compared with this work in table 4.1.3.

Due to the rather large calculated differences in r_e for the $^5\Sigma_u^-$ and $^1\Sigma_g^+$ states, the determination of an accurate experimental value for r_e would be helpful to determine the nature of the ground state. Badger's[18] rule may be employed here on the fourth row metal diatomic molecules following Weisshaar's results[19] on the third row metal elements. Unfortunately, only a very few experimental data (listed in table 4.1.4) have been reported until now, especially of the bond length r_e. The normal form of Badger's rule has the format: $k_e (r_e - d_{ij})^3 = C$, where d_{ij} is a constant that is different depending one the row number of the periodical table in which each atom resides and C may be taken as the same for all molecules (C=1.86mdyn$Å^2$ if k_e is in mdyn/Å and r_e , d_{ij} in Å).However, it is found that allowing C to vary with periodic table row gives considerably better fits[19,20]. The C value in reference 19 varies from 0.53 (3,4) to 5.83 (H,3T) according to the rows of the periodic table.

In order to determine the constant d_{44} and C of the forth row metal diatomic molecules, a linear least squares fit was employed to five pairs of experimentally determined ω_e, r_e (see table 4.1.4 and Fig. 4.1.3), leading to d_{44}= 1.09Å and C=3.41mdyn

Å^2 (linear correlation coefficient is 0.998). Using our experimental result ω_e=184.4cm^{-1}, the bond length of Y_2 may be obtained as an interpolated point on this graph. It is found to be 2.65Å, which is only slightly shorter than Dai's result (r_e=2.76 Å) for the $^1\Sigma_g^+$ state. For the $^5\Sigma_u^-$ state, his result is 3.03Å. This lends additional support to the presumption that $^1\Sigma_g^+$ is very likely the ground state.

Table 4.1.1 Raman frequency shifts (cm^{-1}) for Yttrium dimers in argon matrices

v"	1	2	3	4	5	6	7	8	9	10
Raman Shift (cm^{-1})	183.5	366.1	548.8	730.7	912.5	1093.3	12736	1454.3	1632.3	1810.1
Std.Dev.	0.6	0.4	0.7	0.7	0.7	0.7	0.4	0.6	1.0	1.3

Table 4.1.2 Ground state vibrational frequencies (cm^{-1}) & force constants(mdyne/ Å) for several second row transition metal dimers.

	Y_2 (this work)	Zr_2 (2)	Nb_2 (3)	Mo_2 (4)
ω_e (cm^{-1})	184.4	305.7	420.5	477.1
k_e (mdyne/Å)	0.90	2.51	4.84	6.43

Table 4.1.3 Comparison of theoretical and thermodynamic results for low state parameters of Y_2 with spectroscopic data (this work)

Authors (Ref)	Method	Low state	r_e (Å)	ω_e (cm^{-1})	D_e or D_0 (eV)	T_e (eV)
D.G. Dai and K.Balasubra-Manian (15)	CASSCF + MRSDCI	$^5\Sigma_u^-$	3.03	172	2.56	0.0
		$^1\Sigma_g^+$	2.76	180	3.09	0.55
S.P.Walch and C.W.Bauschlicher-Jr.(14)	CI	$^5\Sigma_u^-$	3.03	171	2.44	0.00
	CI	$^1\Sigma_g^+$	2.74	206	2.93	0.87
	CASSCF	$^1\Sigma_g^+$	2.73	205	1.74	
G.Verhaegan, S.Somoes, and J.Drowart (12)					1.62±0.22	
This work	Isolated matrix			184.4±0.4	3.5±0.4	

Table 4.1.4 Experiment data of the third row metal diatomic molecules

Mol.	State	ω_e (cm^{-1})	r_e (Å)	$k_e^{-1/3}$ (mdyn/ Å)$^{-1/3}$	Ref
Mo_2	$X^1\Sigma_g^+$	477.1	1.938	0.537	(21)
Mo_2	$A^1\Sigma_u^+$	449	1.937	0.560	(21)
Ag_2	$X(O_g^+)\ ^1\Sigma_g^+$	192.4	2.531	0.949	(22,1)
Ag_2	$A(O_u^+)\ ^1\Sigma_u^+$	155.3	2.655	1.095	(22,1)
Sr_2	$B^1\Pi_u$	80.4	3.85	1.816	(23)

REFERENCES

[1] Morse, M. D. *Chem. Rev.* **86**, 1049 (1986).

[2] Hu, Z.; Zhou, Q.; Lombardi, J.R.; Lindsay, D.M. *In Spectroscopy of Mass-selected Zirconium Dimers in Argon, in Physics and Chemistry of Finite Systems: from clusters to Crystals, edited by P.Jena, S.N.Kahana, and B.K.Rao (Kluwer Academic, Dordrecht, 1992).*

[3] Hu, Z.; Shen, B.; Deosaran, S.; Lombardi, J.R.; Lindsay, D.M.; Harbich, W. *Proc. SPIE* **1599**, 65 (1991).

[4] Efremov,Y.M.; Samoilova,.A.N.; Kozhukhovsky, V.B.; Gurvich, L.V. *J. Mol. Spectrosc.* **73**, 430 (1978).

[5] Wang,.H.; Liu,Y.; Haouri, H.; Craig,R.; Lombardi, J.R.; Lindsay, D.M. *J.Chem.Phys*, **106**, 6534, (1997).

[6] Wang, H.; Haouri,H.; Craig,R.; Liu,Y; Lombardi, J.R.;.Lindsay, .D.M. *J.Chem.Phys*, **106**, 2101 (1997).

[7] Ho,.J.; Ervin, K.M.; Polak, K.L.; Gilles, M.K.; .Lineberger, W.C. *J.Chem.Phys*, **95**, 4845, (1991).

[8] Huber, K.P.;.Herzberg, G. *Constants of Diatomic Molecules* (Van Norstrand, New York, 1979).

[9] Klotzbucher, E.W. and Reva, I.D. Poster entitled "Thermal and Photoinduced Reactions of Yttrium Atoms in Inert and Reactive Matrices" presented at the XVII IUPAC Symposium on Photochemistry (Barcelona, Spain, 19.-24. July 1998)

[10] Hu,Z.; Shen, B.; Deosaran,S.; Lombardi, J.R.; Lindsay, D.M.; Harbich,W. *J.Chem.Phys*, **95**, 2206 (1991).

[11] Herzberg, G. *Molecular Spectra and Molecular Structure, I. Spectra of Diatomic Molecules*, D.Van Nostrand Company, Inc. New York, (1950).

[12] Yang,D.S.,Simard,B.,Hackett,P.A.,Breces,A.,Zgierski,M.Z., *International Journal of Mass Spectrometry And Ion Processes.* **159**, 65-74 (1996)

[13] Verhaegan, G.; Somoes,S.; Drowart,J. *J.Chem.Phys.* **40**, 239 (1964).

[14] Casey,S.M.; Leopold,D.G. *J.Phys.Chem*, **97**, 816 (1993).

[15] Walch, S.P.; Bauschlicher, C.W., Jr. In *Comparison of ab Initio Quantum Chemistry with Experimentfor Small Molecules*; R.J.Bartlett., Ed.; D.Reidel: Dordrecht, p39 (1985).

[16] Dai, D.G.; Balasubramanian, K. *J.Chem.Phys.*, **98**, 7098 (1993).

[17] Knight, L.B., Jr.; Woodward, R.W.; Van Zee, R.J.; Weltner,W.,Jr. *J.Chem.Phys.* **79**, 5820 (1983).

[18] Badger, R.M. *J.Chem.Phys.* **2**, 128(1934); **3**, 710(1935)

[19] Weisshaar, J.C. *J.Chem.Phys.* **90**(3), 1429(1989)

[20] Herschbach, .D.R., Laurie, V.W., *J.Chem.Phys.* 35(2), 458, (1961)

[21] Hopkins,J.B.;Langridge-Smith,P.R.R; Morse,M.D.;Smalley,R.E. *J.Chem.Phys.* ,**78** 1627 (1983)

[22] Simard, B.;Hackett, P.A. Chem.Phys.Lett. **186** (4,5) (1991)

[23] Bordas, C.; Broyer,M.;Chevaleyre,J.;Dugourd,Ph. *Chem.Phys.Lett.* **197**(6),562 (1992)

Figure 4.1.1 Scattering depletion spectra of atomic (a) and diatomic yttrium (b) in argon matrices. The dimer spectrum (b) contains an additional band at 485nm, which is attributed to the dimer.

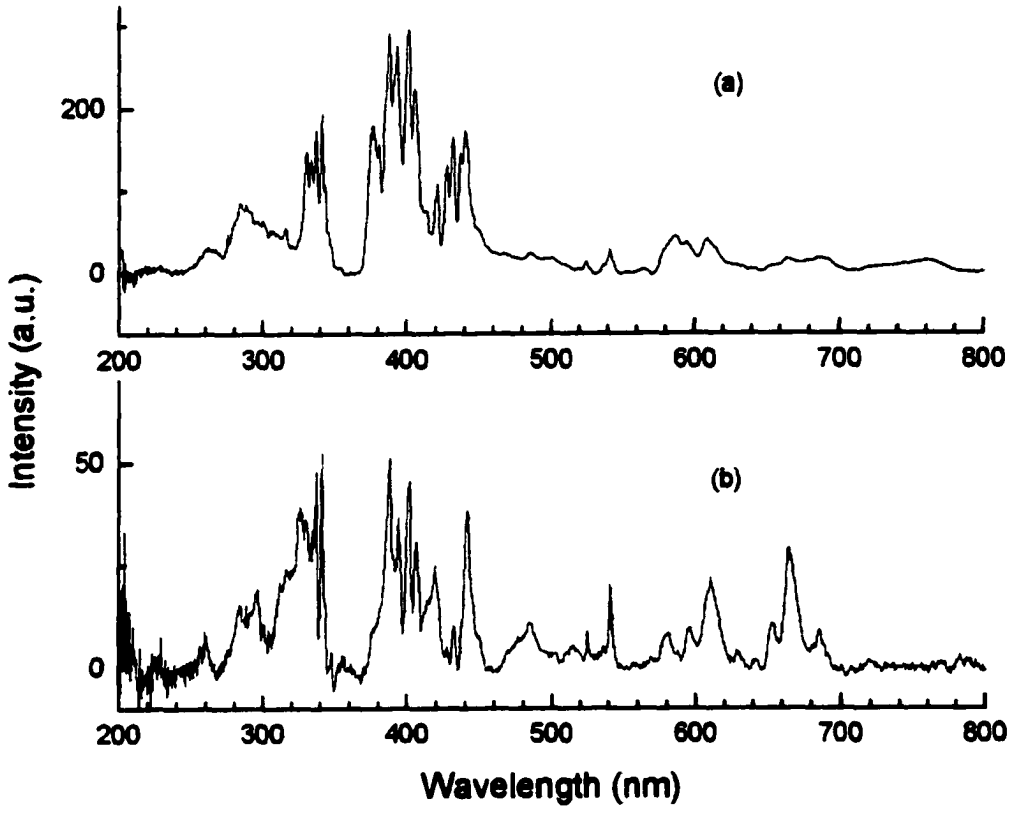

Figure 4.1.2 Resonance Raman and absorption (inset, SDS compared with excitation profile excited with 488nm) for yttrium dimer in an argon matrix.

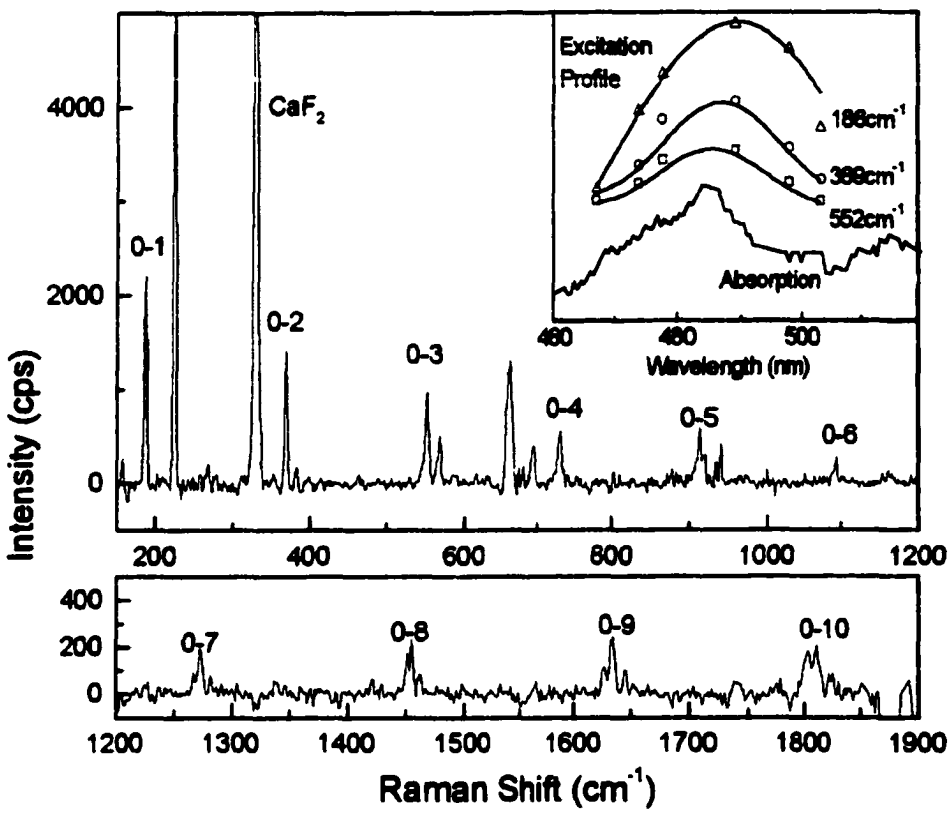

Figure 4.1.3 Badger's rule plot of $k_e^{-1/3}$ vs r_e for metal diatomic molecules from the fourth row of the periodic table.

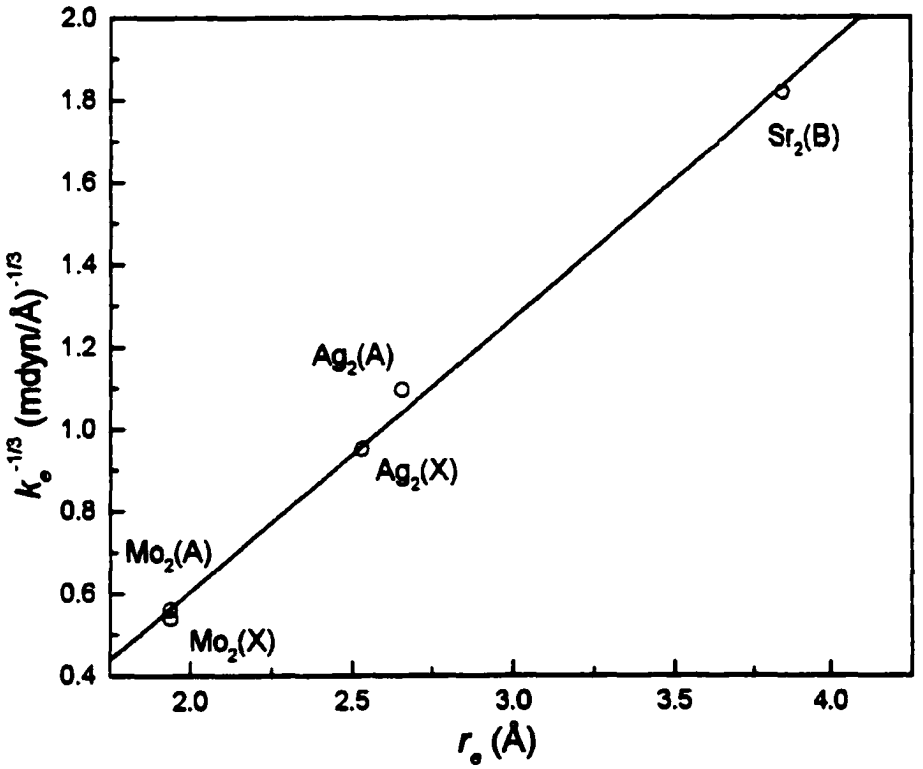

4.2 Absorption, Resonance Raman and Raman Excitation Spectra of Lanthanum Dimers in Argon Matrices

Chem. Phys. to be published

I. INTRODUCTION

Having reported the result of measurements of Raman and absorption spectra of numerous transition metal dimers, (including Ni_2, [1] Ru_2, [2] Rh_2, [3] etc.), we have recently concentrated our studies on the 3B group transition metal dimers: yttrium [4] and lanthanum dimers. It is interesting to study the lanthanum dimers not only because they have seldom been investigated before, [5] but also due to the wide interest in *5d* orbital bonding properties. Lanthanum dimer also provides the opportunity to examine the effect of *4f* orbitals on neighboring dimer bonding.

Very few experimental and theoretical results are available for La_2.[5] The only credible experimental datum on La_2 was obtained by Verhaegen *et al.* [6] by high-temperature Knudsen effusion mass spectrometry in 1963. The absolute entropy method was used to determine $D_0^\circ(La_2) = 2.50 \pm 0.22$ eV. The only other piece of information available about La_2 is the failure of Knight *et al.* [7] to observe an ESR spectrum attributable to La_2. Dolg, Stoll and Preuss [8] have carried out calculations for La_2 using SCF as well as configuration interaction calculations including all single and double substitutions (CISD). All results were approximately corrected for size-consistency errors (+ SCC) using the Langhoff-Davidson formula. They considered 13 low-lying electronic

states as possibilities for the ground state. Bond lengths r_e (Å), vibrational constants ω_e (cm^{-1}) and term energies T_e (eV) were derived from their calculations.

In this paper we report the observation of resonance Raman spectra and the absorption (scattering depletion) spectrum of La_2 in argon matrices. From the Raman spectrum, we measured the Stokes lines at Raman shifts of 234.5 (5) cm^{-1},466.4 (6) cm^{-1}, 696.1 (9) cm^{-1}, and 925.1 (7) cm^{-1}. These data give $\omega_e = 236.0 \pm 0.8$ cm^{-1} with $\omega_e x_e = 0.9 \pm 0.2$ cm^{-1}. The resulting spectroscopic dissociation energy is $D_e = 1.8(3)$ eV.

II. EXPERIMENT

The CCNY cluster deposition source has been described in detail elsewhere. [9] Briefly, an intense (typically 15 mA at 25 keV) argon ion beam from a CORDIS ion source sputters lanthanum cluster ions from a water cooled, lanthanum target (Alfa Aesar 99.9 % (REO)) maintained at about 300 V. Secondary ions were extracted with a modified Colutron model 200-B lens system and then mass-selected using a Wien filter (Colutron 600-B) in conjunction with an approximately 175 mm long drift space and a 6.5 mm diameter aperture. After mass separation, the ion beam is bent by 10° (in order to eliminate neutral sputtered products) and then guided to the deposition region by two electrostatic lenses. Lanthanum dimer (or atomic) ions were then codeposited with argon gas and electrons onto CaF_2 substrate held at 14 K. Ion currents under "soft landing" conditions could be measured on a Faraday plate in the deposition region and were approximately: La^+ (55 nA), La_2^+ (30 nA), La_3^+ (8 nA). Prior to deposition, the selected ions were simultaneously slowed to 10 eV by a surrounding "Faraday cage". Matrices

were grown at about 5-7 μ/h with an Ar : metal ratio of approximately 10^4:1. By comparing the intensities of known atomic excitation features in a dimer deposition with those obtained from depositions of the atom under similar conditions, the dimer fragmentation is estimated to be about 15%.

Matrix samples were interrogated *in situ* using both absorption and Raman spectroscopy. As previously described, the absorption measurements were made by collecting the light at 90° to that incident, a technique we term "Scattering Depletion Spectroscopy" (SDS). Raman spectra were recorded using the visible output of an argon ion laser (Spectra Physics model 2045), and also in the 545nm~575nm region using a dye laser (Rhodamine110). Scattered light was collected at 90° with a Spex 1877E Triplemate Spectrometer (0.6 m) and detected by a liquid nitrogen cooled CCD detector (Spex model "Spectrum One") with DM3000R software.

III. SPECTRA AND ANALYSIS

The insert in Fig. 4.2.1 shows the "scattering depletion" (absorption) spectrum of La_2, which consists two broad transitions centered at 490 nm and 540 nm. No other features attributable to La_2 were observed. The spectrum was obtained following a 3.5 hour deposition of La_2^+ (80 nA-h) at a deposition energy of 10 eV. The broken lines in this insert are Raman excitation profiles obtained by dividing the Raman intensity by the laser power and corrected for the ν^4 dependence of scattering intensity. The remainder of Fig. 4.2.1 shows the resonance Raman spectrum of La_2 when excited at 501.7 nm. A line due to the CaF_2 (at 327 cm^{-1}) substrate is also in evidence. The spectra we obtained by

four exciting Argon CW laser lines (488.0 nm, 496.5 nm, 501.7 nm, 514.5 nm) consist of a single progression of almost equally spaced lines. Each member of the progression can be seen to consist of a closely spaced triplet. The Raman spectrum may be assigned to the first through fourth Stokes transitions of the lanthanum dimer. The observed Raman wavenumbers are listed in table 4.2.1. Some Raman transitions were obscured by very intense atomic fluorescence features at other argon laser CW lines. Since there is no expected isotope effect, the three Raman lines in each member of the progression indicates a "site effect" of dimer molecules in argon matrices. A similar but less characteristic "site effect" spectrum was obtained in previous studies of niobium dimers. [10] We also recorded the spectrum while annealing the sample in steps of temperature from 16 K to 40 K (see Fig. 4.2.2). The annealing was controlled by a Scientific Instruments model 5500 temperature controller. In each set of Raman transition, the middle of the three lines clearly seen in the 16 K spectrum, disappears when temperature exceeds 20 K while the other two lines remain until the temperature reaches 32 K. These features remain until the matrix evaporates at temperatures higher than 36K. From the annealing spectrum we see there are most likely two stable sites with slightly different potential energy at low temperatures for lanthanum dimers in the matrix. The vibrational constants, obtained by analysis of the resonance Raman spectrum are $\omega_e = 236.0\ (8)\ cm^{-1}$ with $\omega_e x_e = 0.9(2)\ cm^{-1}$ and $D_e = 1.8(3)\ eV$.

IV. DISCUSSION

The observed vibrational wavenumber for La_2 leads to an experimental force constant of k_e=2.28(1) mdyne/Å. The corresponding values for Sc_2 [11] and Y_2 [4] are 0.756 and 0.90 mdyne/Å respectively. This trend is in marked contrast to the tendency of the early third row transition metal dimer force constants to decrease in comparison to the corresponding first and second row dimers. A good example of this effect shows readily in the adjacent column: Ti_2 (2.35 mdyne/Å), Zr_2 (2.511 mdyne/Å) and Hf_2 (1.63 mdyne/Å). (For a more complete chart of transition metal dimer force constants [14], or refer to url: http://www.sci.ccny.cuny.edu/~lombardi/). The same anomaly is apparent if we compare force constants along the same row. In the first and second row of transition metal dimers the group 3B force constants are lower than those of the adjacent 4B, 5B and 6B force constants. For La_2 in the third row, the force constant is higher than that of Hf_2. This anomaly is most likely due to the increased bonding afforded by the relatively low promotion energy for La. The ground states of Sc, Y, La and Lu all have a d^1s^2 configuration leading to a ^2D ground state. All have a nearby d^2s^1 configuration (^4F state) which is much more favorable for bonding. The La ^2D-^4F promotion energy (0.36 eV) is much lower than that of Lu (2.33 eV) which itself is much more similar to that of Hf ^3F-^5F ($5d^26s^2$-$5d^36s^1$ 1.94 eV). We thus expect La_2 to exhibit stronger bonding than either Y_2, Lu_2 or Hf_2.

Earlier work on La_2 included an empirical estimate of the vibrational frequency by Goodfriend [12]. He predicted an ω_e of 82.1 cm^{-1}. His results are used in confirmation of an earlier emission study by Carette and Blondeau [13] in which the value of ω_e = 76.9 cm^{-1} was obtained. This was reported despite the comment by Pearse and Gaydon [14] that the

experimental result was unconvincing". Among other things, the unreliability of this experiment is due to the lack of ability to establish a clear spectral origin in the emission spectrum. On the other hand, the theoretical estimate by Goodfriend is flawed by neglecting to account for sharp differences in promotion energy say between La and Lu.

The only other work on La_2 is a calculation by Dolg, Stoll and Pruess [8]. They carry out a quasi-relativistic *ab initio* study of lanthanide elements using pseudopotentials to account for relativistic effects. In all cases fixed integral $4f$ occupation numbers were used. They predicted two low-lying states for La_2. The lowest is a $^5\Sigma_u^+$ $(\sigma_g^2\sigma_u^1\sigma_g^1\pi_u^2)$, with r_e=3.247 Å, and ω_e=130 cm^{-1}. The first excited state lies only 0.11eV higher. This is $^1\Sigma_g^+$ $(\sigma_g^2\pi_u^4)$ with r_e=2.830 Å, and ω_e=167 cm^{-1}. Lack of observation of an ESR spectrum [7] is an indication that most likely the singlet state is indeed the ground state. Our observed force constant would also tend to support the singlet state as the ground state, although both calculated states display wavenumbers considerably lower than that observed.

Note that the observed decrease in force constant for third row dimers is contrary to what would be expected by considering the "Lanthanide contraction". As electrons are added to the f shell, the ionic radius of the lanthanide is reduced due to the inability of additional f electrons to effectively shield outer electrons from the increasing nuclear charge. If this were the only effect, we would expect Hf_2 to have a shorter bond length and higher force constant than Zr_2, the opposite of the above observations. However, taking account of the proper promotion energy effects we might expect Lu_2 to be more comparable to Hf_2 than La_2. Lu has configuration $4f^{14}5d6s^2$ and Hf has just one more d electron. Dolg, Stoll and Preuss [8] calculate a $^1\Sigma_g^+$ $(\sigma_g^2\sigma_u^2\sigma_g^2)$ ground state for Lu_2 with

r_e=3.78 Å and ω_e=74 cm^{-1}. The much weaker vibrational wavenumber, corresponding to a bond order near 1, is in sharp contrast to the likely bond order of 2-3 for the lowest calculated states of La_2. The magnitude of our experimental force constant is also evidence of bond order higher than one in La_2.

Table 4.2.1 Raman shifts (cm^{-1}) of dilanthanum in an argon matrix. Each line in the progression is composed of a triplet, most likely due to matrix sites. Each reported wavenumber is an average of 9 measurements; the standard deviation is in parentheses. The reported values for ω_e and $\omega_e x_e$ were determined using the data of site a, which was shown by annealing (Fig. 4.2.2) to be the most stable site.

υ''	1	2	3	4
Site a	234.5 (5)	466.4 (6)	696.1 (9)	925.1 (7)
Site b	237.6 (7)	471.9 (6)	704.6 (8)	936.4 (4)
Site c	241.7 (7)	479.2 (4)	715.9 (7)	951.1 (5)

REFERENCE

[1] Wang, H., Haouari, H., Craig, R., Lombardi, J.R., and Lindsay, D.M., J.Chem.Phys., **104**, 3420 (1996).

[2] Wang, H., Liu, Y., Craig, R., Haouari, H., Lombardi, J.R., and Lindsay, D.M., J.Chem.Phys., **106**, 2101 (1997).

[3] Wang, H., Liu, Y., Craig, R., Haouari, H., Lombardi, J.R., and Lindsay, D.M. J.Chem.Phys., **106**, 6534 (1997).

[4] Fang, L., Liu, Y., Chen, X., Shen, X., Lombardi, J.R., and Lindsay, D.M., Low Temperature Physics. **26**, xxxx, (2000) in press.

[5] Morse, M.D., Chem. Rev., 1986, Vol. **86**, 1078.

[6] Verhaegen, G., Smoes, S., Drowart, J., J.Chem. Phys. **40**, 239 (1964).

[7] Knight, L.B., Jr, Woodward, R. W., Van Zee, R. J., Weltner, W., Jr., J. Chem. Phys., **79**, 5820 (1983).

[8] Dolg, M., Stoll, H., and Preuss, H., J. Mol. Struct. (Theochem) 277, 239-249 (1992).

[9] Hu, Z., Shen, B., Lombardi, J.R., and Lindsay, D.M., J. Chem. Phys. **96**, 8757 (1992).

[10] Hu, Z., Shen, B., Zhou, Q., Deosaran, S., Lindsay, D.M. and Lombardi, J.R., SPIE Vol. 1599, Recent Advances in the Use of Light in Physics, Chemistry, Engineering and Medicine, **65** (1991).

[11] Walch, S.P., Bauschlicher, C.W., In *Comparison of ab initio Quantum Chemistry with Experiment for Small Molecules*. Ed.by Barlett,R.J (Reidel, Boston, 1985)

[12] Goodfriend, P.L., Spectrochimica Acta, Vol. 40A, No. 3, pp. 283-285.

[13] Carette, P., Blondeau, J., C. R. Acad. Sc. Paris, t. 269, 16-18 (7 juillet 1969).

[14] Pearse, R.W.B., Gaydon, A.G., *The Identification of Molecular Spectra*, 4th Ed. Chapman and Hall, London (1976).

Figure 4.2.1 Raman spectra of dilanthanum in an argon matrix at λ_{ex} = 501.7 nm. Insert: Scattered Depletion Spectrum and Raman excitation profile using n=1 transition at 234.5cm^{-1} .

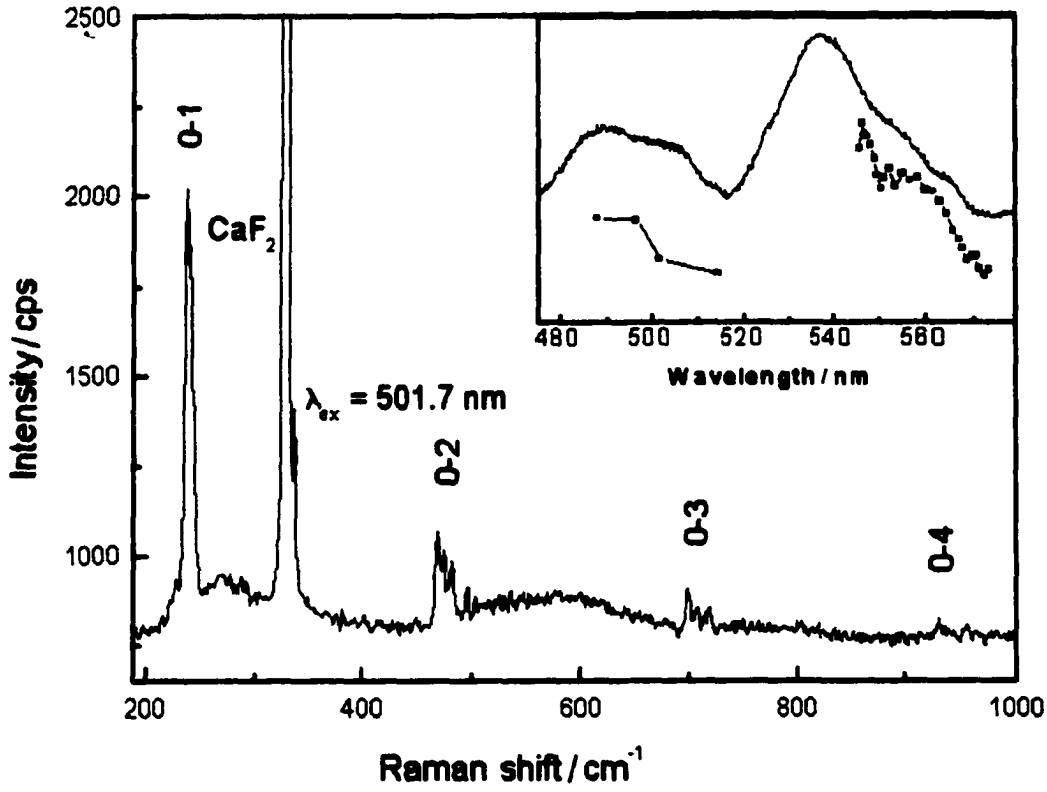

Figure 4.2.2 Raman spectrum of lanthanum dimers during the annealing of argon matrices.

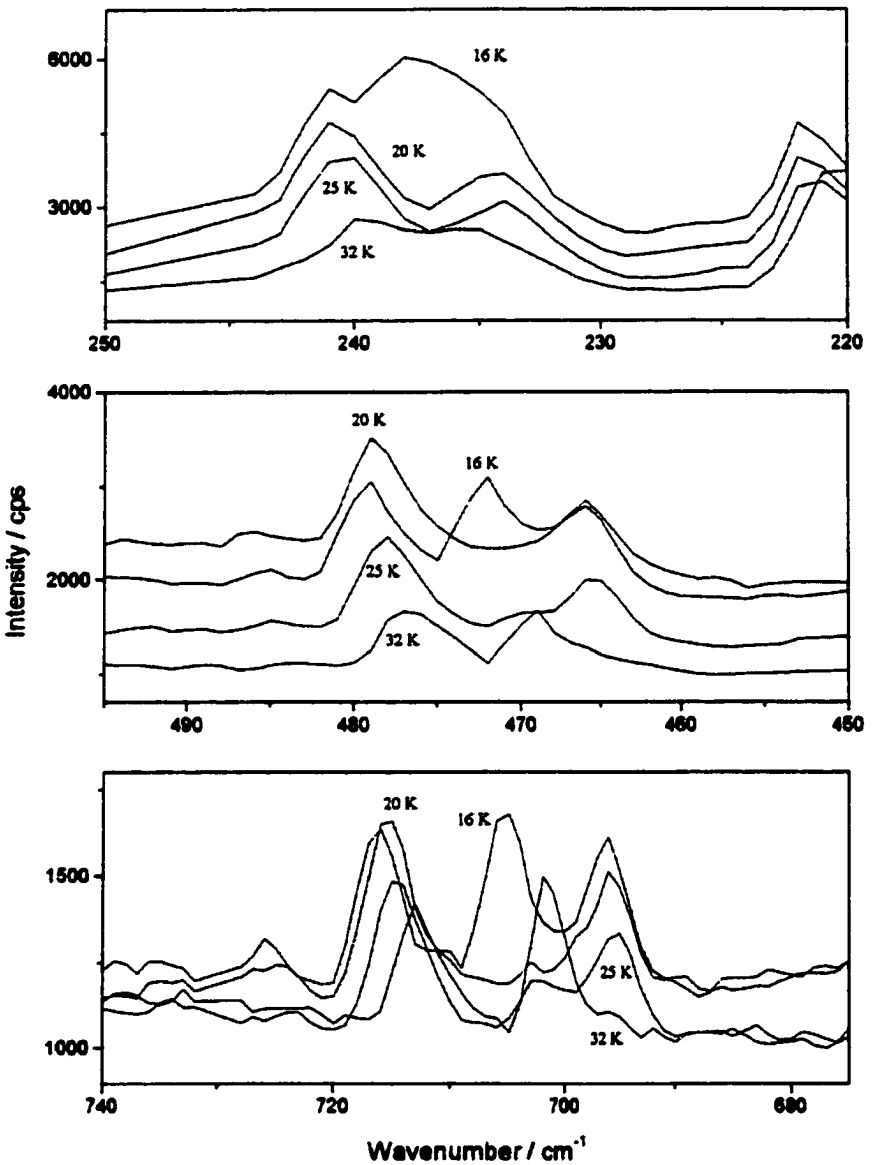

4.3 Spectroscopy of mass-selected gadolinium dimers in argon matrices

X. Chen, L. Fang, X. Shen and J. R. Lombardi

J. Chem. Phys. **112**, 9780 (2000)

I. INTRODUCTION

In a remarkable experiment on the dimer of gadolinium, Van Zee, Li and Weltner[1] showed that the observed ESR spectrum could only be fit using an $S = 9$ spin Hamiltonian. This result led to the assignment of the ground state to be $^{19}\Sigma$, the highest spin diatomic molecule ever observed. The implication is that there are 18 unpaired spins, which can only be possible if the fourteen inner shell $4f$ electrons are ferromagnetically coupled.

An *ab initio* calculation by Dolg, Stoll and Preuss [2] included a set of quasi-relativistic energy adjusted pseudopotentials for the core electrons including the $4f$ shell. They found the dimer ground state to be a $^5\Sigma_u^-$ state arising from the configuration $(4f)^7(4f)^7\sigma_g^2\sigma_u^1\sigma_g^1\pi_u^2$. Possible higher spin states were not considered since there were not sufficient valence electrons included in their calculations. More recent calculations with the inclusion of $4f$ shell in the valence space were carried out by Dolg, Liu and Kalvoda. [3] Both density functional and *ab initio* pseudopotential calculations agree on a $^{19}\Sigma_u^-$ ground state, which is about 1.3 eV lower in energy than the $^5\Sigma_u^-$ state. Although the above configuration indicates a formal bond order of 2, their estimated vibrational frequency of 135 ± 15 cm^{-1} is indicative of a somewhat weaker bond. Kant and Lin [4] obtained a thermodynamic value for the dimer dissociation energy ($D_e = 1.78 \pm 0.34$ eV) using third law methods.

In this paper we report the observation of resonance Raman spectra, the absorption ("scattering depletion") spectrum and the Raman excitation profile of mass selected Gd_2 in argon matrices. From the absorption spectrum, two optical transitions in the 570-660 nm region were observed. Since our samples are optically thin, Raman excitation profiles often provide higher sensitivity, which enabled us to observe transitions to several excited electronic states. The Raman data give $\omega_e = 138.7 \pm 0.4$ cm^{-1} with $\omega_e x_e = 0.3 \pm 0.1$ cm^{-1}, which gives a spectroscopic dissociation energy ($D_e = \omega_e^2 / 4\omega_e x_e$) of 2.1 ± 0.7 eV.

II. EXPERIMENT

The CCNY cluster deposition source has been described in detail elsewhere. [5] Briefly, an argon ion beam (typically 15 mA at 25 keV) sputters a cooled, gadolinium target (Alfa Aesar, 99.9% (REO)). The sputtered products are extracted by electrostatic lenses, mass-selected using a Wien filter, bent by 10° to eliminate neutrals and then guided into the deposition region. Gadolinium dimer (or atomic) ions were then codeposited with argon gas and electrons onto a ~ 16 K substrate, composed of a CaF_2 plate. Ion currents under soft landing conditions could be measured on a Faraday plate in the deposition region and were: Gd^+ (50 nA), Gd_2^+ (8 nA). Prior to deposition, the selected ions were simultaneously slowed to 10 eV by a surrounding "Faraday cage". Matrices were grown at about 5-7 μ/h with an Ar : metal ratio of approximately 10^4 : 1. By comparing the intensities of known atomic excitation features in a dimer deposition

with those obtained from deposition of atom under similar conditions, the dimer fragmentation is estimated to be about 10%.

Matrix samples were interrogated *in situ* using both absorption and Raman spectroscopy. As previously described, [5, 6] the absorption measurements were made by collecting the light at 90° to that incident, a technique we term "Scattering Depletion Spectroscopy" (SDS). Raman spectra were recorded using a dye laser (Coherent, Model CR599) with R110, R6G and DCM, pumped by the "green-blue" lines of an argon ion laser (Coherent, Model INNOVA 70) for excitation. Raman excitation profiles were obtained by observing the Raman spectra while tuning the dye laser in small steps through the absorption region 570-660 nm. Scattered light was collected at 90° into a Spex 1877E 0.6 m Triplemate Spectrometer and detected by a liquid nitrogen cooled CCD detector (Spex model "Spectrum One") with DM3000R software. All Raman results were calibrated using the CaF_2 (substrate) line at 327 cm^{-1}. This value is slightly lower than the previously used value of 330 cm^{-1}, and results from a recent more careful temperature dependent study. The absorption (SDS) spectrum was recorded following a 5 hour deposition of 8 nA of Gd_2.

III. SPECTRA AND ANALYSIS

A portion of the absorption spectrum, shown as insert in Fig.4.3.1, consists of two unstructured bands with maxima at about 585 nm and 620 nm. Those were the only absorption features that we could definitely assign to the dimer. This assignment is

verified by the observation of resonance Raman spectra for excitation into these bands. The Raman excitation profiles, obtained by dividing the Raman intensity (of the first Stokes line) by intensity of CaF_2 Raman line, are superimposed in this insert.

Raman spectra were observed throughout the region 570-660 nm but not upon excitation at wavelengths further to the blue. At longer wavelength up to 680 nm, Raman intensities drop abruptly and observation of Raman lines is subject to severe interference from intense fluorescence. Fig. 4.3.1 shows a typical Raman spectrum for a 40 nA-h sample of digadolinium in argon. A (nonresonant) Raman line due to the CaF_2 substrate is also in evidence. The spectrum consists of a single progression of almost equally spaced lines with increasing linewidth. The shapes of these Stokes lines were well accounted for by simulating overlapping Gaussians corresponding to 15 possible isotopic combinations, which accounts for more than 95% of the total abundance, spaced according to their relative reduced masses. The linewidths of the Gaussians adopted in this simulation scale as v", which implies that the lifetime of higher vibrational states are shorter than that of lower states. Because of the increasing linewidth and decreasing intensity with increasing Raman shift, only four transitions could be accurately positioned. The average Stokes shifts for 44 excitation wavelengths are (one standard deviation uncertainty in parentheses): 138.3(4), 275.6(6), 412.8(6), and 549.2(12) for v" = 1 to 4 respectively. A least squares fit of these data give ω_e = 138.7(4) cm^{-1} with $\omega_e x_e$ = 0.3(1) cm^{-1}.

IV. DISCUSSION

The experimental values for ω_e and $\omega_e x_e$ enable us to determine the dimer force constant, k_e = 0.89(1) mdyn/Å, and the spectroscopic dissociation energy, D_e = 2.1(7) eV. The latter result is in reasonable agreement with previous experimental value of 1.78±0.34 eV, [4] which is obtained by means of a combination of Knudsen effusion and mass spectrometric methods. The observed force constant is similar in magnitude to that of Y_2 [7] (0.90 mdyn/Å) and Hf_2 [8] (1.63 mdyn/Å), but considerably lower than that for La_2 [9] (2.38 mdyn/Å). This is a surprising result. It is well known that 4*f* electrons are, on average, much closer to the nucleus than 6*s* and 5*d* electrons; so much so that they do not participate in bonding. Thus we might on a simple level expect the force constant of Gd_2 to lie between that of La_2 and Hf_2, rather than being much lower than either, as observed. Clearly other factors are important, and it is likely that the 4*f* electrons play at least an indirect role in bonding. One factor is the inability of *f* electrons to effectively shield the outer 6*s* and 5*d* electrons from the nucleus. This results in a contraction of the 6*s* and 5*d* shells, leading to generally lower atomic and ionic radii across the lanthanide series, which in turn should lead to increasing force constants. However, heavy atomic nuclei cause relativistic effects to become more severe. The Dirac-Fock and Hartree-Fock calculations of Desclaux [10] show that there is a larger relativistic effect in Gd than for most other lanthanides. This effect tends to contract the 6*s* orbital while leading to an expansion of the 5*d* orbital. [11] This should result in increasing participation of 5*d* electrons and decreasing participation of 6*s* electrons in bonding, implying a decreased force constant. Since lanthanides generally have $4f^n6s^25d$ atomic configurations, the $6s^25d \rightarrow 6s5d^2$ promotion energy is also important. This is because the $6s5d^2$ configuration

is more favorable for bonding. It is this latter effect which explains the rather high (k_e = 2.38 mdyn/Å) force constant of La_2 since the promotion energy is only 0.33 eV. [12] In Hf, the promotion energy is 1.75 eV, [13] explaining the relatively weaker bond in Hf_2. The promotion energy of Gd is 0.79 eV. [12] Although this is lower than some of its neighbors, it is not sufficiently low as to allow easy promotion. This, combined with the relativistic shrinking of the 6*s* orbital, tends to suppress the possibility of strong bonding, leading to a lower force constant than either La_2 or Hf_2.

Note, however, that our experimental force constant is still considerably higher than that predicted by Goodfriend [14] (ω_e = 70.7 cm^{-1}) assuming a Morse potential and using the dissociation energy of Kant and Lin [4] (which is experimentally the same as ours – we also assume a Morse potential to determine D_e). Goodfriend's analysis depended on determination of a sum of Slater radii of the outermost occupied orbital, using a shielding constant from Hartree-Fock calculations. It is likely that these parameters were overestimated by Goodfriend.

More sophisticated calculations have been carried out by Dolg and coworkers. [2, 3] These studies were inspired partly by the rather large ground state spin observed in the ESR by Van Zee *et al.*. [1] As mentioned, they established a $^{19}\Sigma$ ground state, which required ferromagnetic coupling of the 4*f* electrons in a $(4f)^7(4f)^7\sigma_g^2\sigma_u^1\sigma_g^1\pi_u^2$ configuration, suggested by Dolg *et al.*. [2] Investigation of the relative energy order of $^{19}\Sigma_u^-$ and $^{5}\Sigma_u^-$ states invites comparison with Mn_2 and Mn_2^+ where inner-shell coupling is antiferro- [15] and ferro-magnetic [16] respectively. With a $5d^16s^2$-$5d^26s^1$ atomic configuration, delocalized unpaired valence electrons in Gd_2 make it more similar to

Mn_2^+ even though Gd_2 is a neutral molecule. Similar to the bonding in Mn_2^+, [17] high-spin coupling for Gd_2 may be expected since *5d6s-4f* exchange is likely to be larger than the *4f-4f* interaction. In an earlier calculation, Dolg, Stoll and Preuss [2] held the *4f* occupation numbers at a fixed integral, while carrying out a quasi-relativistic *ab initio* pseudopotential calculation. The result was prediction of a $^5\Sigma_u^-$ ground state for Gd_2. More recently Dolg, Liu and Kalvoda [3] employed a fully relativistic density functional calculation which allows for spin-realignment in the $4f^7$ cores. The *4f* occupancy remains near 7, confirming the model of a relatively inactive Gd *4f* shell. However, the *4f* electrons interact with the valence *5d6s* electrons, enabling strong ferromagnetic coupling between the two $4f^7$ atomic cores. This results in a predicted $^{19}\Sigma_u^-$ ground state in agreement with the ESR results. Dolg, Liu and Kalvoda [3] conclude on the basis of several different calculations that the predicted dissociation energy is 1.4 ± 0.4 eV, somewhat lower than either experimental result (1.78 ± 0.35 eV [4] or 2.1 ± 0.7 eV this work). However, their predicted vibrational frequency of 135 ± 15 cm^{-1} matches our experimental result exactly. This may be taken as additional confirmation of the $^{19}\Sigma_u^-$ ground state assignment.

References

[1] Van Zee, R. J.; Li, S.; Weltner, W., Jr. *J. Chem. Phys.* **100**, 4010 (1994).

[2] Dolg, M.; Stoll, H.; Preuss, H. *J. Mol. Struct. (Theochem)* **277**, 239 (1992).

[3] Dolg, M.; Liu, W.; Kalvoda, S. *Int. J. Quantum. Chem.* **76**, 359 (2000).

[4] Kant, A.; Lin, S. S. *Monatsh. Chem.* **103**, 757 (1972).

[5] Hu, Z.; Shen, B.; Lombardi, J. R.; Lindsay, D. M. *J. Chem. Phys.* **96**, 8757 (1992).

[6] Hu, Z.; Shen, B.; Zhou, Q.; Deosaran, S.; Lombardi, J. R.; Lindsay, D. M. *Proc. SPIE* **1599**, 65 (1991).

[7] Fang, L.; Chen, X.; Shen, X.; Liu, Y.; Lindsay, D. M.; Lombardi, J. R. "Spectroscopy of Yttrium Dimers in Argon Matrices", *Low Temperature Physics*, 26, xxxx (2000) in press.

[8] Hu, Z.; Dong, J.; Lombardi, J. R.; Lindsay, D. M. *J. Phys. Chem.* **97**, 9263 (1993).

[9] Liu, Y.; Fang, L.; Shen, X.; Chen, X.; Lombardi, J. R.; Lindsay, D. M. "Absorption, Resonance Raman and Raman Excitation Spectra of Lanthanum Dimers in Argon Matrices", *Chem. Phys.*. to be published.

[10] Desclaux, J. P. *At. Data Nucl. Data Tables* **12**, 311 (1973).

[11] Pitzer, K. S. *Accounts of Chemical Research* **12**, 271 (1979).

[12] Martin, W. C.; Zalubas, R.; Hagan, L. *Atomic Energy Levels-The Rare Earth Elements*, Natl. Bur. Stand. Ref. Data Ser. 60 (U.S. Dept. of Commerce, Washington, D. C., 1978).

[13] Moore, C. E. *Atomic Energy Levels (Vol III)*, Nat. Stand. Ref. Data Ser., Nat. Bur. Stand. (U.S.), 35 (U.S. Dept. of Commerce, Washington, D. C., 1971).

[14] Goodfriend, P. L. *Spectrochim. Acta* **40A**, 283 (1984).

[15] Baumann, C. A.; Van Zee, R. J.; Bhat, S. V.; Weltner, W., Jr. *J. Chem. Phys.* **78**, 190 (1983).

[16] Van Zee, R. J.; Weltner, W., Jr. *J. Chem. Phys.* **89**, 4444 (1988).

[17] Bauschlicher, C. W., Jr. *Chem. Phys. Lett.* **156**, 95 (1989).

Figure 4.3.1 Resonance Raman spectrum (λ_{ex} = 629.8 nm) of Gd_2 in an argon matrix, and dimer absorption spectrum (inset, compared with excitation profile using n = 1 transition at 138.3 cm^{-1}).

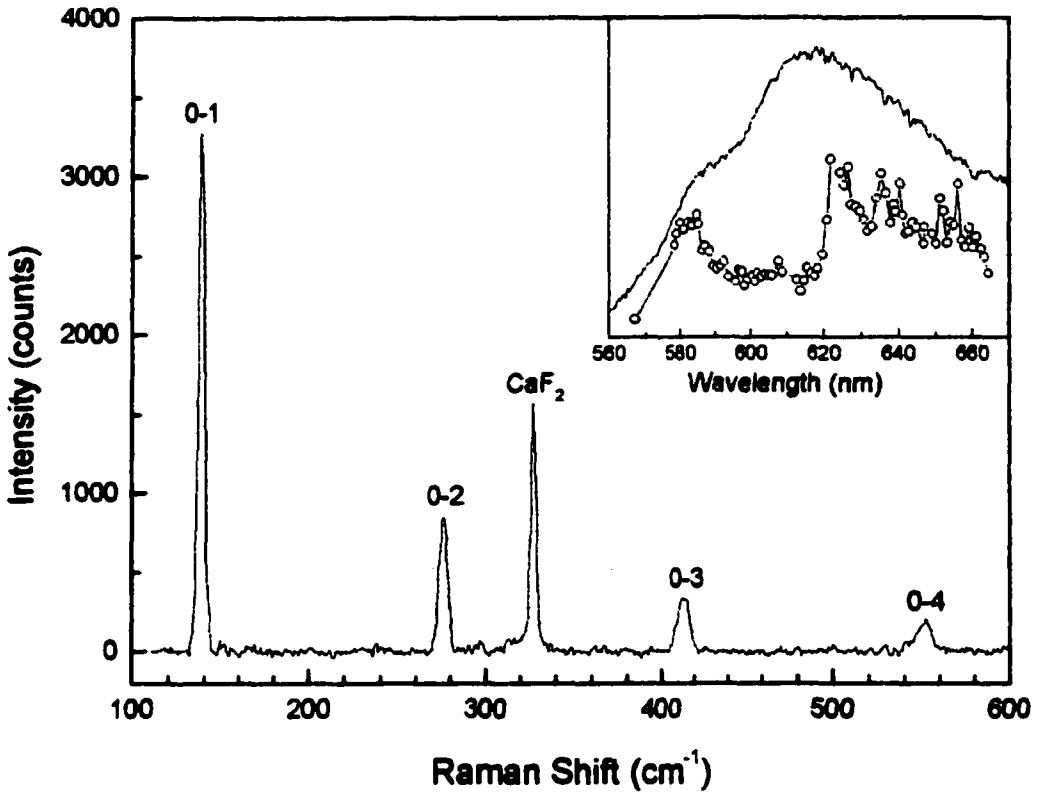

4.4 Absorption, excitation and resonance Raman spectra of Ce_2, Pr_2 and Nd_2

J. Chem. Phys. **113**, xxxx (2000) in press

I. INTRODUCTION

The intrusion of 4*f* electrons observed throughout the lanthanide metals provides us with the possibility of insight into the effects of *f* electrons on both atomic and metallic properties. However, studies of small clusters, such as dimers enable us to determine the effects, through indirect, on bonding as well. The effects must of necessity be indirect, since the 4*f* electrons are held close to the nucleus and are themselves therefore unavailable for bonding. The possibility for bonding is left to the occupied 5*d* or 6*s* shells, which have greater spatial extent than the 4*f* electrons, and are thus more available for the overlap needed to form a strong chemical bond.

At first examination, the effect of adding *f* electrons in moving across the lanthanide series results in a steady monotonic contraction of atomic radii. Since the previously observed force constant in La_2 [1] is relatively high, while those of Gd_2 [2] or for example Hf_2 [3] (with a filled f-shell) are somewhat lower, we might expect a steady monotonic decrease in force constant across the lanthanide dimers. With this in mind we report here on the force constants obtained in Ce_2, Pr_2 and Nd_2 matrix isolated species which have been produced and separated by mass-selection after sputtering a metal target. The results show for Ce_2 $\omega_e = 245.4 \pm 4.2$ cm^{-1}, for Pr_2, $\omega_e = 244.9 \pm 1.2$ cm^{-1}, and for Nd_2 $\omega_e = 148.0 \pm 1.9$ cm^{-1}. In Nd_2 a sufficiently long progression is obtained to

determine $\omega_e x_e$=0.7(4) cm^{-1} leading to a spectroscopic dissociation energy of 1.0 ± 0.5eV. It is clear from these results that other factors, such as promotion energies and relativistic corrections must be considered in explaining the observed variation of force constants across the lanthanide series.

II. EXPERIMENTAL

The CCNY cluster deposition source has been described in detail elsewhere. [4] Clusters, produced by sputtering a cerium (or praseodymium, neodymium) target (Alfa Aesar 99.9 % (REO)) with an argon ion beam (15 mA at 25 keV), were mass selected with a Wien filter and then co-deposited with the matrix gas (Argon) and electrons onto a CaF_2 substrate at around 16K. Ion currents could be measured on a Faraday plate in the deposition region. In figure 4.4.1 we present sputtering mass scans observed in our apparatus for four lanthanide elements. The three main peaks show the argon, atom and the dimer. The small peak between argon and atom is assigned to atom with doubly positive charge. The current ratios of the dimer ion to the atom ion are almost identical (1:4) for all these three elements. This ratio was observed for Gadolinium to be about 1:6. Prior to deposition, the selected ions were simultaneously slowed to 10 or 15 eV by a surrounding "Faraday cage". Matrices were grown at about 5-7 μ/h with an Ar : metal ratio of approximately 10^4:1. By comparing the intense atomic line in the excitation spectra of both the dimer and atom, the fragmentation ratio is determined to be 5%(Ce_2), 15%(Pr_2), and 40%(Nd_2). This latter fragmentation of Nd_2 is considerably higher than

observed in previous experiments. However, sufficient population of dimer apparently remains in the matrices to obtain good Raman spectra.

Matrix samples were interrogated *in situ* using both absorption and Raman spectroscopy, and excitation spectroscopy. As previously described,[4,5] the absorption measurements were made by collecting the light at 90° to that incident, a technique we term "Scattering Depletion Spectroscopy" (SDS). The spectrum is given by the ratio of the scattering light at the center (signal) of the sample to that at the edge (reference). Excitation spectroscopy is recorded by applying a high pass filter before detection of PMT. Raman spectra were recorded using the visible output of an argon ion laser (Spectra Physics model 2045), and also in the 540nm~680nm region using a dye laser (Rhodamine110, R6G, DCM). The Raman shift is calibrated by using the standard CaF_2 shift at 327.0cm^{-1}. The excitation profile is obtained by taking the intensity ratio of the corresponding resonance Raman peak of the dimer to the nonresonance Raman line of CaF_2 vs. excitation laser wavelength. Scattered light was collected at 90° with a Spex 1877E Triplemate Spectrometer (0.6 m) and detected by a liquid nitrogen cooled CCD detector (Spex model "Spectrum One") with DM3000R software.

III. SPECTRA AND ANALYSIS

Ce_2: The absorption spectrum (SDS) of an approximately 80nA-h sample of Ce_2 in argon is shown in inset of figure 4.4.2 We observe two overlapping bands of absorption, which are not observed in the absorption spectra of the atom. This assignment is also

verified by the observation of resonance Raman spectra for several excitation wavelengths in the range of 457.9~514.5nm as well as range of 540~570nm step scan of R110 dye laser. The excitation profile gives two peaks at 485nm and 547nm (inset of Fig. 4.4.2). It can readily be seen that the excitation profile provides a more sensitive picture of the optical spectroscopy than the normal absorption spectrum. In the Raman spectrum there appears a site effect similar to that in lanthanum dimer previously observed in this lab (Fig. 4.4.2). This appears as a triplet of lines for each member of the progression. By annealing from 16K to around 40K, we conclude the most stable site is the lowest of the three peaks. By heating the matrices to 25K, the higher frequency two peaks disappear. The most stable one is lost when temperature goes to 39K, the normal temperature at which the matrix evaporates. The less stable two sites are shifted 6.5 cm^{-1} and 15.3 cm^{-1} higher than the first line. The principle features of the Raman spectra are a vibrational progression (labeled v'=0→v"=1,2). To obtain the vibrational frequencies, we averaged over the eight spectra 457.9~514.5nm. Data at the 540~570nm region show broad character and are difficult to accurately assign. The progression is: 242.3(10), 481.5(12) cm^{-1}, which gives the force constant k_e = 2.48(6) mdyne/Å.

Pr_2: Due to the strong absorption of the atom at the same region, a 130nA-h deposit of Pr_2 shows no obvious absorption structure. However, we do observe a broad band under the atomic lines from 400 to 600nm. The inset in figure 4.4.3 shows both the absorption spectrum of the deposition of atoms and one of the dimer. The more sensitive Raman excitation profile reveals the structure of two absorption bands peak at 465nm and 535nm, which we attribute to the dimer. Raman spectra averaged over 18 scans (Fig.

4.4.3) in the dye region give Stokes shifts of: 241.7(3), 480.2(3) cm^{-1}, k_e=2.49(2) mdyne/Å. For the region of 457.9~514.5nm, there is only one weak site of $7cm^{-1}$ shifted to higher frequency from the first line.

Note that the frequencies observed in the Raman spectra of Ce_2 and Pr_2 are almost identical, leading to questions as to whether we are indeed observing distinct species. We must therefore examine more carefully the differences between the two spectra as well as eliminate the possibility of contamination of one deposition with another. The insets of figure 4.4.2 and figure 4.4.3 show that the two spectra differ considerably in the peak shape or position of the absorption spectra. The praseodymium spectra show strong atomic features which cerium does not have. The more sensitive excitation profile (dotted line at the bottom of Fig. 4.4.2 and 4.4.3) gives different peak maxima. The Ce_2 peaks are at 485nm and 547nm, while in Pr_2 the peaks are closer to 465nm and 535nm. The excitation spectrum using a 720nm high pass filter shows a strong fluorescence emission when exciting the Pr_2 at around 600nm, which is not present in Ce_2. Additional differences show up in a detailed examination of site effects. See Fig. 4.4.4, with the same excitation laser, the Raman spectrum of Ce_2 shows three peaks and Pr_2 has only two. The relative intensity of the two peaks, which are reproducible, differs between the two samples.

In order to determine whether it is possible that there is some contamination of Ce metal in our Pr sample or the opposite, we took a high resolution mass spectrum of our metal targets using a Thermal Quest/Finnigan XSQ-700 Quadruple mass spectrometer. The results showed no detectable traces of Pr in our Ce sample, and no detectable traces of Ce in our Pr sample. The resolving power of the spectrometer was easily sufficient to

distinguish between the two species. There is also the possibility that after a Ce deposition, some Ce metal remained in the instrument and contaminated our Pr deposit, although there is no visible evidence of this. Since the melting point of Ce is 795°C, it is not likely that the source of possible contamination is any part of the apparatus which remain cold during deposition. This leaves only the metal target holder. However, in successive experiments on Ce_2, Pr_2, Nd_2 and then repeating Pr_2, the lines we observed for Pr_2 which were not observed in Nd_2 but observed again in the second deposition of Pr_2. If there were Ce contamination from the target holder, we would also have seen these lines in the Nd_2 deposit. We thus conclude that the coincidence of Ce_2 and Pr_2 frequencies is fortuitous, and that we have indeed made separate measurements.

Nd_2: There is a broad absorption of neodymium dimer centered at 640nm when compared to the atomic spectra (inset of Fig.4.4.5). The excitation profile reveals another peak around 520nm, which was overlapped in the absorption spectrum by atomic structure. Resonance Raman (as in Fig. 4.4.5) spectra give a progression of: 145.8(5), 291.2(8), 436.6(10), 577.7(9) cm^{-1}, averaged over 43 spectra from 488nm to 680nm. Using standard techniques we obtain ω_e=148.0(19) cm^{-1}, $\omega_e x_e$=0.7(4) cm^{-1}, k_e=0.93(2) mdyne/Å. Assuming a Morse potential and that $D_e=\omega_e^2/4\omega_e x_e$ we obtain D_e=1.0(5) ev. This is in reasonably good agreement with the third law experimental result of D_e=0.8(3) ev. The first Raman transition encounters interference from the Rayleigh tail in the excitation region lower than 600nm. The second peak is not sufficiently intense to develop a reliable Raman excitation profile. The band at around 350cm^{-1} is fluorescence. We estimate that the fragmentation of this molecule is as high as 40%. This ratio is larger

than that of the largest previously observed in other experiments. This may due to the low bond strength and dissociation energy [6]. For the other dimers with low dissociation energy such as Ni_2 [7] and Co_2 [8], the fragmentation are also fairly high. The fragmentation may also occur in the ionized dimer before neutralization. In any case there is sufficient dimer remaining to obtain clear Raman spectra without serious interference from the atom.

IV. DISCUSSION

The experimental values for ω_e enable us to determine dimer force constants for each of the observed lanthanides. In table 4.4.1 we present the resulting force constants, along with several other selected properties of the lanthanide elements.

Note that at first the force constant for La_2 (k_e = 2.28 mdyne/Å) seems anamously high in comparison with Y_2 (k_e = 0.90 mdyne/Å) [11] and Hf_2 (k_e = 1.63 mdyne/Å). [3] However, this can be explained by observation of the low $5d^16s^2 \rightarrow 5d^26s^1$ promotion energy (0.33 eV). The $6s^1$ configuration is known to be much more favorable for bonding than the filled $6s^2$. If Y_2 may be presumed to have a bond order of 1, then we expect the La_2 force constant to represent a bond order of 2 or more, indicating strong participation of d as well as s electrons in bonding. By contrast, Gd_2 has a force constant (k_e = 0.89 mdyne/A) much closer to that found in Y_2. The promotion energy in Gd is much larger than that of La so that we might expect a considerably weaker bond in the dimer.

Examination of Ce_2 provides no surprise in that the force constant (k_e = 2.48 mdyne/Å) is similar to that of La_2. The atomic configuration differs by a single f electron,

and the promotion energy, as in La, is low (0.29 eV). Skipping to an examination of Nd_2 we observe a somewhat lower force constant (k_e = 0.93 mdyne/Å), which, considering the rather high promotion energy (1.05 eV) we might expect to be similar to Gd_2 despite the differences in atomic configuration.

Comparing k_e with third law dissociation energy for the above four lanthanides shows a plausible inverse correlation between bond strength and promotion energy. Note, however, for Pr_2 these expectations are not followed. The force constant remains high, just as in La_2 and Ce_2 despite the high $6s \rightarrow 5d$ promotion energy (1.00 eV), and somewhat lower value of D_0. This high value for k_e suggests somewhat stronger bonding than expected, corresponding to a likely bond order considerably greater than 1. This seems especially surprising in that the ground state configuration of Pr is $4f^3 6s^2$. The 4f orbital has dropped lower than the 5d orbital between Ce and Pr. Not only do we have an unfavorable $6s^2$ configuration, there are also no d electrons available for bonding either. We might try to remedy this problem with the observation that the $4f^3 6s^2 \rightarrow 4f^2 5d^1 6s^2$ promotion energy is not too high (0.55 eV). This might be low enough to enable three electrons to be available in the valence shell for bonding. The difficulty with this argument is that the $5d^1 6s^2$ configuration is, as Ce, unfavorable for bonding and, as in Ce, we must invoke almost an additional 0.3 eV to achieve the favorable $5d^2 6s^1$ configuration. (The promotion energy for $4f^3 6s^2 \rightarrow 4f^2 5d^2 6s^1$ in Pr is 0.83 eV.)

It is clear that we must examine more carefully the influence of *f* electrons on bonding in the valence shell. Any discussion of the effect of *f* electrons on the bonding in transition metals and lanthanides must consider two contravening effects. One is due to the incomplete shielding of the *5d* and *6s* electrons by the *f* electrons and the other is the

increasing influence of relativity effects with increasing nuclear charge. It is well understood that 4*f* electrons cannot effectively shield the outer electrons of the 5*p*, 5*d* and 6*s* orbitals, leading to a rather higher effective charge felt by these electrons. The resulting orbital contraction (sometimes called the "lanthanide contraction") leads, among other things, to the observation of nearly equal atomic radii for the second and third row transition metals (e.g. Hf and Zr, Ta and Nb, etc.). If this was the only effect we might expect a rather monotonic change in force constants across the lanthanides following the monotonic decrease in both atomic and ionic radii (see table 4.4.1). This is obviously not the case either for force constants or dissociation energies.

Clearly, relativistic effects must also be of consequence. Due to the contact term in the Dirac Hamiltonian, the 6*s* orbital is contracted by relativistic effects, while the 4*f* and 5*d* electrons experience an expansion. These effects have been explored in great detail in a very useful article by Desclaux [10], who has calculated orbital energies and expectation values for various powers of the radius for atoms with Z = 1 through Z = 120. Comparison is made between relativistic Dirac-Fock calculations and those of previous non-relativistic results. In table 4.4.1 we present the ratio of the relativistic value of <r> to the non-relativistic value for both the 4*f* orbital and the 6*s* orbital (Since the 5d orbital is not occupied for Pr and Nd, no calculations were made). Note first that for the 4*f* orbital (and presumably the 5*d* orbital, when occupied) the ratio is greater than one, indicating a relativistic expansion, while for the 6*s* orbitals the ratio is less than one, resulting in a contraction due to relativity. Even more telling, perhaps is that for Pr, the effects of relativity are considerably greater than either of its neighbors in both the 4*f* and 6*s* orbital. In both cases inclusion of relativity results in a larger orbital radius than that

expected without consideration of relativity. Careful consideration of table 4.4.1 of atomic and ionic radii shows that the "lanthanide contraction" slows at Pr, most likely due to this effect. It is difficult to imagine that this effect is entirely responsible for the higher than expected force constant in Pr_2 . Much more dramatic effects are found in Au_2 where the force constant is higher than that of Cu_2 and Ag_2. Au has been shown by Desclaux [10] to have one of the largest relativistic contractions, and this contraction is thought to be responsible for the observed higher dimer force constant.

Relativistic configuration-interaction calculations by Schwerdtfeger and Dolg [12] show remarkably large relativistic correction to the bond length and vibrational frequencies of AuLa and AuLu. As an example the calculated Au-La force constant increase by over 160% due to inclusion of relativistic effects. Thus it would not be surprising that the additional relativistic contraction to the Pr radial expectation values were responsible for the higher than expected Pr_2 force constant. It is obvious that more accurate relativistic calculations are necessary in order to unravel the various countervailing tendencies. We are currently examining some of the remaining lanthanide dimers in order to aid in this search.

Table 4.4.1 Selected properties of several lanthanide dimers.

	La_2	Ce_2	Pr_2	Nd_2	Gd_2
Atomic Configuration	$5d^16s^2$	$4f^15d^16s^2$	$4f^36s^2$	$4f^46s^2$	$4f^75d^16s^2$
Atomic radii (pm)	187	183	182	181	179
Ionic radii (pm)	107	103	101	99	94
Promotion Energy *					
$f^md^ns^2 \rightarrow f^md^{n+1}s^1$(eV) [9]	0.33	0.29	1.00	1.05	0.79
$f^md^ns^2 \rightarrow f^{m-1}d^{n+1}s^2$ (eV)			0.55	0.84	
$f^md^ns^2 \rightarrow f^{m-1}d^{n+2}s^1$ (eV)			0.83	1.09	
Relativity ratio [10]					
4f orbital		1.054	1.067	1.059	1.036
6s orbital	0.9575	0.9548	0.9579	0.9557	0.9390
D_0 (Third Law)	2.50	2.57	1.30	0.82	1.8
k_e (mdyne/Å)	2.28(1)	2.48(6)	2.49(2)	0.93(2)	0.89(1)

* The promotion energy numbers are energy needed to promote electrons in favor of bonding (s^1 configuration). All the energy levels are relative to ground atomic configuration.

Reference

[1] Liu, Y.; Fang, L.; Shen, X.; Chen, X.; Lombardi, J. R.; Lindsay, D. M.; "Absorption, Resonance Raman and Raman Excitation Spectra of Lanthanum Dimers in Argon Matrices", *Chem. Phys.*. to be published

[2] Chen, X.; Fang, L.; Shen, X.; Lombardi, J. R.; *J. Chem. Phys.* **112**, 9780 (2000)

[3] Hu, Z., Dong, J., Lombardi, J. R., and Lindsay, D. M., *J. Phys. Chem.* **97**. 9263 (1993).

[4] Hu, Z.; Shen, B.; Lombardi, J.R.; and Lindsay, D.M., *J. Chem. Phys.* **96**, 8757 (1992).

[5] Hu, Z.; Shen, B.; Zhou, Q.; Deosaran, S.; Lindsay, D.M. and Lombardi, J.R. SPIE Vol. 1599, Recent Advances in the Use of Light in Physics, Chemistry, Engineering and Medicine, **65** (1991).

[6] Fedrigo, S.; Harbich, W. and Buttet, J.; *Phys. Rev. B.* **58** (11), 7428 (1998).

[7] Wang, H.; Haouari, H.; Craig, R.; Lombardi, J. R. and Lindsay, D. M.; *J. Chem. Phys.* **104** (10), 3420 (1996).

[8] Dong, J.; Hu, Z.; Craig, R.; Lombardi, J. R. and Lindsay, D. M.; *J. Chem. Phys.* **101** (11), 9280 (1994).

[9] Martin, W. C.; Zalubas, R.; Hagan, L. *Atomic Energy Levels-The Rare Earth Elements*, Natl. Bur. Stand. Ref. Data Ser. 60 (U.S. Dept. of Commerce, Washington, D. C., 1978).

[10] Desclaux, J. P.; *At. Data Nucl. Data Tables* **12**, 311 (1973).

[11] Fang, L., Chen, X., Shen, X., Liu, Y., Lombardi, J. R. and Lindsay, D. M.; "Spectroscopy of Yttrium Dimers in Argon Matrices", Low Temperature Physics. 26, xxxx (2000) in press

[12] Schwerdtfeger, P., Dolg. M., *Phys. Rev. A* **43** (3), 1644 (1991).

Figure 4.4.1 Sputtering Mass Spectrum of four lanthanide elements. The lowest peak in each spectrum is due to Ar. The next high peak is due to the lanthanide atom and the next due to the dimer respectively.

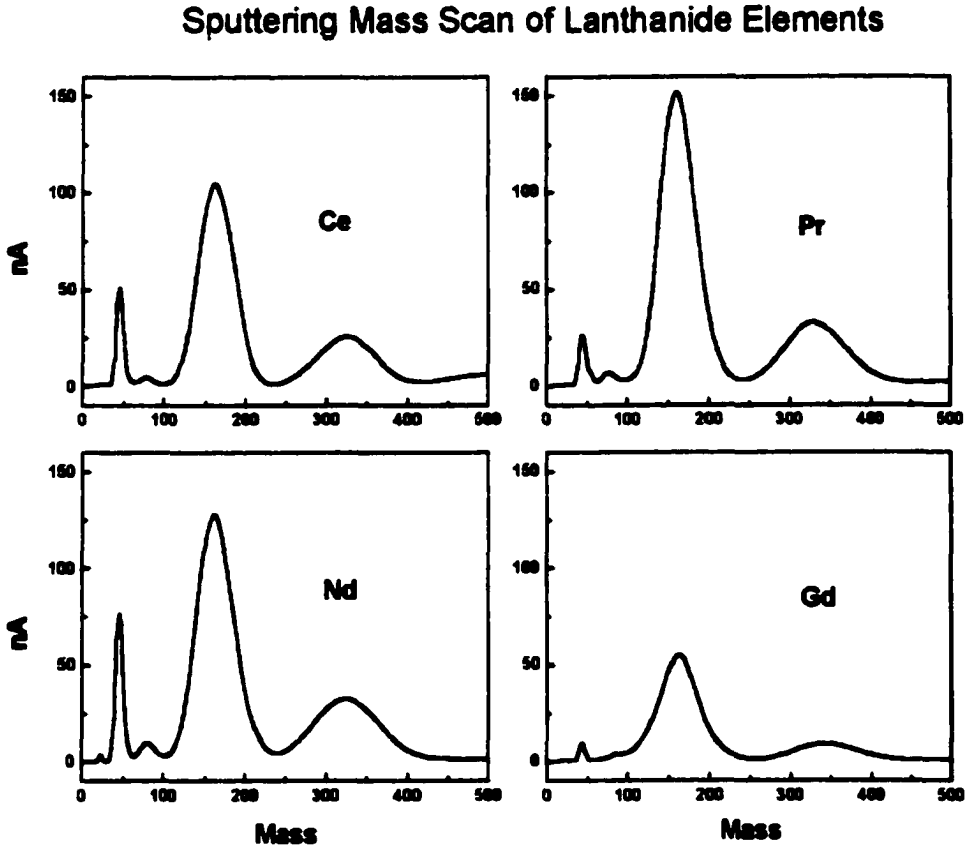

Figure 4.4.2 Resonance Raman (excited by 496.5nm) and absorption (inset, top to bottom, SDS and Raman excitation profile using the n=1 transition) spectra for cerium dimer in argon matrix.

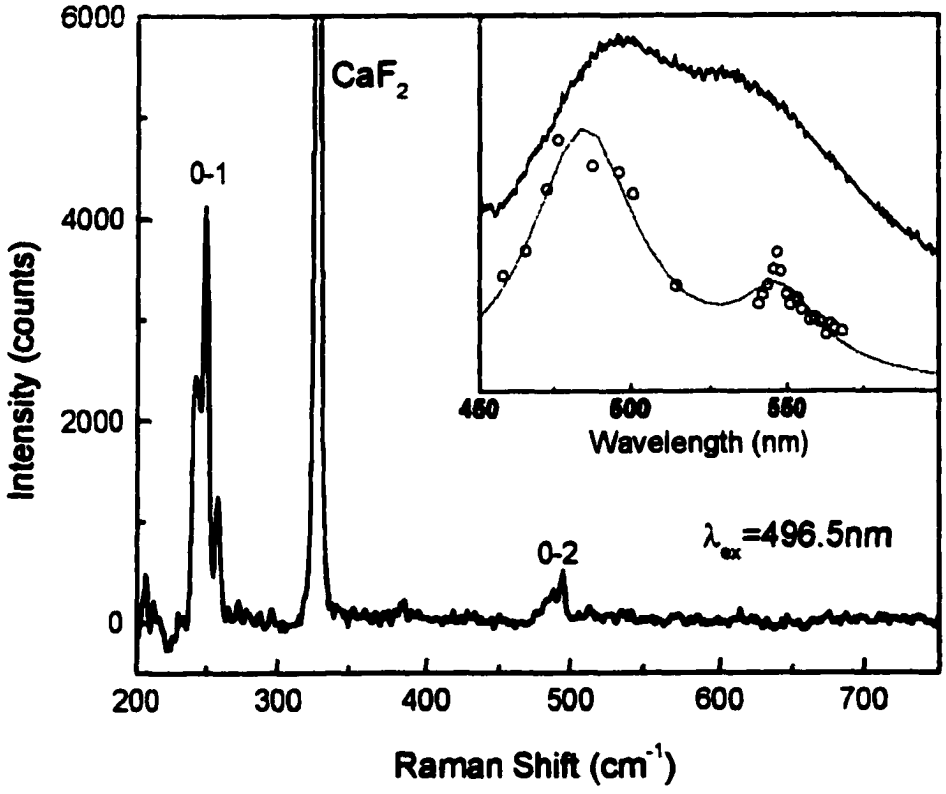

Figure 4.4.3 Resonance Raman (excited by 545.46nm) and absorption (inset, top to bottom, SDS of atom, dimer and Raman excitation profile using the n=1 transition) spectra for praseodymium dimer in argon matrix.

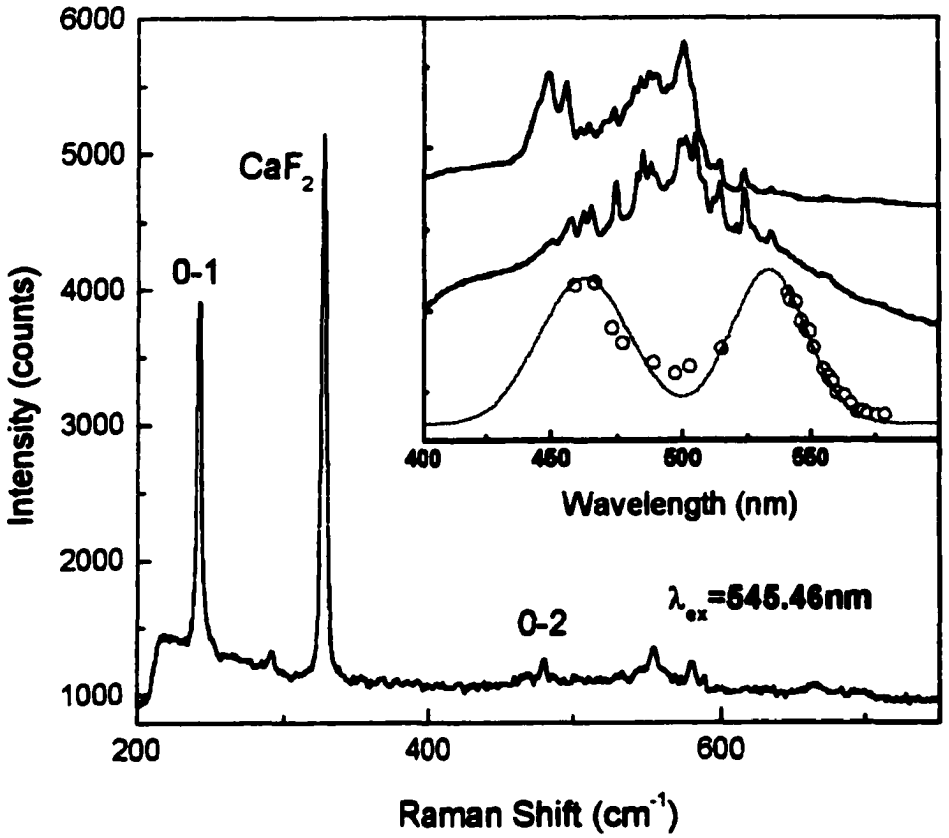

Figure 4.4.4 Site effects comparison of the first resonance Raman transition between Pr_2 and Ce_2 (excited by 496.5nm).

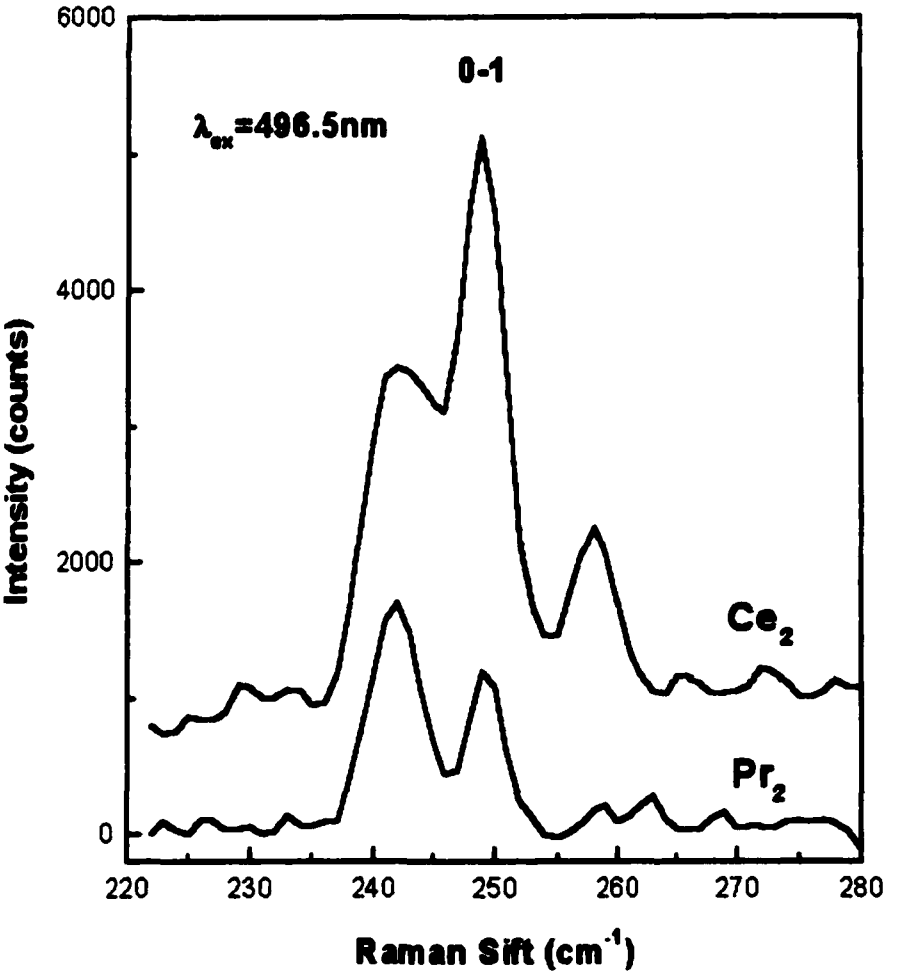

Figure 4.4.5 Resonance Raman (excited by 667.30nm) and absorption (inset, top to bottom, SDS of atom, dimer and Raman excitation profile) spectra for neodymium dimer in argon matrix.

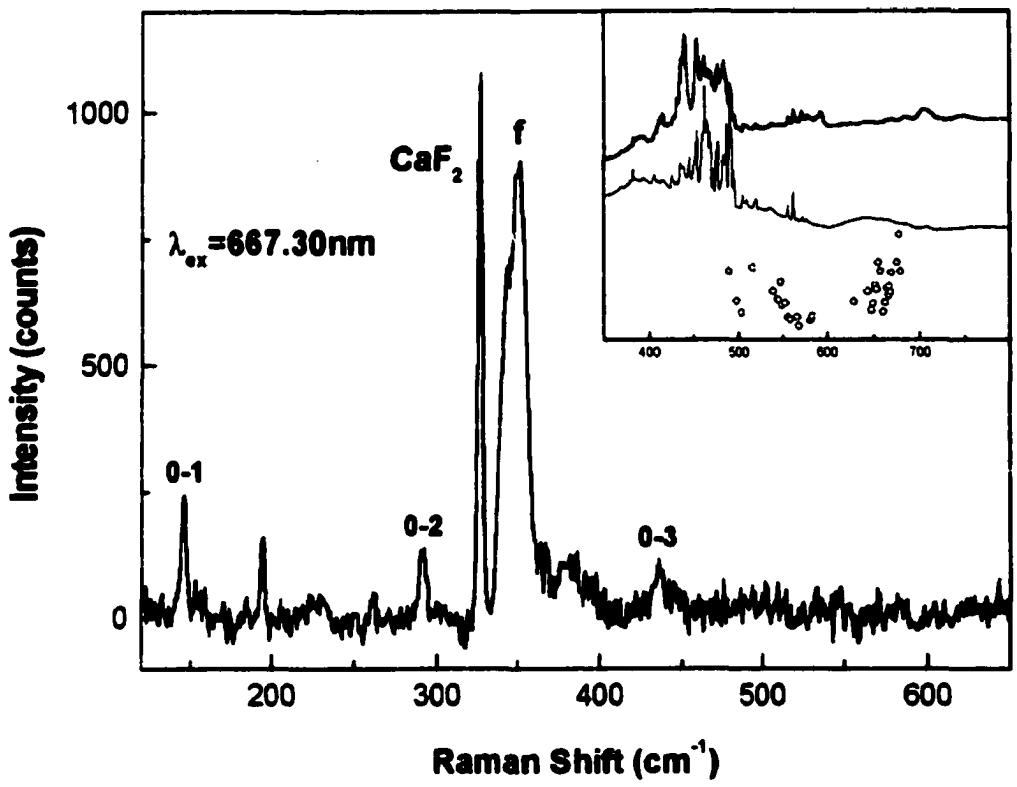

4.5 Raman Spectrum of Mass-Selected Terbium Dimers in Argon Matrices

J. Phys. Chem. to be published

I. INTRODUCTION

In this article we extend our recent investigations of the Raman spectroscopy of lanthanide dimers[1,2,3] to Tb_2. Relatively little previous work has been carried out on this molecule. In 1972, J. Kordis[4] *et.al* measured the dissociation energy by means of Knudsen effusion mass spectrometric study. This work was confirmed by Kant and Lin[5] at around the same time.

We report the observation of resonance Raman spectra, the absorption ("scattering depletion") spectrum and the Raman excitation profile of mass selected Tb_2 in argon matrices. From the absorption (scattering depletion) spectrum, one optical transition in the region 623-673 nm was observed. By excitation into this region with dye laser radiation, two Raman series were observed, with one up to 7 Stokes transitions, and the other up to 4 transitions. These data give for the ground (X) state ω_e = 137.6 ± 0.4 cm^{-1} with $\omega_e x_e$ = 0.31 ± 0.05 cm^{-1}, leading to a spectroscopic dissociation energy of 1.9 ± 0.3 eV, force constant k_e=0.88±0.1mdyne/Å. and the other progression has an origin at 313.9cm^{-1}, the progression 450.0 cm^{-1}, 585.9 cm^{-1}, 721.4 cm^{-1}, which gives ω_e = 136.3 ± 0.2 cm^{-1} with $\omega_e x_e$ = 0.14 ± 0.05 cm^{-1}, leading to a spectroscopic dissociation energy of 4.1±1.2eV., which we assigned to an excited (A) state.

II. EXPERIMENT

The CCNY cluster deposition source has been described in detail elsewhere[7,8] Briefly, an argon ion beam (typically 10 mA at 25 keV) sputters a cooled, terbium target (Alfa Aesar, 99.9% (REO)). The sputtered products are extracted by electrostatic lenses, mass-selected using a Wien filter, bent by 10° to eliminate neutrals (produced during sputtering) and then guided and focused by an einzel lens into the deposition region. Terbium dimer (or atomic) ions were then codeposited with argon gas and electrons onto a ~ 16 K CaF_2 plate substrate. Prior to deposition, the selected ions were simultaneously slowed to 15 eV by a surrounding "Faraday cage " to ensure soft landing. Ion currents under hard landing conditions (V_{dep}=300V) could be measured on the Faraday plate in the deposition region and were: Tb^+ (110 nA), Tb_2^+ (25 nA). Matrices were grown at about 6 μm/h with an Ar : metal ratio of approximately 10^4 : 1. By comparing the intensities of known atomic excitation features in a dimer deposition with those obtained from deposition of atom under similar conditions, the dimer fragmentation is estimated to be less than 10%.

Matrix samples were interrogated *in situ* using both absorption and Raman spectroscopy. As previously described[7,8], the absorption measurements were made by collecting the light at 90° to that incident, a technique we term "Scattering Depletion Spectroscopy" (SDS). Raman spectra were recorded using a dye laser (Coherent, Model CR599) with DCM, pumped by the "green-blue" lines of an argon ion laser (Spectra Physics 2045) for excitation. Raman excitation profiles were obtained by observing the Raman spectra while tuning the dye laser in small steps through the absorption region 620-680 nm. Scattered light was collected at 90° into a Spex 1877E 0.6 m Triplemate

Spectrometer and detected by a liquid nitrogen cooled CCD detector (Spex model "Spectrum One", and CCD30) with DM3000R software connected to a computer. All Raman results were calibrated using the CaF_2 (substrate) line at 327 cm^{-1}. The absorption (SDS) spectrum was recorded following a 5 hours deposition of 18 nA of Tb_2.

III. SPECTRA AND ANALYSIS

A portion of the absorption spectrum, shown as Fig. 4.5.1 are the only absorption features that we could definitely assign to the dimer. This assignment is verified by the observation of resonance Raman spectra for excitation into these bands. The Raman excitation profiles, obtained by dividing the Raman intensity (of the first Stokes line) by intensity of CaF_2 Raman line, are superimposed in this figure.

Raman spectra were observed throughout the region 623-673 nm , Fig. 4.5.2 shows a typical Raman spectrum (excited at 652.7nm) for a 90 nA-h sample of diterbium in argon matrices. A nonresonant Raman line at 327cm^{-1} due to the CaF_2 substrate is also in evidence and is used as a wavelength calibration. The Raman spectrum consists of two distinct progressions, the average Raman shift for over 47 spectra at different wavelengths (between 623nm and 673nm) is listed in Table 4.5.1 and Table 4.5.2.

Data in Table 4.5.1 give for the ground (X) state ω_e = 137.6 ± 0.4 cm^{-1} with $\omega_e x_e$ = 0.31 ± 0.05 cm^{-1}, leading to a force constant k_e = 0.88 ± 0.01 mdyne/Å, and spectroscopic dissociation energy of 1.9 ± 0.3 eV. Our value for the dissociation energy is only slightly higher than that obtained by the third law techniques by Kant and Lin[5] which is 1.4 ± 0.3 eV or that obtained by Kordis and Gingerich[4], which is 1.33 ± 0.26

eV. The latter also use the Guggenheimer[8] method to predict an ω_e = 135cm^{-1} in good agreement with our experimental results.

Lines shown in Table 4.5.2 are assigned to a low lying electronic (A) state at T_0=313.9cm^{-1}, with ω_e = 136.3 ± 0.2 cm^{-1} and $\omega_e x_e$ = 0.14 ± 0.05 cm^{-1}, leading to a spectroscopic dissociation energy of 4.1 ± 1.2eV.

As can be seen from Figure 4.5.1, the Raman excitation profile of the ground X state is almost identical to the absorption spectrum (SDS), and in fact appears more sensitive. The bands are centered at approximately 633nm and 645nm. The excitation profile of the origin band of the A transition, though much less sensitive, appears to have a somewhat different profile, peaking at longer wavelength. Due to the low signal/noise ratio of this spectrum it is not possible to draw any reliable conclusions from this.

IV. DISCUSSION

Terbium lies next to gadolinium in the periodic table. The ground state configuration of Tb atom is [Xe] 4f ^{9}6s^2 while that for Gd is [Xe] 4f ^{7}5d^{1}6s^2.The promotion energy for 4f ^{9}6s^2 → 4f ^{8}5d^{1}6s^2 in Tb (utilizing only the lowest spin-orbit levels) is only 0.035eV. Thus it is not surprising that the dimer force constants are almost identical: k_e =0.88mdyn/Å for Tb_2 while k_e = 0.89mdyne/Å for Gd_2[3]. Both force constants are comparable to that for Y_2 (0.90mdyne/Å)[9] and therefore most likely correspond to a bond order of 1. The lack of ability to form stronger bonds, as for example in La_2[1] (k_e =2.28mdyne/Å) can at least partly be attributed to the rather high 6s→5d promotion energies, 1.87eV and 0.79eV for Tb and Gd respectively. The 6s→ 5d

promotion energy is likely to be important since a $6s^1$ configuration is thought to promote stronger chemical bonding. La, for example, has a promotion energy of only 0.33eV, leading to a likely bond order of more than two.

Note that although the observed first excited (A) state lies only at T_0=313.8cm^{-1}(0.039eV) above the ground state, its dissociation energy (4.1eV) is considerably higher. It is thus likely that the excited state dissociates to atomic states separated by 2.2eV (4.1eV-1.9eV) from those of the ground state. It is possible that the s→d promotion energy for one atom 1.9eV accounts for this difference. It is consistent then to postulate that the ground state arises from two ground state $4f^96s^2$ (or $4f^85d^16s^2$) atoms while the first excited state from one $4f^96s^2$ (or $4f^85d^16s^2$) and one $4f^95d^16s^1$ (or $4f^85d^26s^1$) atom.

Dolg, Stoll and Preuss[10] have carried out density functional calculations employing psuedopotentials with configuration-interaction on homonuclear diatomic lanthanides. For all the dimers, they predict several low lying states. Most important among these are a $^5\Sigma_u^-$ state from a $4f^n4f^n\sigma_g^2\sigma_u^1\sigma_g^1\pi_u^2$ state configuration, as well as a $^1\Sigma_g^+$ from a $4f^n4f^n\sigma_g^2\sigma_u^2\sigma_g^2$ configuration. Their results indicate the $^5\Sigma_u^-$ to be the ground state in Tb_2. Our results would tend to confirm this prediction in that the $^5\Sigma_u^-$ has a lower formal bond order (and vibrational frequency) than the $^1\Sigma_g^+$ state. This raises the question as whether the A state may be the $^1\Sigma_g^+$. This assignment is somewhat less likely, since the vibrational frequency observed is not much different than that of the ground state, although the dissociation energy is much larger. Clearly a more detailed theory is in order to establish firmly the nature of these states.

Table 4.5.1 Vibrational progression for the ground (X) state of Tb_2.

v''	1	2	3	4	5	6	7
Raman Shift (cm^{-1})	137.6	273.6	409.3	544.5	679.2	813.5	946.3

Table 4.5.2 Vibrational progression for the first excited (A) state of Tb_2

v'	0	1	2	3
Raman Shift (cm^{-1})	313.9	450.0	585.9	721.4

REFERENCE

[1] Liu, Y.; Fang, L.; Shen, X.; Chen, X.; Lindsay, D. M.; Lombardi, J. R.; *Chem. Phys.*, to be published.

[2] Shen, X.; Fang, Li; Chen, X; Lombardi, J.R., *J. Chem. Phys.* **2000**, 113, xxxx, in press

[3] Chen, X.; Fang, Li; Shen, X; Lombardi, J.R., *J. Chem. Phys.* **2000**, 112, 9780

[4] Kordis, J., Gingerich, K.A., and Seyse, R.J., *J. Chem. Phys.* **1972**, 61, 12

[5] Kant, A.; Lin, S. S. *Monatsh. Chem.* **1972**, 103, 757

[6] Hu, Z.; Shen, B.; Lombardi, J. R.; Lindsay, D. M. *J. Chem. Phys.* **1992**, 96, 8757

[7] Hu, Z.; Shen, B.; Zhou, Q.; Deosaran, S.; Lombardi, J. R.; Lindsay, D. M. *Proc. SPIE* **1991**, 1599, 65

[8] Guggenheimer,K.M. *Proc. Phys. Soc.* **1946**, 58, 456

[9] Fang, L.; Chen, X.; Shen, X.; Liu, Y.; Lindsay, D. M.; Lombardi, J. R. *Low Temperature Physics* **2000**, 26, xxxx, in press

[10] Dolg, M.; Stoll, H.; Preuss, H. *J. Mol. Struct. (Theochem)* **1992**, 277, 239

Figure 4.5.1 Resonance Raman spectrum (λ_{ex} = 652.6 nm) of terbium dimer in argon matrices.

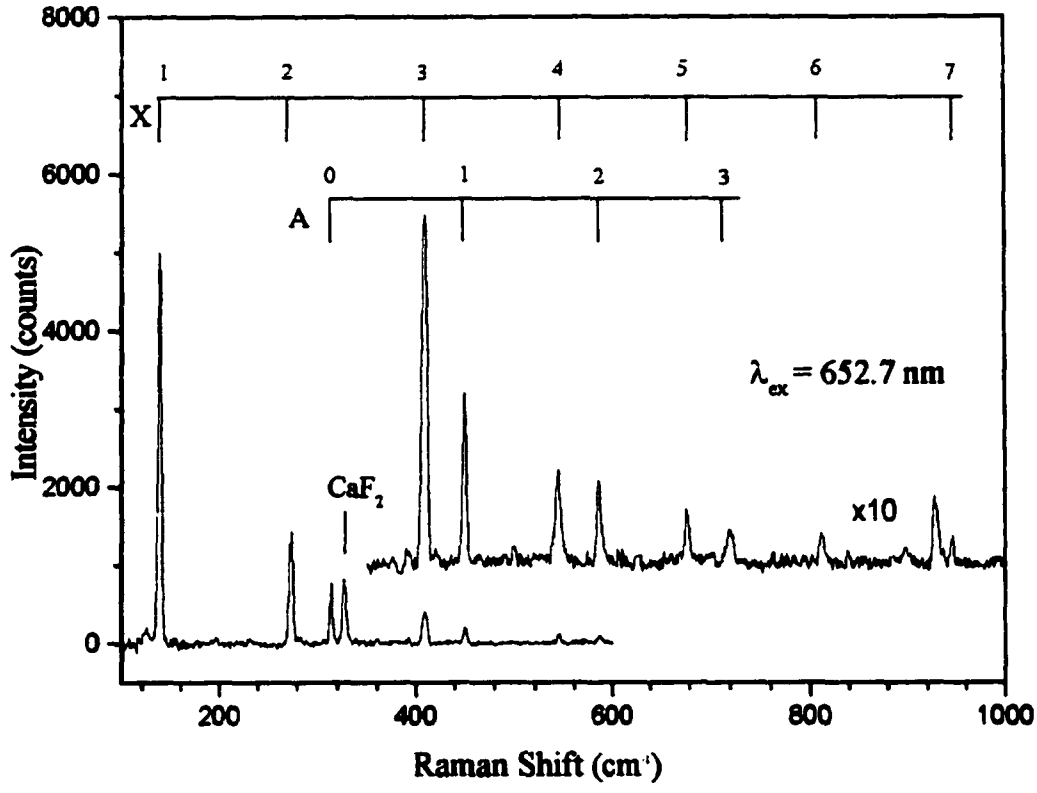

Figure 4.5.2 Absorption (scattering depletion) spectrum (right hand scale) and Raman excitation profile for ground state (X) and excited state (A) transition of terbium dimers in argon matrices.

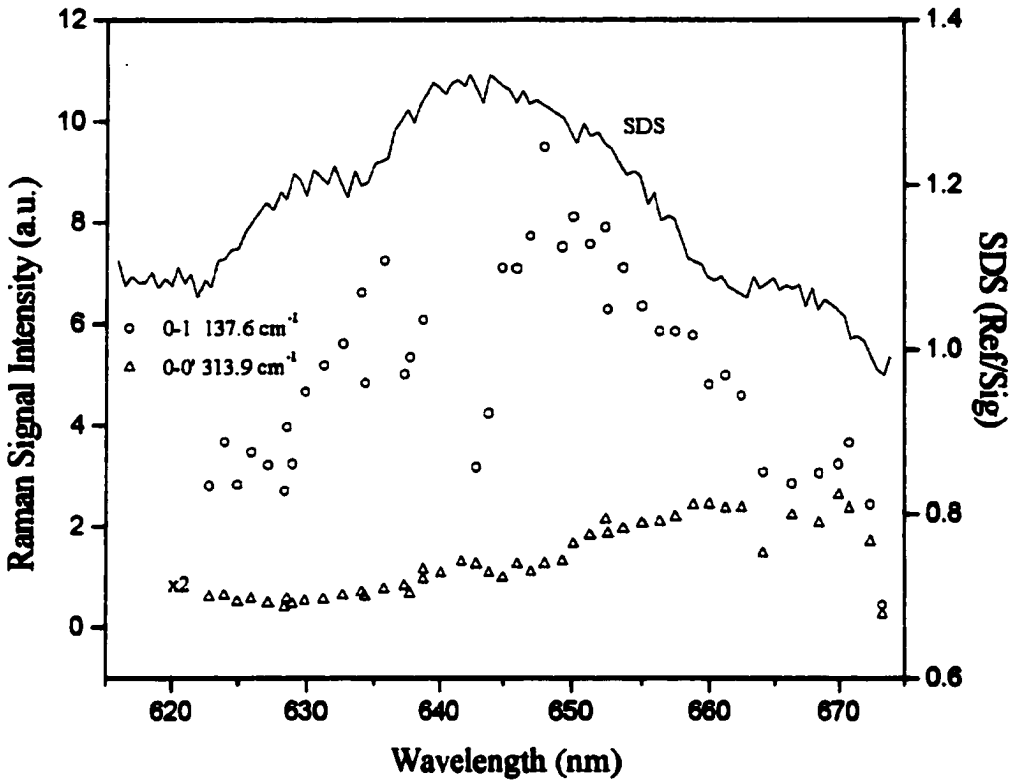

4.6 Raman and Absorption Spectrum of Mass-Selected Lutetium Dimers in Argon Matrices

J. Chem. Phys., submitted

I. INTRODUCTION

We have recently examined the optical and resonance Raman spectra of several metal dimers, including Y_2[1], Hf_2[2] and La_2[3]. The observation of an anomalously high dimer force constant for La_2 in comparison to its near neighbors led us to extend our work to the spectra of several of the lanthanide dimers, including Ce_2, Pr_2, Nd_2[4], Gd_2[5], and Tb_2[6].This work produced the interesting result that all measured dimer force constants fell into only two distinct groups: near 2.3 mdyne/Å or near 0.9 mdyne/Å.

Lutetium holds a unique position among the lanthanides in that its atom configuration ($4f^{14}5d6s^2$) involves a filled *f* shell along with one *d* electron. However, just prior to Lu is Yb ($4f^{14}6s^2$) which, like most of the other lanthanides, has a $4f^n6s^2$ configuration. This has been interpreted to imply that the lanthanides should actually be considered to run from La through Yb, and Lu should occupy the position preceding Hf in the periodic chart [7]. It is thus worth examining the Raman spectrum of Lu_2 to determine if its force constant fits the periodic trends better than La_2.

In this article we examine the optical and resonance Raman spectra of Lu_2. With the SDS technique[8], we obtained the absorption spectrum of Lu_2 in argon matrices. Two broad absorption regions were found between 415-545nm peaking at 418nm, 430nm, 452nm, 470nm, 502nm, 540nm, and between 635-660nm, peaking at 640nm, 652nm.

Resonance Raman spectra were obtained by excitation into one of these regions with the visible light of an Ar ion laser between 458-514nm. Two progressions were assigned to lutetium dimers. We interpret them to represent two distinct electronic states: the ground state X and an excited state A. For the ground (X) state, we obtain $\omega_e = 121.6 \pm 0.8$ cm^{-1} with $\omega_e x_e = 0.16 \pm 0.10$ cm^{-1}, leading to a spectroscopic dissociation energy of 2.86 ± 1.8 eV, force constant $k_e = 0.76 \pm 0.01$ mdyne/Å. The first electronic (A) state has an origin at 210.7 cm^{-1}, and almost identical vibrational parameters. These results provide clear evidence that Lu_2 fits the periodic trends much better than La_2 and provides support for the proposed replacement of La with Lu in the periodic table.

II. EXPERIMENT

The CCNY cluster deposition source has been described in detail elsewhere[9,10] Briefly, an argon ion beam (typically 10 mA at 25 keV) sputters a cooled, lutetium target (Alfa Aesar, 99.9% (REO)). The sputtered products are extracted by electrostatic lenses, mass-selected using a Wien filter, bent by 10° to eliminate neutrals (produced during sputtering) and then guided and focused by an einzel lens into the deposition region. Lutetium dimer (or atomic) ions were then codeposited with argon gas and electrons onto a ~ 16 K CaF_2 plate substrate. Prior to deposition, the selected ions were simultaneously slowed to 10 eV by a surrounding "Faraday cage " to ensure soft landing. Ion currents under hard landing conditions (V_{dep}=300V) could be measured on the Faraday plate in the deposition region and were: Lu^+ (400 nA), Lu_2^+ (10 nA). Matrices were grown at about 5

μm/h with an Ar : metal ratio of approximately 10^4 : 1. By comparing the intensities of known atomic excitation features in a dimer deposition with those obtained from deposition of atom under similar conditions, the dimer fragmentation is estimated to be less than 30%.

Matrix samples were interrogated *in situ* using both absorption and Raman spectroscopy. As previously described [9,10], the absorption measurements were made by collecting the light at 90° to that incident, a technique we term "Scattering Depletion Spectroscopy" (SDS). Raman spectra were recorded using a dye laser (Coherent, Model CR599) with DCM, pumped by the "green-blue" lines of an argon ion laser (Spectra Physics 2045) for excitation. Raman excitation profiles were obtained by observing the Raman spectra while tuning the dye laser in small steps through the absorption region 620-680 nm. Scattered light was collected at 90° into a Spex 1877E 0.6 m Triplemate Spectrometer and detected by a liquid nitrogen cooled CCD detector (Spex model "Spectrum One", and CCD30) connected to a computer with DM3000R software. All Raman results were calibrated using the CaF_2 (substrate) line at 327 cm^{-1}. The absorption (SDS) spectrum was recorded following a 5 hours deposition of 10 nA of Lu_2.

III. SPECTRA AND ANALYSIS

In figure 4.6.1 we show the absorption spectrum of Lu_2 in argon matrices, and for comparison that of the atom. As mentioned in the previous section, we estimated the dimer fragmentation ratio to be around 30%. The remaining differences may be attributed

to the dimer, for which we identify bands at 418nm, 433nm, 452nm, 472nm, 505nm, 540nm, and 640nm, 652nm. We also show in figure 4.6.1 the Raman excitation profile of several lines for the range 458~514nm in which Raman intensity was observed. Although the absorption spectrum in this region displays some interference from the fragmented atomic spectrum, the Raman profiles show clearly parts due to the dimer.

The Raman spectra themselves show two distinct progressions with vibrational spacing of approximately 121 cm^{-1}. In figure 4.6.2 we show a typical spectrum excited at 501.7nm. The first progression originates at the laser line and may be assigned to the ground electronic (X) state. It consists of six lines which are listed in table 4.6.1. The listed frequencies represent averages over 14 spectra. Using standard methods , we obtain from these lines ω_e = 121.6 ± 0.8 cm^{-1} and $\omega_e x_e$ = 0.16 ± 0.10 cm^{-1}. The resulting force constant is k_e = 0.76 ± 0.01 mdyne/Å, and assuming a Morse potential we infer the dissociation energy of D_e = 2.9 ± 1.8 eV. Several of the observed lines (n=2,3,4) appeared doublet with additional lines shown in table 4.6.1. These cannot be due to isotopes, however they persist even after annealing the matrix to 36K. Normally such splittings are attributable to higher energy sites in matrix, which can be removed by annealing. Lacking any other simple explanation, it is likely that these lines are due to a site occupied with sufficiently low in energy to remain even when the matrix is cooled slowly.

A second progression originates (Table 4.6.2) at 210.7cm^{-1} and we assigned these lines (up to n=7) to a low lying excited (A) state at T_0 = 210.7cm^{-1} with ω_e = 121.4 ± 1.0 cm^{-1} and $\omega_e x_e$ = 0.15 ± 0.11 cm^{-1}. For this state k_e = 0.76 ± 0.01 mdyne/Å, and D_e = 3.1 ± 2.2 eV. These parameters are almost exactly the same as those of X state, implying a common configurational origin.

Our value for the dissociation energy of the lowest lying state is considerably higher than that obtained by thermodynamic measurements D_e =1.43 ± 0.34 eV[11]. However our errors in this parameter are considerable due to the large relative uncertainty in our value of $\omega_e x_e$, and in this case the thermodynamic measurements should be considered more reliable.

IV. COMPARISON OF LANTHANIDE PROPERTIES

This work was originally inspired by an earlier measurement of the force constant in La_2 which seemed to be anomalously high[3], in comparison to nearby dimer force constants, especially those of Y_2[1] and Hf_2[2] Subsequently we examined several of the intervening lanthanide dimers, including Ce_2[4], Pr_2[4], Nd_2[4], Gd_2[5], Tb_2[6]. The remaining species were not examined for reasons of economy and time. In addition from previous experience, we felt that due to the rather low value of their thermodynamic dissociation energies, the remaining dimers were likely to be unstable either in our sputtering source or easily fragmented under our deposition conditions.

In table 4.6.3 we show a comparison of several properties of lanthanide atoms and dimers including the thermodynamic dissociation energies[11], and our measured force constants.

When we first embarked on this study we expected the force constants might either vary monotonically across the lanthanides following Badger's rule (k_e $(r_e-d_{ij})^3$ = C)[12] or possibly track the measured dissociation energies (see table 4.6.3). Instead, they

fall into two sharply distinct groups, either close to 2.28 mdyne/Å (La_2, Ce_2, Pr_2) or close to 0.88 mdyne/Å (Nd_2, Gd_2, Tb_2, Lu_2). Due to the much lower dissociation energies, it is likely that remaining lanthanide dimers are also around 0.88 mdyne/Å or less. This is confirmed in several cases by the calculations of Dolg, Stoll and Preuss[13]. Following Pauling's rule[14] that force constants are a linear function of the bond order, and recognizing the similarity to Y_2 (k_e =0.90 mdyne/Å) we may safely ascribe the lower group of force constants to a bond order of around 1, while the higher group then corresponds to a bond order between 2 and 3. This observation is highly suggestive of a possible shift in ground state configuration between Pr_2 and Nd_2. In earlier work we attributed the relatively high force constant in La_2 to the very low 6s → 5d promotion energy in La (see table 4.6.3), however this does not adequately explain the similarly large value in Pr_2[4]. At this point it might be useful to turn to theory for guidance. Calculations in molecules with such high atomic number are difficult due to increasing importance of relativistic effects[15]. Dolg, Stoll and Preuss[13] use quasi-relativistic pseudopotentials in a configuration interaction and correlation density functional study of lanthanide dimers. They found four low lying states, a $^5\Sigma_u^-(\sigma_g^2\sigma_u^1\sigma_g^1\pi_u^2)$, a $^1\Sigma_g^+(\sigma_g^2\pi_u^4)$, a $^1\Sigma_g^+(\sigma_g^2\sigma_u^2\sigma_g^2)$ and a somewhat higher $^5\Delta_u(\sigma_g^2\sigma_u^1\pi_u^2\delta_g^1)$. It is most likely that La_2, Ce_2 and Pr_2 have the same ground state, whereas, Nd_2, Gd_2, Tb_2 and Lu_2 have another one. The $^1\Sigma_g^+(\sigma_g^2\pi_u^4)$ is a likely candidate for the first three since it has the highest formal bond order (3). This leaves either the $^1\Sigma_g^+(\sigma_g^2\sigma_u^2\sigma_g^2)$ or the $^5\Sigma_u^-(\sigma_g^2\sigma_u^1\sigma_g^1\pi_u^2)$ for the rest. The $^1\Sigma_g^+$ state has a formal bond order of 1. However the observation of an extremely large magnetic moment in Gd_2[16] indicates a $^{19}\Sigma_g^+$ ground state. Assuming strong

ferromagnetic coupling of the two sets of $4f^7$ electrons, this high spin state most likely originates from the $^5\Sigma_u^-(\sigma_g^2\sigma_u^1\sigma_g^1\pi_u^2)$ state.

Further we have observed low lying electronic states in Tb_2 and Lu_2 both of which show almost exactly the same force constant as the ground state in each species. Those observations hint that the two states originate from the same configuration in each molecule, perhaps representing a second-order spin-orbit splitting. The spin-orbit coupling constant for Lu[17] is $\zeta(5d) = 1{,}158\ cm^{-1}$, large enough to cause splitting of say the $^5\Sigma_u^-$ by 200 cm^{-1} even if the perturbing state (triplet or quintet Σ or Π state) is as far as 6,700 cm^{-1}. If true, this eliminates either $^1\Sigma_g^+$ as the ground state in Tb_2 and Lu_2. Thus we suggest the $^5\Sigma_u^-$ as the correct ground state for Nd_2, Gd_2, Tb_2 and Lu_2.

Examining our recent works in conjunction with spectra from other source it is now possible to compare visible and near ultraviolet bands of almost all of the lanthanides. In table 4.6.4 we collect the results of either absorption, SDS or Raman excitation profiles of numerous lanthanide dimers. Included for comparison are the bands in Y_2 and Hf_2 as well. Note that all observed dimer spectra show one or more of three distinct bands, centered around an average of 485nm (blue), 549nm (green) and 631nm (red). Even though not all three bands appear for each dimer, the constancy of the observed wavelength across the series is remarkable. Still more remarkable is that the energy spacing of these bands is the same at around 2,380 cm^{-1}. It is, of course, possible that these numbers are coincidental. More likely they reveal an underlying set of electronic states which are common to all lanthanide dimers. The intensity of these bands indicates that they most likely correspond to an allowed atomic transition, say a nearby allowed $6s \rightarrow 6p$ transition. In atomic lutetium the $^4F^\circ$ ($4f^{14}5d6s6p$) state could lead to an

excited $^3\Pi$ giving an equally spaced triplet with Ω = 0, 1, 2. The atomic $6p$ spin orbit coupling constant may be inferred from atomic energy levels [18] to be $\zeta(6p) = 3{,}454\ cm^{-1}$. To the extent that the spin-orbit splitting of the excited state is first order ($A\Lambda\Sigma$), we predict $A = 3{,}454/2 = 1{,}727\ cm^{-1}$ somewhat lower than the observed value of $2{,}380\ cm^{-1}$, but certainly of reasonable magnitude. Nonetheless, labeling for the moment the red transition $\Omega = 2$, green $\Omega = 1$ and blue $\Omega = 0$ (i.e. an inverted state), we may examine more carefully the pattern of appearance of the bands across the lanthanides. Of course, too much should not be read into the lack of observation of a transition, especially for those as broad as observed here. However, it is provocative that for La_2, Ce_2 and Pr_2, the blue and green transitions are observed, while for the remaining dimers starting at Nd_2 (except Ho_2 and Lu_2) it is the green and red transitions which appear. This is the same place (i.e. between Pr_2 and Nd_2) that a break is observed in the force constants, indicating a sharp change in the orbital nature of the ground state. Assuming the selection rules $\Delta\Omega = 0,\pm1$, say with the excited state values of Ω suggested above, the ground state in La_2, Ce_2 and Pr_2 would correspond to an $\Omega = 0$ (e.g. $^1\Sigma_g^+$) state while the others would correspond to $\Omega = 2$ (e.g. $^5\Sigma_u^-$). See figure 4.6.3. Although this scheme is speculative, it is consistent with the assignment suggested above.

In conclusion, despite considerable disparities in properties across the lanthanides, we have obtained remarkable consistency in spectroscopic properties. The observed force constants fall into two narrow categories, while the three observed visible transitions are nearly invariant in wavelength. A full explanation of these observations awaits more accurate calculations.

V. PERIODIC PROPERTIES OF LUTETIUM VS. LANTHANUM

In any case, it is now at least clear how to reinterpret the rather large force constant of La_2. As discussed previously[3], the observed frequency for La_2 leads to a force constant of $k_e = 2.28(1)$ mdyne/Å. The corresponding values for Sc_2[22] and Y_2[1] are 0.756 and 0.90 mdyne/Å respectively. This trend is in marked contrast to the tendency of the early third row transition metal dimer force constants to decrease in comparison to the corresponding first and second row dimers. A good example of this effect shows readily in the adjacent column: Ti_2[23] (2.35 mdyne/Å), Zr_2[24] (2.511 mdyne/Å), Hf_2[2] (1.63 mdyne/Å). (For a more complete chart of transition metal dimer force constants, refer to URL: http://www.sci.ccny.cuny.edu/~lombardi). The same anomaly is apparent if we compare force constants along the same row. In the first and second row of transition metal dimers the group 3B force constants are lower than those of the adjacent 4B, 5B and 6B force constants. For La_2 in the third row, the force constant is higher than that of Hf_2. We previously explained this as due to increased bonding afforded by the relatively low promotion energy for La. The ground state of Sc, Y, La and Lu all have a d^1s^2 configuration leading to a ^{2}D ground state. All have a nearby d^2s^1 configuration (^{4}F state) which is much more favorable for bonding. The La $^2D \rightarrow {}^4F$ promotion energy (0.33 eV) is much lower than that of Lu (2.34 eV) which itself is much more similar to that of Hf $^3F \rightarrow {}^5F$ ($5d^26s^2 \rightarrow 5d^36s^1$, 1.94 eV). We thus expect La_2 to exhibit stronger bonding than either Y_2, Lu_2 or Hf_2.

This analysis raises the question as to whether it would be more suitable to replace La with Lu in the periodic table. The lower value for the Lu_2 force constant measured here fit the trends for the other rows and columns better than that from La_2 In fact this has been suggested by several other observers. Jensen[7] has analyzed just this issue. He shows various trends in atomic radii, ionization potential, melting points and electronegativities which support his contention. Furthermore, Jensen points out that the assignment of La to group 3B in most textbooks is due to early spectroscopic work which indicated an electronic configuration $4f^n5d^16s^2$ for the ground state of lanthanide atoms. However subsequent research showed that except for Ce, Gd and Lu, the ground state $4f^n6s^2$ prevails. Thus Yb has the configuration $4f^{14}6s^2$ and Lu may then be regarded as having a differentiating *d* electron, making it a valid candidate for first member of the *d*-block for sixth period. In addition to Jensen's arguments we would like to add observations of the relativistic corrections to the contraction of the 6*s* shell from the calculations of Desclaux[25]. A plot of the ratio of relativistic $\langle r_{6s} \rangle$ to the non relativistic value is shown in figure 4.6.4. Note the sharp break in slope between Yb and Lu. At least relativistically Lu belongs to the *d*-block elements and the lanthanides should be considered to run from La through Yb. This combined with our measurements of dimer force constants add weight to the arguments in favor of reexamining the common placement of La and Lu in the periodic table.

Table 4.6.1 Vibrational progression for the ground (X) state of Lu_2.

v''	1	2	3	4	5	6
Raman Shift (cm^{-1})	121.1	242.1	363.3	482.2	603.1	722.4
		249.3	373.3	497.4		

Table 4.6.2 Vibrational progression for the first excited (A) state of Lu_2

v'	0	1	2	3	4	5	6	7
Raman Shift (cm^{-1})	210.7	332.5	453.5	571.9	692.1	813.0	933.3	1051.9
	204.5		447.9	578.1	702.0			

Table 4.6.3 Configuration of ground state, promotion (6s→5d) energies (eV), atomic radii (10^{-12}m), ionic (3+) radii, ratio of relativistic to non-relativistic 6s orbital radial expectation values*, dimer dissociation energies** D_0 (eV), and force constant*** k_e (mdyne/Å) of lanthanides.

Element	La	Ce	Pr	Nd	Pm	Sm	Eu	Gd	Tb	Dy	Ho	Er	Tm	Yb	Lu
Configuration($6s^2$)	$5d^1$	$4f^15d^1$	$4f^3$	$4f^4$	$4f^5$	$4f^6$	$4f^7$	$4f^75d^1$	$4f^9$	$4f^{10}$	$4f^{11}$	$4f^{12}$	$4f^{13}$	$4f^{14}$	$4f^{14}5d^1$
P.E.	0.33	0.29	1.00	1.05		1.34	1.60	0.79	1.87	2.17	2.34	2.40	2.53	3.04	2.34
Atomic r_e	187	183	182	181	181	180	199	179	176	175	174	173	173	194	172
Ionic (3+) r_e	107	103	101	99		96	95	94	92	91	89	88	87	86	84
$\langle r_{6s}\rangle_{rel}/\langle r_{6s}\rangle_{non\text{-}rel}$	.958	.955	.958	.956	.954	.951	.949	.939	.945	.942	.940	.937	.935	.932	.916
D_0	2.50	2.57	1.30	0.82		0.52	0.43	1.8	1.4	0.69	0.69	0.74	0.52	0.13	1.43
k_e	2.28	2.48	2.49	0.93				0.89	0.88						0.76

* The numbers are taken from the Dirac-Fock and Hartree-Fock calculation of Desclaux, J. P., *At. Data Nucl. Data Tables*, **12**, 311(1973)

** Dimer dissociation energies from third law measurements of Kant, A. and Lin, S. S., *Monatshefte fur Chimie*, **103**,757-763(1972). See also (for Tb_2) Kordis, J., Gingerich, K. A. and Seyse, R. J., *J.Chem.Phys.*, **61**, 12(1972). See also Connor, J. A., in *Metal Clusters in Catalysis, Studies in Surface Science and Catalysis 29*, B. A. Gates, L. Guczi and H. Knoezinger (Eds.), Elsevier, Amsterdam, (1986).

*** Obtained in our experiments.

Table 4.6.4 Lanthanide dimer optical transitions (nm)

	Blue	Green	Red	Reference
Y_2	485			1
La_2	490	540,560		3
Ce_2	485	547		4
Pr_2	465	535		4
Nd_2		520	640	4
Sm_2		541	599	19
Gd_2		585	620	5
Tb_2			633,645	6
Ho_2	498,504	558,562		20
Yb_2		555		21
Lu_2	505	540	640,652	This paper
Hf_2	450	540	620	2

REFERENCE

[1] Fang, L.; Chen, X.; Shen, X.; Liu, Y.; Lindsay, D. M.; Lombardi, J. R. *Low Temperature Physics* **26**, xxxx (2000), in press

[2] Hu, Z.; Dong, J.; Lombardi, J. R.; Lindsay, D. M. *J. Chem. Phys.* **97**, 9263(1993)

[3] Liu, Y.; Fang, L.; Shen, X.; Chen, X.; Lindsay, D. M.; Lombardi, J. R. *Chem. Phys.*, to be published

[4] Shen, X.; Fang, L.; Chen, X; Lombardi, J. R. *J. Chem. Phys.* **113**, xxxx (2000), in press

[5] Chen, X.; Fang, L.; Shen, X; Lombardi, J. R. *J. Chem. Phys.* **112**, 9780(2000)

[6] Fang, L.; Chen, X.; Shen, X.; Lombardi, J. R. *J. Phys. Chem.*, to be published

[7] Jensen, W. B. *J. Chem. Ed.* **59**, 634(1982)

[8] Hu, Z.; Shen, B.; Zhou, Q.; Deosaran, S.; Lombardi, J. R.; Lindsay, D. M. *Proc. SPIE* **1599**, 65(1991)

[9] Hu, Z.; Shen, B.; Lombardi, J. R.; Lindsay, D. M. *J. Chem. Phys.* **96**, 8757(1992)

[10] Hu, Z.; Shen, B.; Deosaran, S.; Lombardi, J. R.; Lindsay, D. M.; Harbich, W. *J. Chem. Phys.* **95**, 2206(1991)

[11] Connor, J. A. in *Metal clusters in catalysis, Studies in Surface Science and Catalysis* 29, Gates, B. A., Guczi, L. and Knoezinger, H. (Eds.), Elsevier, Amsterdam, 1986

[12] Badger, R. M. *J. Chem .Phys.* **2**, 128(1934); **3**, 710(1935)

[13] Dolg, M.; Stoll, H.; Preuss, H. *J. Mol. Struct. (Theochem)* **277**, 239(1992)

[14] Pauling, L. *The Nature of the Chemical Bond* (Cornell University, Ithaca, NY, 1960)

[15] Pitzer, K. S. *Acc. Chem. Res.* **12**, 271(1979)

[16] Van Zee, R. J.; Li, S.; Weltner, W., Jr. *J. Chem. Phys.* **100**, 4010(1994)

[17] Lefebvre-Brion, H.; Field, R. W. *Perturbations in the spectra of diatomic molecules* (Academic Press, INC., Orlando, Florida, 1986)

[18] Martin, W. C.; Zablubas, R.; Hagan, L. *Atomic Energy Levels-The Rare Earth Elements*, Natl. Bur. Stand. Ref. Data Ser. 60 (U.S. Dept. of Commerce, Washington, D.C., 1978)

[19] Klotzbucher, W. E.; Petrukhina; M. A; Sergeev, G. B. *Mendeleev Commun.* 5-7(1994)

[20] Klotzbucher, W. E.; Petrukhina; .M. A; Sergeev, .G. B. *J. Chem. Phys.* **101**, 4548(1997)

[21] Suzer, S.; Andrews, L., *J. Chem. Phys.* **89**, 5514(1988)

[22] Walch, S. P.; Bauschlicher, C. W., Jr. In *Comparison of Ab Initio Quantum Chemistry with Experiment for Small Molecules*; R. J. Bartlett., Ed.; D. Reidel: Dordrecht, 17-51(1984)

[23] Cosse, C.; Fouassier, M.; Mejean, T.; Tranquille, M.; DiLella, D. P.; Moskovits, M. J. *J. Chem. Phys.* **73**, 6076(1980)

[24] Hu, Z.; Zhou, Q.; Lombardi, J. R.; Lindsay, D. M. In *Spectroscopy of Mass-selected Zirconium Dimers in Argon, in Physics and Chemistry of Finite Systems: from clusters to Crystals, edited by P. Jena, S. N. Kahana, and B. K. Rao (Kluwer Academic, Dordrecht, 1992)*

[25] Desclaux, J. P. *At. Data Nucl. Data Tables* **12**, 311(1973)

Figure 4.6.1 Absorption (scattering depletion) spectrum of lutetium atom (a) and dimer (b) in argon matrices. Insert is the Raman excitation profile for several lines of ground state (X) and excited state (A) transitions.

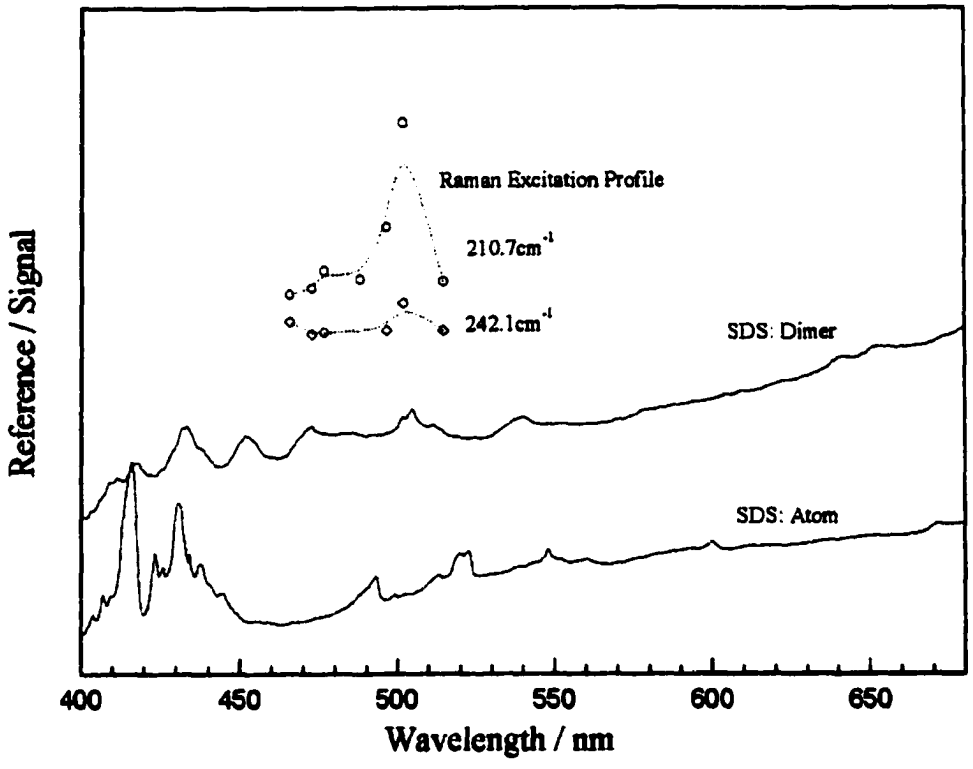

Figure 4.6.2 A typical resonance Raman spectrum at λ_{ex} = 501.7 nm (and parts of the spectrum excited at λ_{ex} = 476.5 nm) of lutetium dimer in argon matrices.

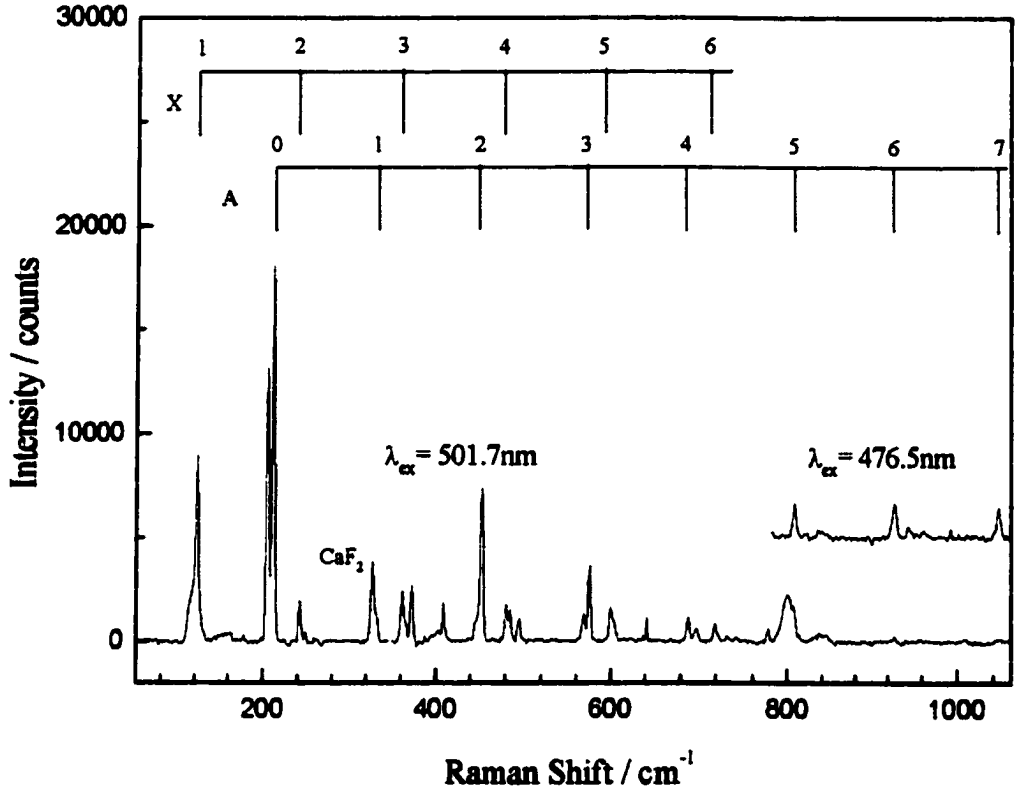

Figure 4.6.3 Optical transitions and suggested assignment for lanthanide dimers.

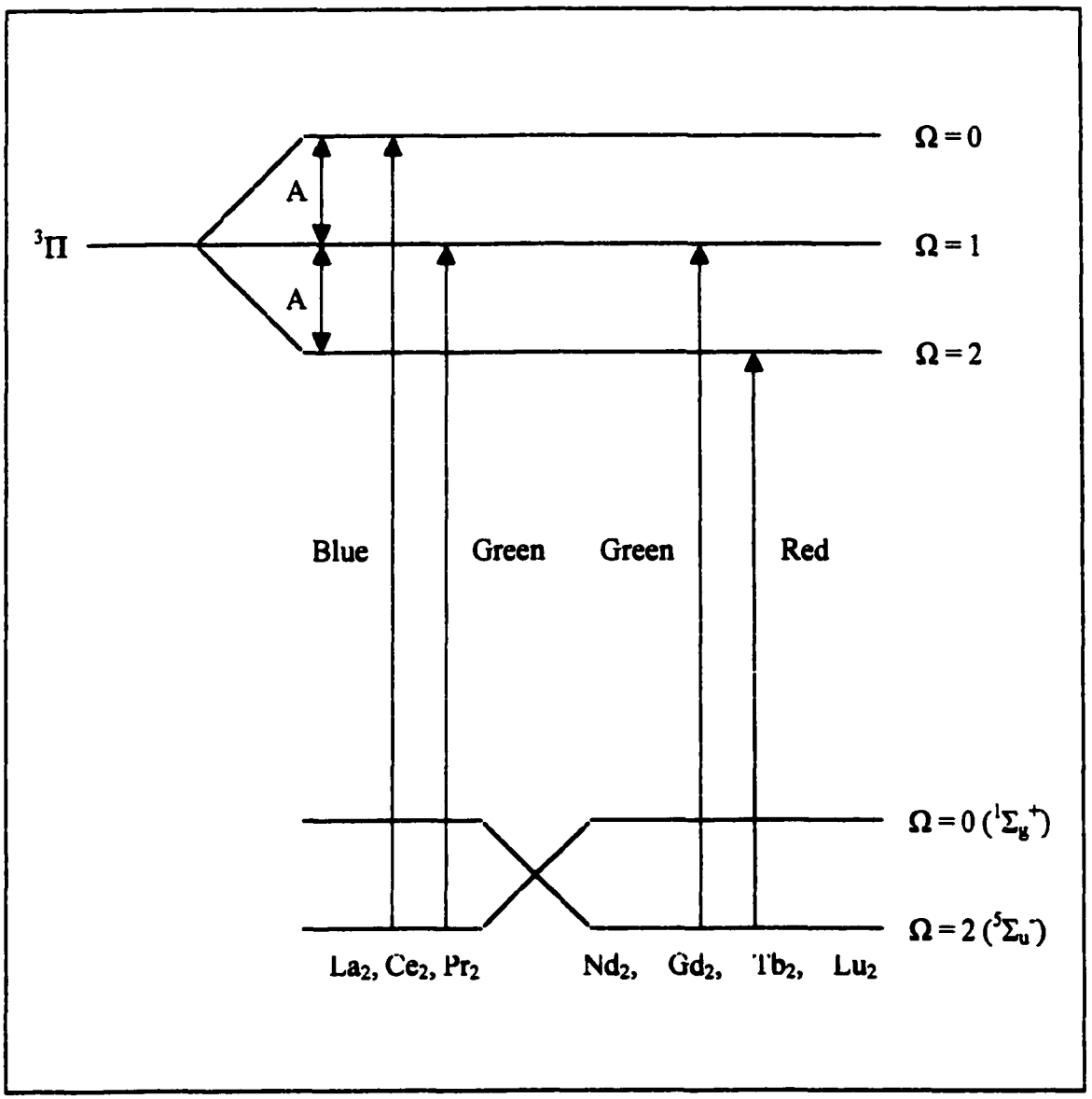

Figure 4.6.4 Ratio of relativistic to non-relativistic 6s orbital radial expectation value, from Desclaux[25].

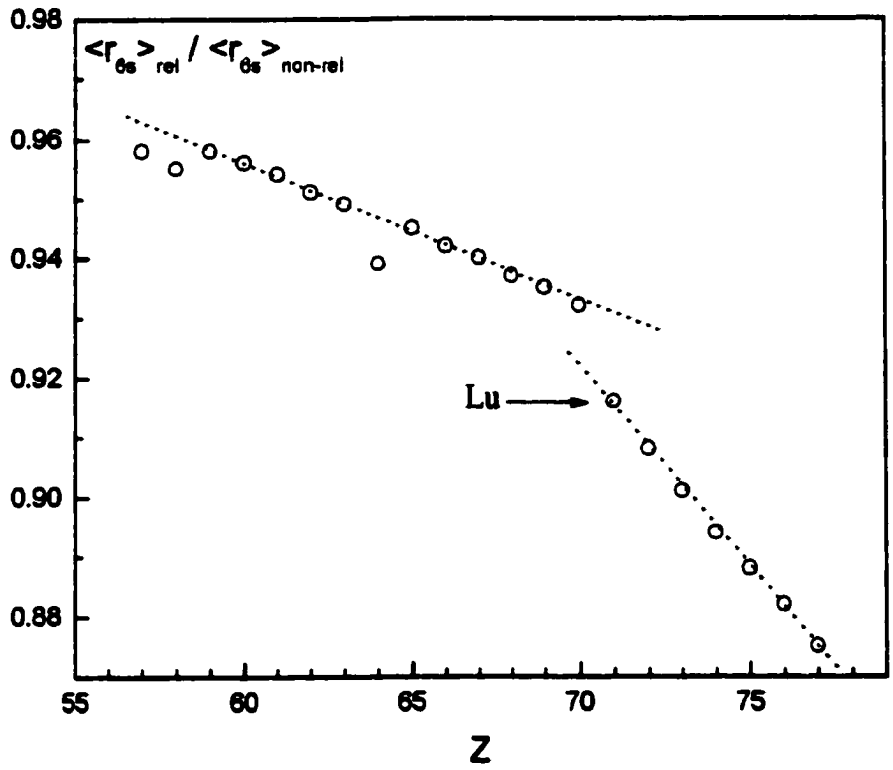

CHAPTER V. Transition Metal Trimers

Structure is the major challenge for investigating metal cluster in both the theoretical and experimental approaches. With information from dimers and atoms, we can extend our exploration to transition metal trimers. Configuration, bonding, frequencies and also geometry are interesting topics for trimer clusters.

In previous investigations of triatomic clusters by the heating method, there has always been incorrect assignments, especially for the absorption. This would not be a problem for our instrument based on mass selection method and abundant knowledge of unambiguous dimer and atom results. Insufficient sputtering production is probably the only limitation. This group has successfully published the trimer of Zr_3, Nb_3, Hf_3 and recently Rh_3, Ru_3, and Ta_3. High quality Raman spectra reveal bonding characteristics of the clusters, as well as geometry information for ground state and low lying excited states. The SDS spectrum and Raman excitation profile suggest the absorption process and excited states properties.

With knowledge of bonding character, we can see how the change takes place from diatomic to triatomic metal clusters. The geometry reveals a lot about configuration and the bonding. Ozin and McIntosh suggested how to predict

the vibrational frequency of higher clusters from that of dimer with central force field calculation [1]. Assuming the interaction between atoms is not changed from dimer to trimer, the trimer vibrational frequency contributes to three atoms. There are three situations possible for trimer geometry, linear, equilateral triangle, and normal triangle. The totally symmetric stretch is the most important for resonance Raman because it bears the character of long progression for overtone and complex transitions. For an equilateral triangle the total symmetric vibration is equally shared and this frequency value should be $\sqrt{3}/2=0.866$ times that of the dimer. In the case of linear symmetry $D_{\infty h}$, only one mode is Raman active. There is no interaction between two end atoms and the totally symmetric frequency of trimer is thought to be the same as that of dimer. When the angle is between 60° and 180°, the frequency number is intermediate. The angle between two arms also determines the other two frequencies in the Raman spectrum, the asymmetric stretch and bending modes. Those two modes are degenerate in an equilateral triangle, and only one line at $\sqrt{2}/2=0.707$ times the symmetric frequency is shown. When the angle is not 60°, two Raman transitions, the antisymmetric vibration and bending

modes are seen besides the symmetric mode. No believable linear metallic trimer has been reported. About half of published trimers have geometry of D_{3h}, and the other half are C_{2v}. It has been suggested that fluxional [2] states with low energy barrier appear in some molecule such as Cu_3 [r1]. In this case, slow experiments like ESR will show an averaged result more like the D_{3h} signal. That may be the reason geometry from ESR differs sometime from that of spectroscopy. Theoretical studies indicate that there will be abundant low-lying excited states for metallic trimers. The Raman spectrum could show their position, frequency, and also geometry. However, the number of states detectable is far less than expected.

The comparison between a dimer and trimer suggests the progression in bonding character from a small cluster to a large one. The ratio of force constant for trimer to that of dimer is 0.5 according to Ozin and McIntosh [1]. In our results, the force constants of Zr_3, Nb_3, Ru_3 and Hf_3 are almost given by the derived factors times the dimer values. For the case of Rhodium, the trimer shows stronger bonding than dimer. It is hard to believe that the trimer force constants would fall into the exact same trends as those of the dimers. Experimental results for Sc_3, Cr_3, Mn_3, Ag_3 are all hardly related with the dimer character. The tendency

of bonding character changes going from dimer to trimer may reveal something about the transition from atom to bulk. Transition metal dimer and trimer force constants from experimental results are summarized in table 5.1. With the results of tantalum trimer, we have successfully published dimer, trimer and tetramer for one element for the first time. We believe further investigation will reveal the force that governs bonding in clusters.

Besides the semi-empirical method with combination of experimental results mentioned above, there are have been a lot of theoretical calculations using molecular orbital methods for clusters. Configuration of both ground state and excited states can be estimated through resonance Raman spectroscopy. One way is comparing with the theoretical results. The other way is from selection rules. The difference between Raman excitation profiles among the possible transition modes is especially helpful. Of course the electronic multiplicity and nuclear equivalent situation provided by ESR experiment are also useful understanding cluster properties.

Table 5.1 Comparison of force constants of dimer and trimer.

	Sc [a]	Ti	V [d]	Cr [g]	Mn [h]	Fe [i]	Co	Ni [k]	Cu [l]	Zn
k_e of Timer	0.55		2.21	1.09	0.38	0.67		0.80	0.91	
k_e of Dimer	0.756	2.348	4.326	3.515	0.094	1.476	1.529	1.162	1.329	0.013
k_e ratio(trimer/dimer)	0.728		0.511	0.310	4.02	0.454		0.688	0.685	
	Y	Zr [b]	Nb [e]	Mo	Tc	Ru [f]	Rh [j]	Pd	Ag [m]	Cd
k_e of Timer		1.19	2.05			1.86	2.10		0.40	
k_e of Dimer	0.896	2.511	4.840	6.433		3.587	2.443	1.382	1.176	0.017
k_e ratio(trimer/dimer)		0.474	0.424			0.519	0.860		0.340	
	Lu	Hf [c]	Ta [f]	W	Re	Os	Ir	Pt	Au	Hg
k_e of Timer		0.71	2.25							
k_e of Dimer	0.762	1.632	4.804	6.144	6.263			2.240	2.115	0.020
k_e ratio(trimer/dimer)		0.435	0.468							

References for Table 5.1

a. M. Moskovits, D. P. Dilella and W. Limm, *J. Chem. Phys.* **80**, 626 (1983)

b. H. Haouri, H. Wang, R. Craig, J. R. Lombardi, D. M. Lindsay, *J. Chem. Phys.* **103**, 9527 (1995).

c. H. Wang, Z. Hu, H. Haouri, R. Craig, Y. Liu, J. R. Lombardi, D. M. Lindsay, *J. Chem. Phys.* **106**, 8339 (1997).

d. D. D. Yang et al. Chem. Phys. Letter, **231**, 177 (1994) S. Alex, S. M. E. Green and D. G. Leopold, 51st International symposium in Molecular Spectroscopy, Columbus Ohio.

e. H. Wang, R. Craig, H. Haouri, Y. Liu, J. R. Lombardi, D. M. Lindsay, *J. Chem. Phys.* **105**, 5355 (1996).

f. "Raman Spectra of Ruthenium and Tantalum Trimers in Argon Matrices"

g. D. P. Dilella, W. Limm R. H. Lipson, M. Moskovits and K. V. Taylor, *J. Chem. Phys.* **77**, 5263 (1982)

h. K. D. Bier, T. L. Haslett, A. D. Kirkwood and M. Moskovits, *J. Chem. Phys.* **89**, 6 (1998)

i. Lai-Sheng Wang, Hang-Song Cheng, Jiawen Fan, *J. Chem. Phys.* **102**, 9480 (1995)

j. L. Fang, X. Shen, X. Chen, and J. R. Lombardi, *J. Chem. Phys.* Submitted for publication

k. M. Moskovits and D. P. Dilella, *J. Chem. Phys.* **72**, 2267, (1979)

l. E. A. Rohlfing and J. J. Valentini, *Chem. Phys. Lett.* **126**, 113 (1986)

m. W. Schulze, H. U. Becker and R. Minkwitz and K. Manzel, *Chem. Phys. Lett.* **55**, 59 (1978)

5.1 Raman spectra of rhodium trimers in argon matrices

J. Chem. Phys. submitted

I. INTRODUCTION

Although rhodium is quite important as a catalyst in many process, there is little experimental information about the properties of small rhodium clusters[1]. The Raman spectra of rhodium dimers in argon matrices have been obtained in our laboratory[2] in 1997. Ozin and Hanlan[3] obtained optical spectra of various rhodium clusters. The only other available experimental information on rhodium trimer is obtained from ESR by Van Zee. *et.al.*[4]. They concluded that rhodium trimer has an equilateral triangle structure (D_{3h} symmetry) with the unpaired spins essentially in non-bonding orbitals involving atomic dδ atomic orbitals. Their result was in agreement with the theoretical calculations of Dai and Balasubramanian[5]. Das and Balasubramanian[6] calculated the potential energy surface of eight low-lying electronic states of Rh_3.

In this paper we report on the observation of resonance Raman spectra of Rh_3 in an argon matrix. Our samples are prepared by neutralizing a mass selected beam of trimer ions. Although the absorption spectrum (scattering depletion spectrum) failed to show any obvious absorption transitions from 200 nm to 850 nm, a rich Raman spectrum was found between 545 nm and 593 nm. Three fundamentals, corresponding to normal modes of a bent (C_{2v})molecule can be assigned, with up to four overtones in the symmetric stretch (a_1). We obtained for this mode ω_e =322.4(6) cm_{-1}, with $\omega_e x_e$ = 0.49(10) cm^{-1}, leading to k_e = 2.10 ± 0.01 mdyne/Å .and an atomization energy of 6.6 ± 1.4 eV. The

asymmetric stretch and bend are found at 259 cm^{-1} and 247.9 cm^{-1} respectively. A line at 400 cm^{-1} is assigned as the original of a low lying excited state.

II. EXPERIMENT

The City College of New York (CCNY) metal cluster deposition source has been described in previous publications[7,8,9]. Briefly, an intense (typically 15mA at 25keV) argon ion beam from a CORDIS ion source sputters on a water cooled rhodium target (Alfa, 99.9% REO) maintained at around 300V. Secondary ions are extracted with a modified Colutron model 200-B lens system and then mass selected using a Wien filter (Colutron 600-B) in conjunction with an approximately 175mm free drift distance and a 6.5mm diameter aperture. After mass selection, the ion beam is bent by 10° using two electric plates to eliminate neutrals and then guided and focused to the deposition region by two einzel-like lenses.

Rhodium trimer ions were codeposited with argon and electrons (generated from a heated tungsten filament) on a polished CaF_2 substrate (~16K). Matrices were grown at ~5μm/hour with an Ar:metal dilution ratio of approximately 10^4: 1. The deposition region was surrounded by a "Faraday Cage" whose potential with respect to the sputtering target controls the kinetic energy (20eV in this experiment) of deposited ions. Ion currents under "soft landing" conditions were approximately: Rh^+(120nA), Rh_2^+(12nA), and Rh_3^+ (12nA). The rhodium trimer sample was prepared with about 6 hours deposition, totally 90nA-h.

Matrix samples were interrogated *in situ* using both absorption and Raman spectroscopy. As previously described[7,8,9], the technique termed SDS was applied. but no obvious absorption feature could be possibly assigned to rhodium trimers.

The Raman spectra were measured by exciting the sample with the visible light (457.9nm-514.5nm) of an argon ion laser (Spectra-Physics model 2045), tunable dye laser and Ti-Sapphire laser. The scattered light was collected at 90° and focused into a Triplemate Spectrometer (Spex 1877E, 0.6m). The scattered light was detected with a liquid nitrogen cooled CCD system (Spectrum One and CCD30). The Raman shifts of Rh_3 were calibrated with the nonresonance Raman line of the CaF_2 (substrate) at 327cm^{-1}.

III. SPECTRA AND ANALYSIS

In figure 5.1.1 we show a typical resonance Raman spectrum of rhodium trimers in argon matrices. Most of the stronger lines are observed over a range of excitation of 540~590 nm, while a few weaker lines show up only in still narrower segments of the excitation range. A summary of the spectral observations is presented in Table 5.1.1. A consistent progression of five lines in 322 cm^{-1} is observed throughout the range, and this is assigned the totally symmetric stretch ν_1. If the molecule were in an equilateral triangular geometry (D_{3h}) we would expect only one more vibration, a doubly degenerate (e') mode at $\nu_1/\sqrt{2}$ [10] or around 228cm^{-1}. Instead we see two lines at 259cm^{-1} and 247.9cm^{-1}. This is characteristic of a bent (C_{2v}) molecule and we may assign these to the $\nu_2(b_1)$ asymmetric stretch and the $\nu_3(a_1)$ bend, respectively. The 259cm^{-1} is somewhat

weaker than the 247.9cm^{-1} line, and we only tentatively assign the still weaker feature at 545cm^{-1} as an overtone $2\nu_2$, indicating considerable anharmonicity, if correct. More certain is the assignment of the line at 496 cm^{-1} to the first overtone ($2\nu_3$) of the bending mode. The only remaining line is that at 400 cm^{-1} which is observed in the range 582~576 nm, centered around 578 nm. It is narrow and moderately intense, but does not fit any scheme of ground state vibrations. All transition metal clusters are expected to have numerous low lying electronic states due to open d-shell atomic configurations. It is not unreasonable to assign this line as the origin of such a state and we designate it is the A state to distinguish it from the X ground state.

The long progression (see Table 5.1.1, The Raman shifts were averaged over 30 spectra at different wavelengths and the standard deviation is included) the symmetric stretch (ν_1) vibration may be fit by standard techniques [11], giving ω_e =322.4(6) cm^{-1}, with $\omega_e x_e$ = 0.49(10) cm^{-1}. From ω_e we may obtain a stretching force constant of k_e = 2.10 ± 0.01 mdyne/Å . This may be compared with the dimer force constant of 2.44 mdyne/Å . If we assume the stretch along the coordinate of the totally symmetric mode (ν_1) to be governed by a Morse potential we may calculate a spectroscopic atomization energy ($Rh_3 \rightarrow 3Rh$) to be $D_e^{at} = \omega_e^2 / 4\omega_e x_e = 6.6 \pm 1.4$ eV.

Despite the fact that, due to our optically thin samples we observed no absorption (SDS) spectra, we are able to obtain a sensitive Raman excitation profile by plotting the observed intensity of individual Raman lines against excitation wavelength. We display several in Figure 5.1.2. A broad band ranging over 540~590 nm with maximum around 575nm is observed for the $n\nu_1$ vibrations. For weaker lines, less distinct profiles are obtained. For the line at 247.9cm^{-1} in the range 576~584 nm, a slow rise to ~ 582nm is

observed followed by an abrupt decline. Other lines show profiles which are too noisy to plot.

IV. DISCUSSION

There have been several previous studies of rhodium trimers. Ozin and Hanlan [3] examined the optical absorption spectrum of various rhodium clusters as well as their behavior under photolysis. Van Zee, Hamrich and Weltner[4] examined dimers and trimers of Co, Rh, and Ir using ESR, while Balasubramanian and coworkers applied the technique of complete active space multiconfiguration self-interaction (CASSCF) plus multireference configuration –interaction (MRSDCI) calculations to both low spin[6] and high spin[5] states of rhodium trimers.

Using argon-metal vapor deposition techniques, varying the relative concentration of metal/argon, Ozin and Hanlan[3] examined the absorption spectroscopy of rhodium clusters in the visible and UV region. As the metal/Argon ratios are increased, new bands are observed which they assign to successively larger clusters. They identified bands at 400 nm and 460 nm which they assigned to Rh_2, one at 490 nm assigned to Rh_3 and a band around 560 nm assigned to higher clusters Rh_n. In our earlier work on rhodium dimer, using the excitation profile, we showed that the band at 490 nm definitely corresponds to the dimer. In this work, we observe saw no Raman excitation of the trimer in the region of 490 nm, but that a band peaking at 575 nm is clearly associated with the trimer. These reassignments illustrate the advantage of using Raman excitation profiles combined with mass-selection to definitively identify optical transitions in metal clusters.

Van Zee *et.al.*[4] examined the ESR spectrum of rhodium trimer and found that the ground state was of high spin, most likely S = 5/2, and observed a hyperfine intensity pattern of 1:3:3:1, which indicates D_{3h} equilateral triangle geometry. Dai and Balasubramanian[5], however, in a calculation involving high-spin low-lying state of the Rh3 predict a $^6A_1$ ground state with an apical angle of 50.8° for the ground state. This state is derived along with a nearby $^6B_2$ (0.02 ~ 0.08 eV) state via Jahn-Teller distortion of an $^6E'(D_{3h})$ state. Our observations of three distinct fundamentals confirm the C_{2v} geometry for the ground state, although using a simple central force field[10] calculation, we obtain an apical angle of 76.9°. These observations are not inconsistent with the ESR experiments if the barrier to pseudo-rotation is sufficiently small that the ESR may be considered to be obtained as an average over all configurations.

Additional confirmation of this is provided by our observation of a low lying (A) state at 400 cm^{-1} (0.05eV). Note, although we cannot develop a clear excitation profile for this state, it is observed only in the relatively narrow region 582~576 nm, almost exactly the same region as the $\nu_2(b_1)$ vibration of the ground (X) state. It is commonly assumed that resonance Raman spectra can only involve totally symmetric ground state species. This is only true if the symmetry of both ground and excited state involved in the optical resonance are the same or in the absence of strong vibronic mixing. Observation of the $\nu_2(b_1)$ vibration indicates that at least for the sub-region 582~576 nm the usual resonance Raman selection rule breaks down allowing transitions to states which are non-totally symmetric. Due to the similarity in excitation profile and the observed energy, it is quite likely that the (A) state at 400cm^{-1} is the $^6B_2$ state predicted by Balasubramanian.

It remains to discuss our determination of the energy of atomization. In their earlier paper on low spin states of Rh_3, Das and Balasubramanian[6] predicted a value of 8.15eV, but in their later high spin calculation[5], revise this to 10.8eV. They do point out that using the trimer dissociation energy ($Rh_3 \rightarrow Rh_2$+ Rh) obtained in photolytic experiments of Ozin and Hanlan[3] (4.16eV) plus the dissociation energy for the dimer (D_e = 2.92 eV)[2] gives an experimental value of 7.08eV. This is in agreement with our spectroscopic value of 6.6 ± 1.4eV, but both values deviate considerably from the revised value calculated by Balasubramanian. They are actually close to his original value.

Table 5.1.1 Resonance Raman lines observed for rhodium trimers in argon matrices. Excitation wavelength is the range of laser excitation wavelengths over which each line is observed.

λ_{ex} (nm)	Raman Lines (cm^{-1})	Assignment
540-590	247.9(8)	$\nu_3(a_1)$
579-583	259	$\nu_2(b_1)$
540-590	321.9(5)	$\nu_1(a_1)$
576-582	400	A state
581-583	496	$2\nu_3$
579-583	545	$2\nu_2$
540-590	641.9(11)	$2\nu_1$
540-590	961.6(17)	$3\nu_1$
540-590	1,279.4(20)	$4\nu_1$
540-590	1,597.4(14)	$5\nu_1$

REFERENCES

[1] Morse, M. D. *Chem. Rev.* **86**, 1049 (1986).

[2] Wang, H.; Haouari, H.; Craig, R. Liu, Y.; Lombardi,.J.R.; and Lindsay, D.M. *J.Chem.Phys.*, **106**(6), 2101(1997)

[3] Ozin, G.A. and Hanlan, .A.J., Inorganic Chemistry, **18**, 1781(1979)

[4] Van.Zee , R.J.; Hamick, Y.M.; Li,S.;and Weltner. Jr. W., *Chem.Phys.Lett.*, **195**,214(1992)

[5] Dai, D.G.; Balasubramanian, K. *Chem.Phys.Lett.*, **195**, 207 (1992).

[6] Das, K.K.; Balasubramanian, K., *J.Chem.Phys*, **93**, 625 (1990)

[7] Hu, Z.; Zhou, Q.; Lombardi, J.R.; Lindsay, D.M. *In Spectroscopy of Mass-selected Zirconium Dimers in Argon, in Physics and Chemistry of Finite Systems: from clusters to Crystals, edited by P.Jena, S.N.Kahana, and B.K.Rao (Kluwer Academic, Dordrecht, 1992).*

[8] Hu, Z.; Shen, B.; Deosaran, S.; Lombardi, J.R.; Lindsay, D.M.; Harbich, W. *Proc. SPIE* **1599**, 65(1991).

[9] Hu,Z.; Shen, B.; Deosaran,S.; Lombardi, J.R.; Lindsay, D.M.; Harbich,W. *J.Chem.Phys*, **95**, 2206 (1991).

[10] Herzberg, G. *Molecular Spectra and Molecular Structure, II. Infrared And Raman Spectra Of Polyatomic Molecules*, D. Van Nostrand Company, Inc. New York, (1950).

[11] Herzberg, G. *Molecular Spectra and Molecular Structure, I. Spectra Of Diatomic Molecules* D. Van Nostrand Company, Inc. New York, (1950).

Figure 5.1.1 Raman spectrum of rhodium trimers in argon matrices excited at 572nm.

A fraction of another Raman spectrum excited at 582nm is shown as insert.

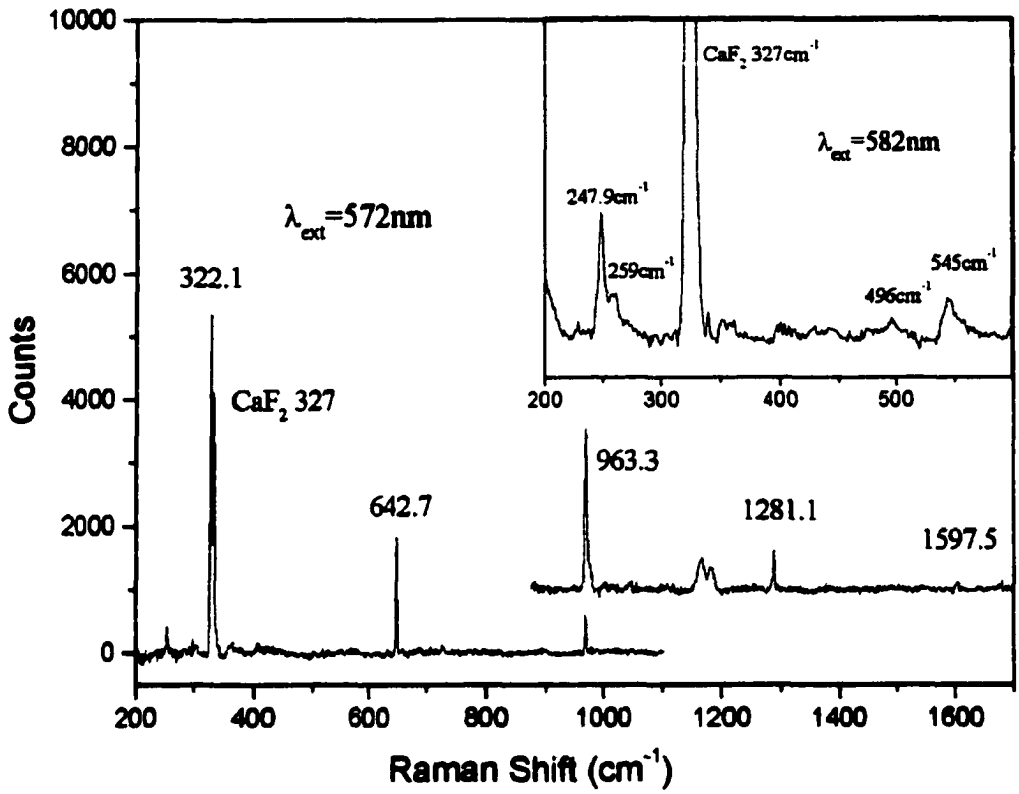

Figure 5.1.2 The Raman excitation profile for the frequency of 322.1cm^{-1}(ν_1), 642.7cm^{-1}($2\nu_1$), and 247.9cm^{-1}. (ν_3)

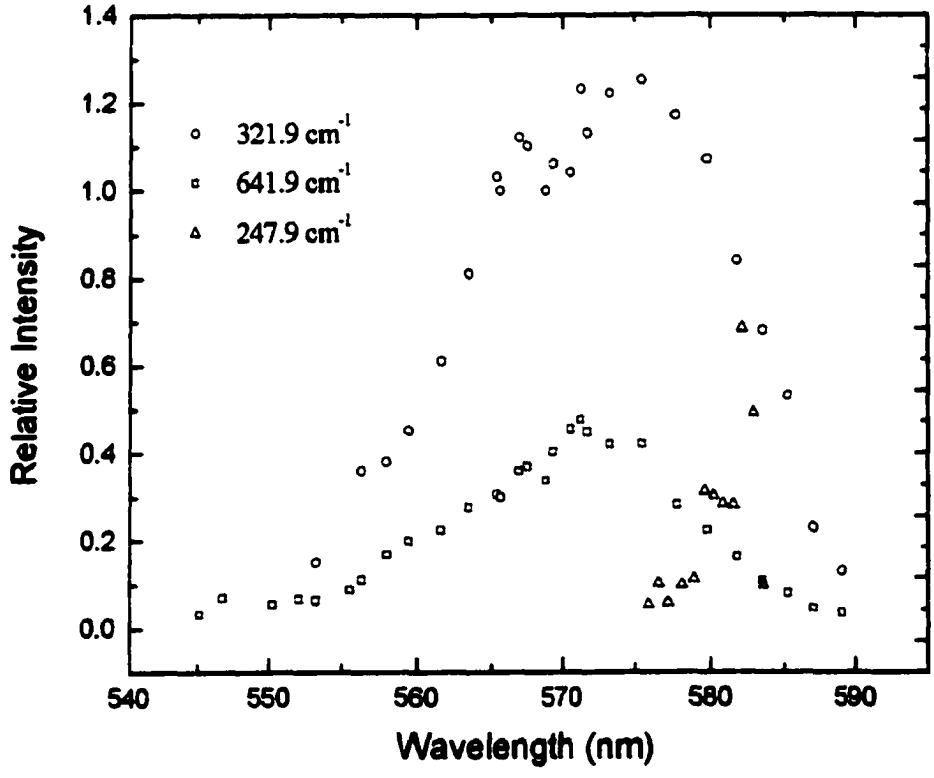

5.2 Raman Spectra of Ruthenium and Tantalum Trimers in Argon Matrices

In preparation

I. INTRODUCTION

In this paper we report on the observation of resonance Raman spectra of Ru_3 and Ta_3 in an argon matrix. To our knowledge there is no previous experimental or theoretical work on Ru_3. We have previously reported the Raman spectrum of ruthenium dimers in argon matrices[1]. Our samples are prepared by neutralizing a mass selected beam of trimer ions. Although the absorption spectrum (scattering depletion spectrum) failed to show any obvious absorption transitions from 200 nm to 850 nm, the resonance Raman spectra of ruthenium trimers in argon matrices have been observed (between 597 nm and 570 nm) for the first time. Three Raman transitions may be assigned to Ru_3. Two of them (303.4 cm^{-1} and 603.7 cm^{-1}) are considered to be a progression in the symmetric stretch, which gives ω_e = 306.5 cm^{-1}, and $\omega_e x_e$ = 1.6 cm^{-1} (k_e = 1.86 mdyne/Å), while the third observed band (581.5 cm^{-1}) is assigned to a low lying excited electronic state.

For Ta clusters we have previously reported on Ta_2[2] and Ta_4[3]. Exciting in the region 575~612nm we find new lines at 251.2 cm^{-1} and 501.9 cm^{-1} which we assign to the fundamental and first overtone of the symmetric stretch, giving ω_e = 251.7 cm^{-1}, and $\omega_e x_e$ = 0.25 cm^{-1} (k_e = 2.25 mdyne/Å).

II. EXPERIMENT

The City College of New York (CCNY) metal cluster deposition source has been described in previous publications[4]. Briefly, an intense argon ion sputtered a water cooled metal target (Exxon Research and Engineering Corporation) maintained at around 300V. Secondary ions were extracted and mass selected using a Wien filter (Colutron 600-B). After mass selection, the ion beam was bent by 10° and then guided and focused to the deposition region.

Ruthenium or tantalum trimer ions were codeposited with argon and electrons on a polished CaF_2 substrate (~16K). Matrices were grown at ~5μm/hour with an Ar:metal dilution ratio of approximately 10^4: 1. The deposition region was surrounded by a "Faraday Cage" whose potential with respect to the sputtering target controls the kinetic energy (24eV in this experiment) of deposited ions. Ion currents under "soft landing" conditions were approximately: Ru^+ (50nA), Ru_2^+ (16nA), and Ru_3^+ (15nA), and Ta^+ (37nA), Ta_2^+ (55nA), Ta_3^+ (20 nA), and Ta_4^+ (40nA). The metal trimer samples were prepared with 6 hours deposition, totally 90 nA-h and tantalum trimer 100 nA-h. Figure 5.2.1 shows the mass-scan of Ta clusters in our apparatus. Due to the unusually high current in Ta_4^+ there can be seen considerable overlap with Ta_3^+ so that we cannot completely discriminate against Ta_4^+ in our sample.

Matrix samples were interrogated *in situ* using both absorption and Raman spectroscopy. As previously described[5], the technique termed SDS was applied, but no obvious absorption feature could be assigned to ruthenium or tantalum trimers.

The Raman spectra were searched by exciting the sample with the visible light (457.9 nm-514.5 nm) of an argon ion laser (Spectra-Physics model 2045), tunable dye laser (R110, R6G and DCM) and Ti-Sapphire laser. The scattered light was collected at 90°, focused into a Triplemate Spectrometer (Spex 1877E, 0.6m, resolution is around 4cm^{-1} at 580 nm in this experiment) and detected with a liquid nitrogen cooled CCD system (Spectrum One and CCD30).

III. SPECTRA AND ANALYSIS – Ruthenium Trimers

Figure 5.2.2 shows a typical Raman spectrum of ruthenium trimers in argon matrices excited at 581 nm. Several fluorescent bands (f) are indicated as well. The Raman shifts were averaged over nine separate spectra at different wavelengths from 574 nm to 587 nm. The averages, along with standard deviations (in parentheses) are 303.4(3) cm^{-1}, 603.7(7) cm^{-1} and 581.5(5) cm^{-1}.

The lowest frequency line is the most intense, and may be assigned as the fundamental of a totally symmetric stretch. Support for this assignment is provided by the work of Ozin and McIntosh[6] who suggest that force constants for higher clusters (n>2) may be obtained from that of the dimer by simple distribution among the various bonds. We have found this to be a reliable guide[7,8]. Assuming a central force field, the totally symmetric fundamental frequency for a homonuclear trimer should be observed at approximately $\sqrt{3}/2$=0.866 times the dimer frequency. This is independent of whether the geometry is that of an equilateral triangle (D_{3h}) or bent (C_{2v}). In previous work on

ruthenium we obtained a dimer frequency of 347.1 cm^{-1} [1], and with this result predict using Ozin and McIntosh a value of 300.6 cm^{-1} for the trimer. We therefore have confidence that the 303.4 cm^{-1} line observed is indeed the totally symmetric stretch. Despite an intensive search we were not able to observe any lines to lower frequency, which could be assigned to other vibrational modes. We therefore cannot determine the molecular geometry from these spectra.

The two higher frequency lines are both candidates for an overtone of the observed fundamental. We take the 603.7 cm^{-1} to be the first overtone for two reasons. One, it is closer to twice the fundamental frequency. The second reason involves the line widths. The 603.7 cm^{-1} line is broader than the 581.5 cm^{-1} (see figure 5.2.2). We attribute this to the distribution of isotopes (^{102}Ru =31.6%, ^{104}Ru=18.6% and ^{101}Ru=17.1%) which is expected to broaden overtones. The spectral origin (0-0 band) of an excited electronic state would be expected to have minimal isotopic broadening and we therefore assign the relatively narrow line at 581.5 cm^{-1} to the origin of a low lying electronic state. The calculated force constant for the ground state is k_e = 1.86 mdyne/Å

The insert in figure 5.2.2 shows the Raman excitation profile for the line at 303.4 cm^{-1}. The intensity maximum is near 579 nm, and despite the absence of any observed absorption (SDS) intensity, we believe this represents an optical transition in the trimer.

IV. SPECTRA AND ANALYSIS – Tantalum Trimers

Due to the relatively low sputtering current of Ta_3^+ and relatively high current due to the neighboring Ta_4^+ peak, only a fairly weak resonance Raman spectrum of Ta_3 could be obtained, by exciting in the region 575~612nm. This is shown in figure 3. Due to the above mentioned overlap, we observe a line at 261.5 cm^{-1} which was previously assigned to Ta_4[3] and most likely due to some fragmentation we also observe a line at 296.5 cm^{-1} which we have previously assigned to Ta_2[2]. The remaining two lines at 251.2 cm^{-1} and 501.9 cm^{-1} were not observed in the previous spectra of Ta_2 and Ta_4 and we assign them to Ta_3. They are the fundamental and first overtone of the symmetric stretch from which we obtain ω_e = 251.7 cm^{-1}. The resulting force constant k_e = 2.25 mdyne/Å. These results are of special interest in the light of previous results from this laboratory on Ta_2 [2]and Ta_4 [3]. Tantalum is the first transition metal for which high quality Raman spectra have been obtained for the dimer, trimer and tetramer. We present comparison of the Ta-Ta stretching force constants obtained for each of these in Table 1.

Table 1. Observed and predicted force constants (mdyne/Å) for dimer, trimer and tetramer of Ta. Predictions use the scheme of Ozin and McIntosh [6].

	Observed	Predicted
Ta_2	4.80	(4.80)
Ta_3	2.25	2.40
Ta_4	1.89	1.60

Ozin and McIntosh have proposed a scheme by which the force constants for larger clusters may be predicted from the knowledge of the dimer force constant. For an equilateral triangle (D_{3h}) trimer, the force constant should be 1/2 that of the dimer, and

for a tetrahedral (T_d) tetramer the factor should be 1/3. These predicted values are presented in the table 1. As can be seen the predictions are quite close to the measured value. For the trimer, the difference may be due to deviations of the geometry from that of an equilateral triangle. Since we were not able to observe any lower frequency modes we are not able to determine any structural information about this trimer.

The only other work we know of concerning Ta_3 is a multiphoton ionization and density functional theory calculation by Heaven *et. al* [9]. They are mostly concerned with carbides of tantalum clusters, but for the dimer predicted a $^1\Sigma_g^+$ ground state with ω_e = 354 cm^{-1}. The trimer is predicted to have a geometry close to an equilateral triangle, but slightly distorted to C_s with a ^2A" ground state, while the tetramer is predicted to be considerably distorted from the tetrahedral geometry and a $^1A_1$ (C_{2v}) state. This latter differs considerably from the experimental results [3], for which only a slight distortion from tetrahedron is observed, and the existence of John-Teller distortion indicates a doubly degenerate ground state.

Reference

[1] Wang, H.; Liu, Y.; Haouari, H.; Craig, R.;Lombardi, J.R, and Lindsay, D.M. *J. Chem. Phys.* **106**, 6534 (1997).

[2] Hu, Z.; Shen, B.; Lombardi, J.R.; Lindsay, D.M. *J. Chem. Phys.* **96**, 8757 (1992).

[3] Wang, H.; Craig, R.; Haouari, H.; Dong, J.; Hu, Z.; Vivoni, A.; Lombardi, J.R., and Lindsay, D.M. *J. Chem. Phys.* **103**, 3289 (1995).

[4] Hu, Z.; Shen, B.; Deosaran, S.; Lombardi, J.R.; Lindsay, D.M.; Harbich, W. *J. Chem .Phys.* **95**, 2206 (1991).

[5] Hu, Z.; Shen, B.; Deosaran, S.; Lombardi, J.R.; Lindsay, D.M.; Harbich, W. *Proc. SPIE* **1599**, 65 (1991).

[6] Ozin; G.A.; McIntosh, D.F. *J. Phys. Chem.* **90**, 5756 (1986).

[7] Wang, H.; Hu, Z., Haouri, H.; Craig, R.; Liu, Y.; Lombardi, J.R.; Lindsay, D.M. *J. Chem. Phys.* **106**, 8339 (1997).

[8] Wang, H.; Craig, R.; Haouri, H.; Dong, J.; Hu, Z.; Vivoni, A.; Lombardi, J.R.;.Lindsay, D.M. *J. Chem. Phys*, **103**, 8389 (1997).

[9] Heaven, M.W.; Stewart, G.M.; Buntine, M.A., and Metha, G.F. *J. Phys. Chem. A* **104**, 3308 (2000).

Figure 5.2.1 Mass-scan of Ta cluster cations in our apparatus. Note the strong overlap of Ta_4^+ and Ta_3^+ due to high Ta_4^+ current.

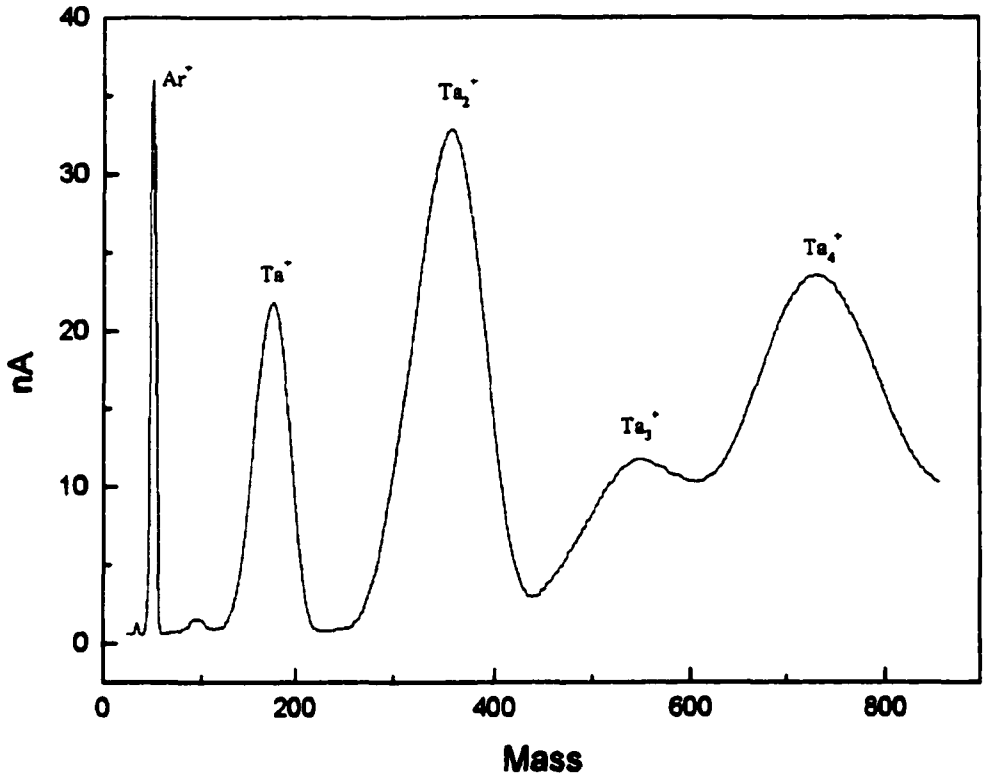

Figure 5.2.2 Raman spectrum of ruthenium trimers in argon matrices excited at 581nm. The Raman excitation profile for the 303.4cm^{-1} line is shown as insert. Several bands due to fluorescence are marked *f*.

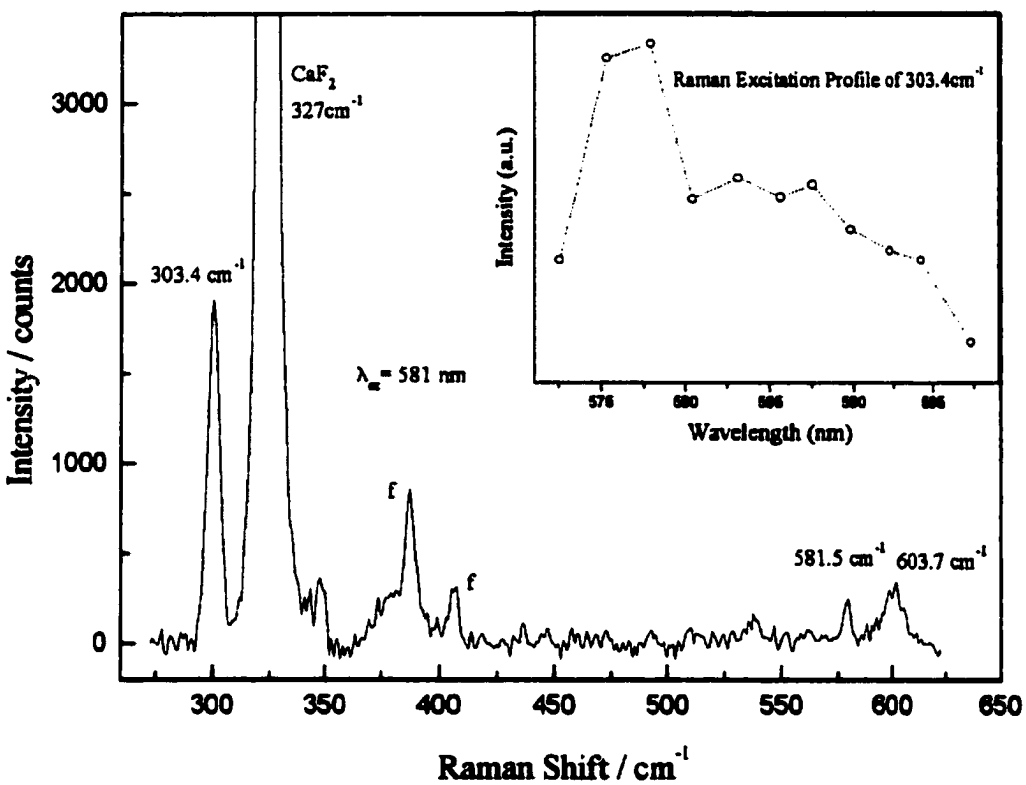

Figure 5.2.3 Raman spectrum of tantalum trimers in argon matrices. Due to incomplete mass filtering we also observe a line due to Ta_4 and some fragmentation leads to a line for Ta_2 as well.

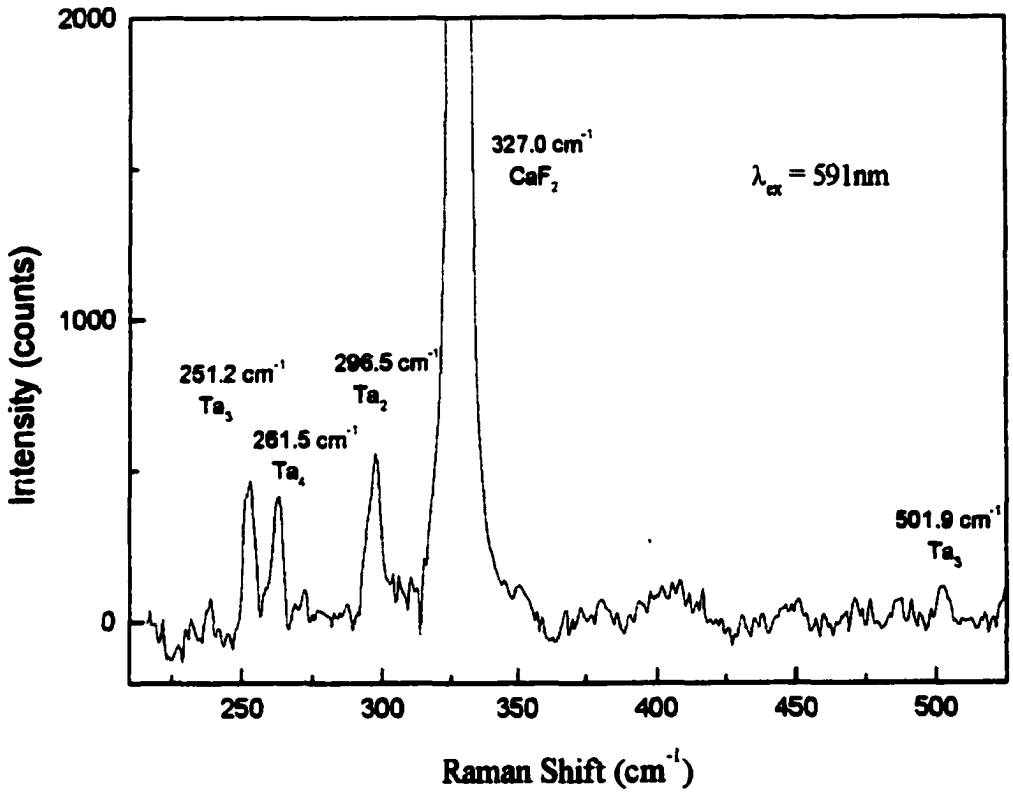

BIBLIOGRAPHY

Chapter I. Introduction

[1.1] *Metal Clusters in Catalysis, Studies in Surface Science and Catalysis 29,* B. A. Gates, L. Guczi and H. Knoezinger (Eds.), Elsevier, Amsterdam, (1986).

[1.2] Cr_2: S. P. Casey, P. W. Villalta, A. A. Bengali, C. L. Cheng, J. P. Dick, P. T. Fenn, D. G. Leopold, *J. Am. Chem. Soc.* **113**, 6688 (1991)

Pd_2: J. Ho, K. M. Ervin, M. L. Polak, M. K. Gilles, W. C. Lineberger, *J. Chem. Phys.* **95**, 4845 (1991)

[1.3] D. S. Yang, B. Simard, P. A. Hackett, A. Breces, M. Z. Zgierski, *International Journal of .Mass Spectrometry And Ion Processes.* **159**, 65-74 (1996)

[1.4] M. D. Morse, *Chem. Rev.* **86**, 1049 (1986).

[1.5a] For example Pt_2, S. Taylor, G. Lemire, Y. M. Hamrick, Z. Fu, M. Morse, J. Chem. Phys. **89**, 5517 (1988)

[1.5b] Pt_2 and AgAu J. C. Pinegar, L. Karlsson, J. D. Langenberg, Q. D. Costello, M. D. Morse. J. Chem. Phys.

[1.6] Cu_2: E. A. Rohlfing, J. J. Valentini, *J. Chem. Phys.* **84**, 6560 (1986)

Mo_2: Y. M. Ffremov, A. N. Samoilova, V. B. Kozhukhovisky, L. V. Gurvich, J. Mol. Spectrosc. **73**, 430 (1978)

Pt_2: H. Wang, Y. Liu, H. Haouri, R. Craig, J. R. Lombardi and D. M. Lindsay, *J. Phys. Chem.* **101**, 7036 (1997).

[1.7] Sc_2: M. Moskovits, D. P. DiLella, W. Limm, *J. Chem. Phys.* **80**, 626 (1984)

Ti_2: C. Cosse, M. Fouassier, T. Mejean, M. Tranquille, D. P. DiLella, M. Moskovits, *J. Chem. Phys.* **73**, 6076 (1980)

Mn_2: K. D. Bier, T. L. Haslett, A. D. Kirkwood, M. Moskovits, *J. Chem. Phys.* **89**, 6 (1988)

Fe_2: T. L. Haslett, M. Moskovits, *J. Mol. Spectrosc.* **135**, 259 (1989)

[1.8] For example: D. M. Lindsay, F. Meyer, and W. Harbich.; *Z. Phys. D* **12**, 15-18(1989)

W. Harbich, S. Fedrigo, and J. Buttet, *Mat. Res. Soc. Symp. Proc.* **206**, 368 (1991)

W. Harbich, S. Fedrigo, J. Buttet, and D. M. Lindsay, *Z. Phys. D* **19**, 157-159 (1991)

S. Fedrigo; W. Harbich, and J. Buttet; *Phys. Rev. B.* **58** (11), 7428 (1998).

[1.9] For example: T. L. Haslett, K. A. Bosnick, and M. Moskovits, *J. Chem. Phys.* **108**, 3453 (1998)

[1.10] For example: Ag_3 of our lab: K. Kernisant, G. A. Thompson, and D. M. Lindsay, *J. Chem. Phys.* **82**, 4739 (1985)

[1.11] M. Dolg,; H. Stoll,; H. Preuss, *J. Mol. Struct. (Theochem)* **277**, 239, (1992)

[1.12] Example: D. G. Dai; K. Balasubramanian, *Chem. Phys.*

Lett., **195**, 207 (1992).

K. K. Das, K. Balasubramanian, *J. Chem. Phys.*, **93**, 625 (1990)

Chapter II. Experimental

[2.1] R. Behrisch, Sputtering by Particle Bombardment, *Topics in Applied Physics*. Vol. 47, (1981)

[2.2] B. Meyer, *Low temperature Spectroscopy,* (1971)

[2.3] For example, Tb and its dimer, J. Kordis, K. A. Gingerich, and R. J. Seyse., *J. Chem. Phys.* 61, 12, 5114 (1974)

[2.4] D. M. Lindsay, F. Meyer, and W. Harbich.; *Z. Phys. D* 12, 15-18 (1989)

[2.5] S. Fedrigo; W. Harbich, and J. Buttet; *Phys. Rev. B.* **58** (11), 7428 (1998).

[2.6] A. R. Gee, D. C. O'Shea and H.Z. Cummings, *Solid State Communications* Vol.4 43 (1965)

Chapter III. Resonance Raman Theory

[3.1] H. A. Kramers and W. Heisenberg, *Z. Phys.* **31**, 681 (1925)

[3.2] P. A. M. Dirac, *Proc. R. Soc.* London **114**, 710 (1927)

[3.3] T. G. Spiro and P. Stein, *Ann. Rev. Phys. Chem.* **28**, 501 (1977)

Robin J. H. Clark, *Vibronic Processes in Inorganic Chemistry*, **301** (1989)

[3.4] S. O. Williams and D. G. Imre, *J. Phys. Chem.* **92**, 3363 (1988)

E. J. Heller, R. L. Sunberg and D. Tannor, *J. Phys. Chem.* **86**, 1822 (1982)

S. Y. Lee and E. J. Heller, *J. Chem. Phys.* **71**, 4777 (1979)

Chapter IV. Transition metal Dimers

[4.1] F. A. Cotton and C. B. Harris, *Inorg. Chem.*, **4** 330 (1965)

[4.2] N. W. Ashcroft, *Solid State Physics*, (1976)

[4.3] G. Herzberg, *spectra of Diatomic Molecules* (Van Nostrand, Princeton, 1950)

Chapter V. Transition metal Trimers

[5.1] G.A. Ozin; D.F. McIntosh, *J. Phys. Chem.* **90**, 5756 (1986)

G. Herzberg, *Infrared and Raman Spectra of Polyatomic Molecules* (Van Nostrand, Princeton, 1945)

[5.2] A. D. P. Dilella, K. V. Taylor and M. Moskovits, *J. Chem. Phys.* **87** (1983) 524. M. Moskovits, *Chem. Phys. Letters.* **118**, (1985) 111